Experimental and computational studies on deflagration-to-detonation transition and its effect on the performance of PDE

A Thesis

Submitted For the Degree of

Doctor of Philosophy

in the Faculty of Engineering

by

Abhishek R Bhat

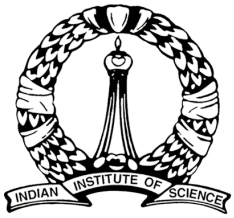

Department of Aerospace Engineering
Indian Institute of Science
BANGALORE – 560 012, INDIA

MAY 2014

I dedicate this thesis to my Grand Parents,
They taught me the value of books.
Which set me on the path of acquiring knowledge.

Acknowledgement

I am thankful to God for allowing me to study and work in this great institute. I would like to pay my homage and gratitude to late Prof P. J Paul for guiding me for my PhD and my ME. My interactions with him during the course work and research period has left a deep impression on my thinking. In particular the quality of fearless and critical thinking. I am greatly indebted to Dr. N. K. S. Rajan and Prof. H. S. Mukunda for helping me with the completion of my theses for past 1 year. My interactions with Dr. Rajan were greatly helpful to increase my understanding of working of electronic equipment and circuits. I would like to acknowledge his help in providing the computational for my research work and for providing unconditional support to me. Prof. Mukunda has provided a new dimension to the understanding of work by emphasizing on critical issues in my work. His fast thinking, constant questioning and bringing out the importance of numbers was a great learning experience. I would like to thank Prof. S. Dassapa for support and enthusiastic discussions on various topics related to energy, which helped me to deeply appreciate the importance of this field. I thank the chairman of the Aerospace Department Prof. D. Ghose for being supportive to my cause. I am grateful to the help provided by support staff of CGPL for conducting my experiments, without their enthusiastic support it would have been practically impossible for me to carry out several experiments. I would like to thank all my friends in and outside CGPL lab for being my friends during the happy and sad times of my life in IISc. I would specially like to thank Arvind Iyer who has been my friend and colleague for past 14 years, his intelligence, dedication and hard work has always been a great example for me. My parents have been constant source of inspiration for me, on which I have greatly depended during the trying times of my PhD. Finally I would like to thank my wife for providing me moral and mental support while being patient herself.

Abstract

This thesis is concerned with experimental and computational studies on pulse detonation engine (PDE) that has been envisioned as a new concept engine; these engines use the high pressure generated by detonation wave for propulsion. The cycle efficiency of PDE is either higher in comparison to conventional jet engines or at least has similar high performance with much greater simplicity in terms of components.

The first part of the work consists of an experimental study of the performance of PDE under choked flame and partial fill conditions. Detonations used in classical PDEs create conditions of Mach numbers of 4-6 and choked flames create conditions in which flame achieves Mach numbers near-half of detonation wave. While classical concepts on PDE's utilize deflagration-to-detonation transition and are more intensively studied, the working of PDE under choked regime has received inadequate attention in the literature and much remains to be explored. Under partial fill conditions and the results show that up to 20 % higher impulse can be obtained by faster initial acceleration of flame which subsequently fails as compared to detonation regime. Most of the earlier studies claim transition to detonation as success in the working of the PDE and non-transition as failure. After exploring both these regimes, the current work brings out that impulse obtained from the wave traveling near the choked flame velocity conditions is comparable to detonation regime. This is consistent with the understanding from the literature that CJ detonation may not be the optimum condition for maximum specific impulse. The present study examines the details of working of PDE close to the choked regime for different experimental conditions, in comparison with other aspects of PDE's.

In the light of these observations that

(a) earlier work on detonation transmission has mostly focused on the transmission of detonation from small to larger tube using various techniques like wave reflection and implosion and that these have shown limited success for detonating fuel-air mixtures under varying conditions and

(b) using blockages to attain DDT is a fundamental technique used by most of the studies on detonation even if it is less efficient as some fuel is always consumed in the initial phase of flame acceleration,

the current study examines transmission of fast flames from small diameter pipe into larger ducts. Experiments were carried out using H_2-air fuel mixtures over an equivalence ratios of 0.55 to 1.0 with polycarbonate tube of 50 mm diameter and length

of 2 m. The smaller tube used for transmission was of 5 mm diameter and length of 0.25 m. This approach *minimizes the amount of fuel consumed* in the smaller pipe for flame acceleration also leading to decrease in the time and length of transition process. Further it allows achieving of the plateau pressure at the head end in lesser time. Comparison with earlier experiments showed that for 50 mm tube the transition length was reduced from 50 cm to 35 cm for stoichiometric H_2-air mixtures and reduction in spiral length from 50 cm to 30 cm. For leaner mixtures with the use of unsymmetrical blockages with spiral of BR 0.35 detonation was achieved within 70 cm for equivalence ratio up to 0.55.

The study of flame acceleration was carried out using three different setup's for stoichiometric mixture of H_2-air using the transmission method described earlier. First set of experiments were carried out in tubes of 42 mm diameter and length of 1 m and 2 m. A second set of experiments was carried out in the tube of 25 mm diameter using different blockages. A third set of experiments was carried out in 30 mm diameter tube again with varying blockages. The results obtained from these three case studies show the importance of initial flame acceleration in obtaining higher specific impulse.

Earlier experiments have shown that for full fill condition, L/D $\approx$ 18 is found to be optimum for maximum specific impulse for wide range of H_2-air mixtures. However, the current work has uncovered the feature that this condition is true only for full fill; no such optimum value is obtained for partial fill cases.

The second part of the study aims at elucidating the features of deflagration-to-detonation transition with direct numerical simulation (DNS) accounting for *multireactions* and *multispecies*. The choice of full chemistry and DNS is based on two features:

(a) the induction time estimation at the conditions of varying high pressure and temperature behind the shock can only be obtained through the use of full chemistry.

(b) the complex effects of fine scale of turbulence that have sometimes been argued to influence the acceleration phase in the DDT cannot be captured otherwise. Turbulence in the early stages causes flame wrinkling and helps flame acceleration process.

Therefore, the numerical scheme demands robustness to capture the DDT process; WENO-5 scheme based of Lax-Fredrich flux has consistently demonstrated higher resolution in capturing various shock interactions compared to second order numerical schemes and hence has been adapted. The code based on WENO-LF was specifically developed for complex chemistry and multi-component diffusion. Diffusive fluxes were calculated using fourth order central differencing scheme. The values of diffusion

constants were calculated using Wilks formula. Code was parallelized using MPI and showed nearly linear speedup. Final code was tested using various test cases from literature before adoption here.

Due to the requirement of resolving fine scales the mesh requirements become very severe. Therefore, the code was used to study the DDT in H_2-O_2 stoichiometric mixture in micro-channels. 2D domain with adiabatic walls was used to study the transition. The study of flame propagation showed that the wrinkling of flame has major effect on the final transition phase as flame accelerates through the channel. *The present simulations demonstrate the detonation initiation at the tip of the accelerating flame as against the transition in boundary layer which is mostly seen in larger channels*. Further, flame becomes corrugated prior to transition. This feature was investigated using nonuniform initial conditions. Under these conditions the pressure waves emanating from corrugated flame interact with the shock moving ahead and transition occurs in between the flame and the forward propagating shock wave.

The primary contributions of this thesis are:
(a) Elucidating the phenomenology of choked flames, demonstrating that under partial fill conditions, the specific impulse is superior to detonations and hence, allowing for the possibility of choked flames as a more appropriate choice for propulsive purposes instead of full detonations, (b) The use of smaller tube to enhance the flame acceleration and transition to detonation. The comparison with earlier experiments clearly shows the enhancements achieved using this method, and (c) The importance of the interaction between pressure waves emanating from the flame front with the shock wave which leads to formation of hot spots finally transitioning to detonation wave.

The thesis is composed of 6 chapters. Chapter 1 is devoted to literature survey and the basic theoretical aspects of detonation wave and pulse detonation engine. Chapter 2 deals with a description of experimental work that has been carried out in this thesis. This chapter starts with the study of partial filling of tubes with different L/D. This is followed by the study of detonation transmission and the description of results obtained. This chapter also contains a description of propagation of choked flames and the comparison of impulse obtained from these experiments. The last part of this chapter gives theoretical basis for choked flame engines. Chapter 3 discusses the study on transmission of accelerating flame using transparent polycarbonate tube for different arrangements and H_2-air equivalence ratios. Chapter 4 gives the details of the numerical method used for studying the flame acceleration and transition to detonation. It

also presents several test cases for non-reactive and reactive flows to validate the solver. Chapter 5 presents various test cases used to study the deflagration-to-detonation transition and the motion of flames and their transition to detonation. Study of flame acceleration and transition to detonation were carried out. Initiation using wrinkled initial profile was also studied. This leads to production of several pressure waves at flame front, due to Ritchmeyer-Meshkov instability and these waves collide with each other forming regions ahead of the flame which leads to transition in between the flame and the forward propagating shock wave. Chapter 6 presents the overview of the work presented in this thesis and the future work.

Contents

1 Introduction **1**

1.1 Preliminaries of detonation waves 3

1.1.1 Rayleigh and Hugoniot Relations 4

1.1.2 Fast deflagration or Choked Flame 6

1.1.3 Zeldovich Neumann and Doring Model 7

1.1.4 Detonation Instability 8

1.1.5 Propagation of a Detonation Wave in a Pipe Closed at One End 10

1.1.6 Single cycle Impulse of Pulse Detonation Engine (PDE) 12

1.1.7 PDE Cycle 15

1.2 Literature Survey 16

1.2.1 Initiation 16

1.2.2 Choked Flames and Quasi Detonation 20

1.2.3 Pulse Detonation Engines 22

1.3 Summary 24

2 Experiments **26**

2.1 Experimental studies on partially filled tubes 27

2.1.1 Details of setup and Instrumentation 28

2.1.2 Experimental Procedure 29

2.1.3 Results and discussion 31

2.1.4 Brief Summary 37

2.2 Study of flame acceleration and its effect on Specific impulse 38

2.2.1 Introduction 38

2.2.2 The Experimental Setup 40

2.2.3 Experimental Procedure 40

2.2.4 Results and Discussion . . . 41
2.3 Experiments on 42 mm Diameter tube . . . 43
2.3.1 Extension tube length variation . . . 48
2.3.2 Study of detonation cell structure obtained . . . 48
2.4 Experiments with 25 mm Diameter tube . . . 50
2.5 Propagation of Detonation in transparent tube . . . 55
2.5.1 Experimental setup . . . 55
2.5.2 Results and Discussions . . . 56
2.6 Theoretical model for impulse produced by various detonation regimes . 60
2.7 Summary . . . 65

3 Initiation of detonation using extension tube **67**
3.1 Introduction . . . 67
3.2 Experimental Setup . . . 67
3.3 Results and discussion . . . 68
3.3.1 Experiments with S1 . . . 68
3.3.2 Experiments with S2 . . . 70
3.3.3 Experiments with H_2-O_2 mixtures . . . 74
3.4 Summary . . . 74

4 Numerical Method **76**
4.1 Introduction . . . 76
4.2 Governing Equations . . . 77
4.3 Weighted Essentially Non Oscillatory Scheme (WENO) . . . 79
4.3.1 Introduction . . . 79
4.3.2 Boundary Conditions . . . 82
4.4 Test Cases . . . 83
4.4.1 Real gas test case . . . 83
4.4.2 Shock BL interaction . . . 84
4.4.3 Detonation 2D structure . . . 85
4.4.4 One dimensional H_2-O_2 flame structure . . . 87
4.5 Summary . . . 88

5 Numerical study of DDT **89**
5.1 Study of DDT in micro channel with stoichiometric H_2-O_2 89
5.2 Numerical setup and domain 89
5.3 Results and discussion 90
5.3.1 Grid dependence study 93
5.3.2 Effect of reaction mechanism 93
5.3.3 Flame length variation and transition 94
5.4 Initial condition variation 98
5.4.1 Initial flame acceleration 98
5.4.2 Flame deceleration 99
5.4.3 Second phase of acceleration 100
5.4.4 Transition to detonation 101
5.4.5 The strength of precursor shock 101
5.5 Strong Initiation 104
5.6 Summary 106

6 Conclusions and future work **107**
6.1 Conclusions 107
6.2 Future work 109

A Reaction Mechanisms **120**

List of Figures

1.1 Range of specific impulse variation with Mach number for various air-breathing engines. 2
1.2 T-S diagrams of Humprey, Brayton and PDE cycles. 3
1.3 The schematic diagram of a Detonation Tube 4
1.4 Rayleigh and Hugoniot curves showing the heat addition at upper and lower CJ points and generalized choked curve passing through upper and lower CJ points. 5
1.5 Choked Flame and double discontinuity. 6
1.6 Variation of properties behind shock wave for CJ detonation wave. . . . 9
1.7 Plot shows the variation of flow velocity in the frame of reference of detonation wave with the tail end of detonation wave moving with -D_{cj}. 11
1.8 Propagation of Taylor wave from closed to open end in a pipe at different times, showing that tail of Taylor wave propagates close to half of CJ velocity. 13
1.9 Head end pressure vs time for a single cycle of PDE. 14
1.10 Single cycle of PDE operation. 15

2.1 Single cycle working of PDE under partial fill condition. 28
2.2 Detonation tube with various attachments. Spark plug, pressure transducers and fuel air inlet. 28
2.3 Schematic Details of Experimental Setup. 30
2.4 Oscilloscope connected to signal conditioner. 31
2.5 Pressure history at head end for various fill fraction (FF) cases for 2m tube. 32
2.6 Comparison of impulse with fill fraction for different impulse models; symbols refer to present experiments for two different trials. 34

2.7 Variation of specific impulse with the fill fraction (ff) and fill length (fl). Increase in specific impulse with length for the same fill length is clearly seen when comparing with fill length. Values collapse to similar curves when plotted against fill fraction. 35
2.8 Comparison of the experimental specific impulse data with the results of models on partial-fill condition; symbols are the present experiments, two trials. 36
2.9 Schematic Details of Experimental Setup for transmission. 39
2.10 Transmission tube of 5 mm diameter. 41
2.11 Pressure time data obtained at 4 locations for ϕ =1. 42
2.12 5 mm tube attached perpendicular to the 42 mm tube. 43
2.13 Plots showing the pressure measurements at 50 cm and 70 cm form closed end, with attachment and without attachment. 44
2.14 Comparison of pressure profile at head end for same fill length of 1 m. Datum pressure is altered for clear comparison. 45
2.15 Specific impulse obtained in 1 m and 2 m tubes with and without attachment at various fill lengths. 46
2.16 Comparison of head end pressures of 1 m tube with 0.5 fill fraction, with and without small tube attachment. 46
2.17 Head end pressure obtained in completely filled 2 m tube without and with extension tube. Datum pressure is altered for clear comparison. . . 47
2.18 Specific impulse vs fill fraction for different lengths of extension tubes. 48
2.19 Closed end 49
2.19 Open end 50
2.20 Various spirals used in the experiment. 51
2.21 Specific impulse vs fill fraction for 25mm dia 1m tube. 52
2.22 The head end pressure profile with attachment and without attachment. . 53
2.23 The variation of specific impulse with the shock velocity measured between the three transducers. V1 corresponds to initial velocity while V2 corresponds to later section. 54
2.24 The pressure profiles at head end and at the middle transducer for the four configurations. 57
2.25 Images of flame motion through the tube captured using high speed camera. 58

2.26 Combustion wave velocity variation along the length of the tube for various cases. 59
2.27 Schematic representation of pressure and velocity variation with distance for the choked state. Various states of mixture are 0: fuel-air mixture, 1: condition after shock, 2: burnt products, 3: state after Taylor wave. 60
2.28 Schematic representation of pressure and velocity variation with distance for the initial acceleration phase. 62
2.29 Variation of theoretical specific impulse Vs shock velocity. Dots are experimental results referring to Fig 2.23. 65

3.1 Comparison of flame velocity with and without extension tube, as flame propagates through the tube with spiral of BR 44%. Detonation fails to propagate without extension tube, the initial process of flame acceleration is significantly delayed as can be seen from the right figure. 69
3.2 Comparison of head end pressure profile with and without extension tube. 69
3.3 X-t diagram of flame front as it moves through the tube. 70
3.4 Flame acceleration and transition for the three cases studied for ϕ=0.63. The final velocity is close to D_{cj}=1733 m/s. 71
3.5 Pressure and velocity comparison of success and failure cases for ϕ=0.55 using tangential attachment. 72
3.6 Flame acceleration for different placement of first orifice plate from the closed end of tube for ϕ=0.55. 73

4.1 Forward and backward stencil spread over 6 points used for the interpolation of fluxes. 80
4.2 Real gas test case with O_2 as test gas; results at 80μs. 83
4.3 Density contours at 1s. Shows the accurate capturing of vortex structure behind the reflected shock. The height of the triple point and secondary vortex is also correctly captured. 84
4.4 Comparison of density profile along the wall at 1 s after the initial state. 85
4.5 Temperature profile of 2D H_2-O_2-Ar detonation. The fine instability structures seen developing behind the detonation front have been very accurately captured using the current scheme while they are diffused in the reference case. 86

4.6 Numerical schlieren of 2D H_2-O_2-Ar detonation. We can see the fine structures behind the detonation front using 22 points in induction zone which are clearly visible using WENO5 while they are diffused in reference test case even after using 44 point in the induction zone. 86
4.7 Temperature distribution across H_2-O_2 flame. CEA gives value of temperature of 3086 K. 87
4.8 Mass fraction of species across flame. CEA values for various species are OH=0.13, H_2=0.019, H=0.005, O=0.034. 88

5.1 The variation of pressure with x for different times. Black: time up to 83.72 μs, Green: time up to 86.07 μs, Red: time up to 86.20 μs. There is a strong exponential growth prior to final transition. 90
5.2 The variation of peak pressure inside the domain with time. 91
5.3 Comparison of flame acceleration for three channels with the theory. Value of coefficient A used for the three cases is 13, 14 and 15 for 0.2, 0.25 and 0.5 mm respectively (left to right). Dash lines are curve fits, Solid lines for the three channels respectively. 92
5.4 Comparison of velocity variation with time for 0.25 and 0.5 mm cases using 5 μ and 10 μ mesh. Net variation of less than 3 % has been observed 93
5.5 Comparison of Flame velocity vs time for the two reaction mechanisms. 94
5.6 Variation of flame length (normalized by channel width) with time. . . . 95
5.7 Variation of flame length (normalized by channel width) vs time normalized with respect to time at maximum flame length. 95
5.8 Pressure and temperature profiles 0.5 mm channel. [As flame propagates through the tube it gets elongated. Close to the transtion the shock develops close to the flame which decreases the flame length and final transition takes place at the tip of the flame.] 96
5.9 Profiles of species mass fraction as flame accelerates through the channel of 0.5 mm width. 97
5.10 Flame and shock velocity vs time. 98
5.11 Pressure profile at different times. 99
5.12 Pressure build up in front of flame leading to transition 100

5.13 Density gradient images of final phase of flame propagation prior to transition. 102
5.14 Temperatures profile of flame propagation close to transition. Images show the transition in the duration of 1μs before transtion. 103
5.15 Simulation with coarse mesh. 103
5.16 1-D plots of pressure and temperature for different times for wrinkled initiation with slip condition. In this case explosion takes place between the flame and shock and final transition to detonation occurs. 104
5.17 Pressure and temperature variation in domain for strong initiation with no slip condition at the wall. 105

List of Tables

2.1 L=Length, ID=Internal Diameter, ϕ=Equivalance ratio, BR=Blockage Ratio. 27
2.2 Variation of front shock velocities V1,V2 and V3 (m/s) between transducers with ϕ=Eq Ratio. 42
2.3 The spirals used in the experiments (dimensions in mm). 50
2.4 Specification of various spirals used. 55
2.5 Spiral combination's used for the experiments. O refers to orifice plate with blockage ratio of 50 %. 56
2.6 Calculated parameters for the four configurations using head end pressure data. For this configuration the theoretical impulse calculated using Wintenberger et al. [1] model is 1.24 Ns/m^2 and Endo et al. [2] model is 1.0Ns/m^2 59
2.7 Parameters of CJ detonation wave used for calculations. 64

3.1 List of experiments conducted showing success and failure for the various cases. T=tangential, A=Axial, R=Radial Attachment. 71
3.2 Values of DDT criteria predicted by Dorofeev et al. [3]. 74
3.3 Values of minimum distance L from closed end for two blockage ratios, for DDT to be successful. 74

4.1 Initial state of the gas across the discontinuity. 83
4.2 Initial conditions. 84

A.1 19 step Reaction mechanism of Jachimowski [4]. Third body factors are given below the respective reactions. 120
A.2 34 step Reaction mechanism derived from larger methane mechanism by Westbrook [5]. 121

Nomenclature

Symbol	Units	Description
$()_x$	-	$\frac{d()}{dx}$
$()_{cj}$	-	Property value at CJ location
$()_c$	-	Property value at Choked condition
$()_f$	-	Property value after flame
$()_s$	-	Property value after shock
M	-	Mach number
D	m/s	Detonation Velocity
Y_i	-	Specie mass fraction
λ	cm	cell size
I	N/m^2	Impulse
I_{sp}	s	Specific Impulse

Acronyms

CJ	Chapman-Jouguet point
ZND	Zeldovich Neumann Doring
PDE	Pulse detonation engine
BR	Blockage Ratio
DDT	Deflagration to detonation transition
ID	Internal Diameter
L_{DDT}	Length of DDT
O	Orifice plate
PT	Pressure transducer
ff	fill fraction

Chapter 1

Introduction

Combustion is the process of chemical reaction between fuel and oxidizer accompanied with the release of heat. It has been used for centuries by humans for various purposes. Combustion process involves coupling between fluid dynamics and chemical kinetics. This coupling gives rise to two equilibrium solutions for the system:

Deflagration wave, which propagates at subsonic velocity with respect to the reactants. Across deflagration wave temperature increases while pressure remains nearly constant. Combustion of premixed fuel air mixture in Bunsen burner is an example of deflagration.

Detonation wave, which propagates at supersonic velocity with respect to the reactants and it is accompanied by large rise in pressure and temperature. The explosion in fuel-air mixture is a typical example of detonation wave. Deflagration waves have been in use and studied since time immemorial while detonation waves were first reported in literature by Berthelot and Vielle [6] and by Mallard and Le Chaterlier [7].

At present most of engines use deflagration wave for the conversion of chemical energy into mechanical energy and our understanding in this field has greatly advanced in past century. On the other hand the engines using detonation as a conversion mechanism are still under initial phase of development. First successful flying PDE engine was reported in 2008 [8] which produced the thrust of 900 N. PDE's will be 5-10% more efficient as compared to current air-breathing engines.

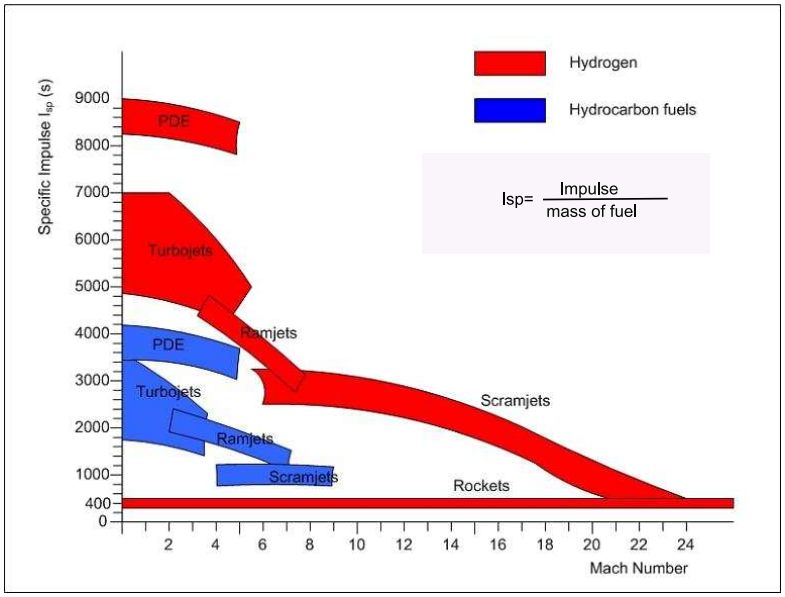

Figure 1.1: *Range of specific impulse variation with Mach number for various air-breathing engines.*

Pure PDEs are being considered for military applications, for propulsion of missiles, unmanned air vehicles, and other small-scale applications. As combined cycle applications PDEs have been considered to replace the afterburners, so as to improve the specific fuel consumption during the after-burning period and to reduce the emissions Lam et al. [9].

In addition to the propulsion applications, they have also been proposed for power generation applications. In combined cycle with turboprop engine increase in performance has been predicted by Kumar [10].

PDE has lesser moving parts and higher combustion efficiency as it works close to constant volume cycle. Figure 1.1 shows the variation of specific impulse with Mach number for different air breathing engines. PDE has a higher efficiency as compared to jet engines in Mach number range of 0 to 4. This is because most of the jet engines work on Brayton cycle in which heat addition takes place at constant pressure as deflagration is the primary mechanism of heat release. In contrast, a pulse detonation engine works close to Humpry cycle in which heat release takes place close to constant volume. Figure 1.2 shows the comparison of these three cycles. Average release of heat in case of PDE cycle takes place at higher temperature as compared to Brayton which leads to

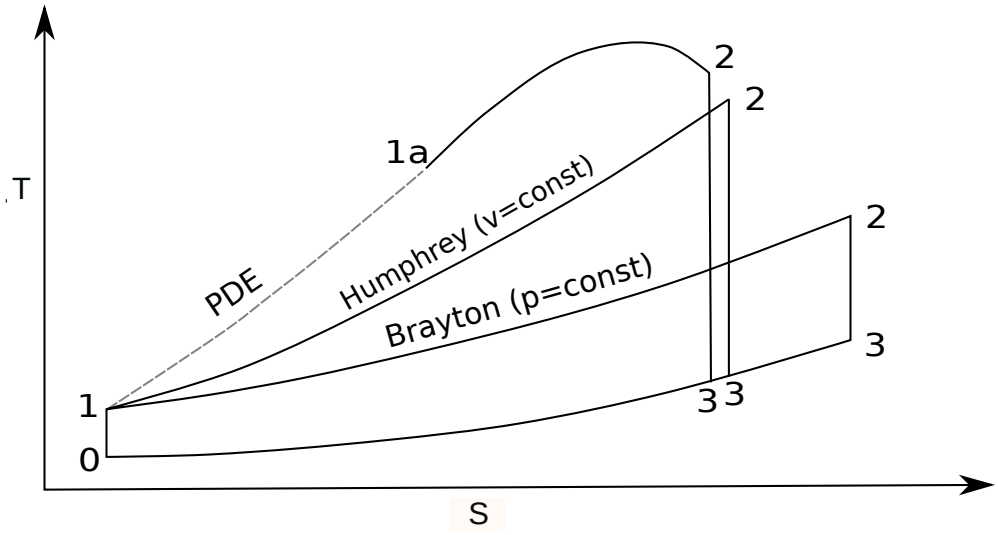

Figure 1.2: *T-S diagrams of Humprey, Brayton and PDE cycles.*

higher thermal efficiency for PDE as compared to jet engines.

1.1 Preliminaries of detonation waves

The core of a pulse detonation engine is a detonation tube (see Fig 1.3), which is closed at one end and open at the other. The tube is filled with reactive mixture, which on ignition with favourable condition transits to a detonation wave moving through the tube from the closed end to the open end.

The following sections explain the basic theory of the formation of a detonation, and the choked flame condition. For details one may refer to the many texts in this subject, eg Lee [11], Fickett and Davis [12]. The most basic treatment of a flame is made by considering the system in the frame of reference moving with the flame. This treatment results in the Rankine-Hugonit relations which is discussed in Sec 1.1.1 The fast deflagration wave (called as choked flame in some literature) is the transient which appears before the formation of the shock. This is analysed in Sec 1.1.2. Once a detonation is formed, the dynamics of the fluid behind the detonation wave is discussed in Sec 1.1.5

The detailed treatment to detonation wave is given by the ZND model which is covered in Sec 1.1.3. While the ZND model itself provides the details, it is a steady state

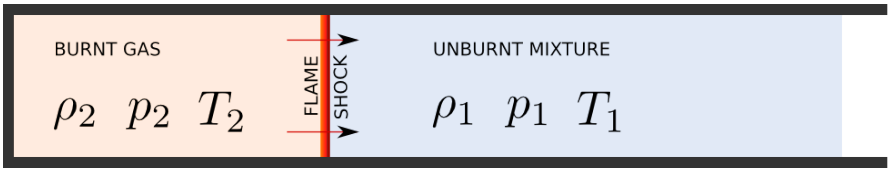

Figure 1.3: *The schematic diagram of a Detonation Tube*

model. However, in practice it is found that the detonation is unstable. Section 1.1.4 discusses about this important aspect.

Finally, this section closes with the practical PDE cycle, discussed in Sec 1.1.7

1.1.1 Rayleigh and Hugoniot Relations

The conservation equations of mass, momentum, and energy in one-dimension provide us with the equations for Releigh line Eqn 1.1 and Hugoniot curve Eqn 1.2. Subscripts 1 and 2 refer to the conditions at the unburnt and burnt conditions. q is the heat added due to the chemical reactions. Manipulating the above equations, the following two relations can be obtained for ideal gases with constant properties and no change in molecular mass due to chemical reactions.

$$y - 1 = \gamma M_1^2 (1 - \varepsilon) \tag{1.1}$$

$$\left(y + \frac{\gamma - 1}{\gamma + 1}\right)\left(\varepsilon - \frac{\gamma - 1}{\gamma + 1}\right) = \frac{4\gamma}{(\gamma + 1)^2} + \frac{2\gamma q}{a_1^2}\left(\frac{\gamma - 1}{\gamma + 1}\right) \tag{1.2}$$

where $y = p_2/p_1$ and $\varepsilon = \rho_1/\rho_2$. Eqn 1.1 represents a straight line in $\varepsilon - y$ plane with the slope of the line $= -\gamma M_1^2$. This family of lines are called the Rayleigh lines. All of these pass through the point (1,1), indicating no change. Since Eqn 1.1 enforces that the slope is always negative, the admissible values of $(y.\varepsilon)$ would be

Condition on M_1	Condition on y	Condition on ε	Comment
$M_1 > 1$	$y > 1$	$0 < \varepsilon < 1$	Detonation ($p \uparrow, \rho \uparrow$)
$M_1 < 1$	$0 < y < 1$	$\varepsilon > 1$	Deflagration ($p \downarrow, \rho \downarrow$)

It must be noted here, that in the case of deflagration, the incoming stream is subsonic, hence, the changes caused by the deflagration wave will cause changes in the upstream conditions. Hence, this does not represent the practical situation. However, in

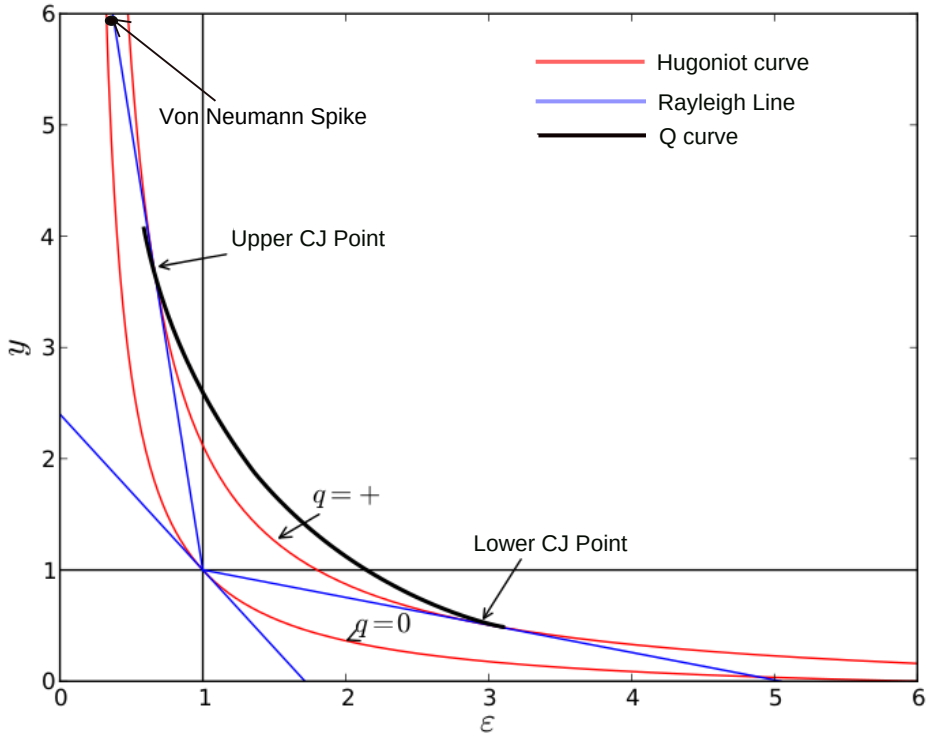

Figure 1.4: *Rayleigh and Hugoniot curves showing the heat addition at upper and lower CJ points and generalized choked curve passing through upper and lower CJ points.*

the case of a detonation wave, the incoming stream is not affected, and this represents the actual system.

It can be seen from Eqn 1.2 the relation represents a hyperbola and for $q = 0$ this curve passes through the point $(1, 1)$. For positive values of q, the curve no longer passes through the point $(1, 1)$, shifts away from the origin, though the asymptotic values remain the same. Figure 1.4 shows the Rayleigh lines and Hugoniot curves for $q = 0$ and a positive value of q. For $M_1 = 1$, the Rayleigh line is tangential to the zero heat addition Hugoniot at the point $(1, 1)$ and this line does not cross the Hugoniot curve anywhere else. However, if the slope of Rayleigh line is increased, $(M_1 > 1)$, the line will always cross $q = 0$, Hugoniot somewhere in the region $y > 1$ and for $M_1 < 1$ in the region $y < 1$. These two intersections correspond to the normal shock wave and the expansion shock.

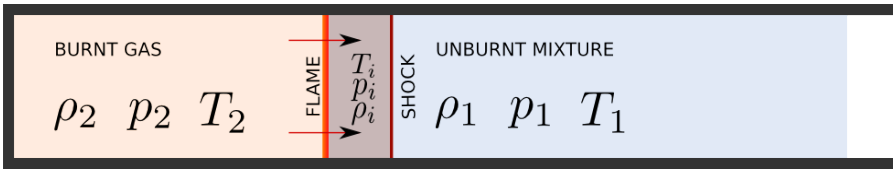

Figure 1.5: *Choked Flame and double discontinuity.*

For the case where the heat addition is positive, there are some values of M_1 for which there exists no point of cross over between the Rayleigh lines and the Hugoniot curves. As M_1 is increased, the Rayleigh line touches the positive heat addition Hugoniot and this point of contact is called the Chapman-Jouguet (CJ) point. The Mach number of the burnt stream (M_2) is unity at the CJ point. The point where $q = 0$ intersects with the Reyleigh line is known as Neumann spike, it represents the post shock state of reactants before reaction begins. On further increasing M_1, the line cuts the Hugoniot curve at two points, one below the CJ point and one above the CJ point. These two intersection points correspond the weak and strong detonation respectively. The weak detonation has $M_2 > 1$ and for strong detonation $M_2 < 1$. Similarly at the lower side, we can get weak deflagration, strong deflagration and lower CJ point, all of which correspond to $M_1 < 1$. Only the weak deflagration is physically realizable in the lower side.The mach number of combustion wave at upper and lower CJ states is given by:

$$M_1 - M_1^{-1} = \sqrt{(2q(\gamma^2 - 1)/a_1^2)} \tag{1.3}$$

1.1.2 Fast deflagration or Choked Flame

Fast deflagration waves refer to flames behind a shock wave. The shock wave moves at supersonic speeds, and the flame is a deflagration wave which moves at speeds that are subsonic with respect to the fluid which is compressed by the shock. Figure 1.5 shows the schematic representation of the flame-shock complex moving at supersonic speeds. These are distinct from detonation waves because in the former the shock and flame are decoupled while they are strongly coupled in the present case. The state at the end of reaction is that of a choked condition, hence the name Choked Flame. Choked flames are unstable under favorable circumstances, it may progress to form a detonation wave. In other cases, when it may not be able to feed the shock and continues to accelerate as a

deflagration wave or fail Lee [11]. The experiments have clearly shown the existence of choked flame under the condition of high blockage [13, 14]. Theoretical development of these combustion waves using three states as shown in Fig 1.5 leads to the well known double discontinuity model [15–17] with both the shock and flame propagating at different speeds as shown in Fig 1.5. The results from this section show that the fast deflagration will propagate at almost the half of CJ speed for a similar mixture.

A second point of view is provided by the work of Brailovskya and Sivashinsky [18] in which they show the existence of multiple regimes for the detonation propagation if the friction term is included in the one dimensional Euler equations. They showed the presence of friction term leads to multiple solutions for detonation velocity depending on the friction factor which in turn is affected by the blockages. Their solution assumed the propagation of detonation as a combustion front which propagates in such a way that at the end of reaction zone the velocity of products immediately goes to zero. This case leads to the condition that there is no Taylor wave (see Sec 1.1.5) present at the end of reaction zone and system undergoes near constant volume explosion with the combustion wave moving at half detonation velocity.

Another point of view which is similar to earlier one is provided by Lee and Moen [19] who shows that the flame accelerates from the closed end of the tube towards the open end to reach the first critical velocity which belongs to the first choking regime. Here the flame propagates at the speed of sound in the burnt gas. The flame continues to accelerate further and reaches the second choking regime where the flame and the shock move at the same velocity which corresponds to CJ detonation velocity for quiescent gas and CJ deflagration velocity for the shocked gas. The curve corresponding to this generalized state is shown in Fig 1.4 as Q-curve. It represents the locus of all the processes which end in choked condition.

1.1.3 Zeldovich Neumann and Doring Model

The RH equation's (see Sec 1.1.1) with Chapman-Jouguet provide us with the overall properties of detonation wave like velocity, CJ pressure and density. To study the detailed structure of the detonation wave it is very important to consider the reactions and also the variation of properties inside the detonation wave. The first model explaining the detailed structure of detonation wave was independently given by Zeldovich, Neumann and Doring [11] and hence is named after them as ZND model. This model is

based on steady state one dimensional conservation equations taking the reaction rate into account. In this model detonation is considered as a shock wave followed by a reaction zone which ends in the CJ state. The governing equation are:-

$$\begin{aligned}(\rho u)_x &= 0\\ (P+\rho u^2)_x &= 0\\ (E+P/\rho)_x &= 0\\ (\rho u Y_i)_x &= \dot{\omega}_i\end{aligned}$$

E is the total internal energy. Y_i is the species mass fraction and $\dot{\omega}_i$ is the reaction rate for the particular specie. These equations can be solved in the shock attached coordinates, with the boundary condition determined by the non reactive RH condition at the shock. These equations are integrated in time and space to give the entire structure of the detonation wave. Figure 1.6 shows the variation of different properties behind the shock wave for a single specie single reaction system with dimensionless value of activation energy $E_a = 50$ heat release $q = 50$ and $\gamma = 1.2$. While pressure and density decrease across the combustion zone there is an increase in temperature. The induction zone is clearly visible, it plays critical role in the stability of detonation wave.

1.1.4 Detonation Instability

ZND model explains steady state profile of detonation wave. However in experiments and numerical simulation detonation waves have been found to be unstable [12]. Starting with the work of Erpenbeck [20] there have been number of theoretical, numerical and experimental studies carried to analyze the instability of detonation wave. Experimental studies have mostly considered recording and analyzing the cellular structure of detonation wave whereas numerical studies have concentrated on carrying out the direct simulation of detonation wave mostly in 1D and 2D. Numerical simulations highlighted the interaction of front shock wave with the reaction zone behind it. The theoretical studies [21, 22] have been carried out by linearizing the reactive Euler equations over the base steady state profile taken from ZND theory. These studies have shown that four most important parameters, namely, (1) Activation energy E_a, (2) Heat of reaction q, (3) Specific heat ratio γ, and (4) Detonation overdrive $f = (D/D_{cj})^2$ affect the stability

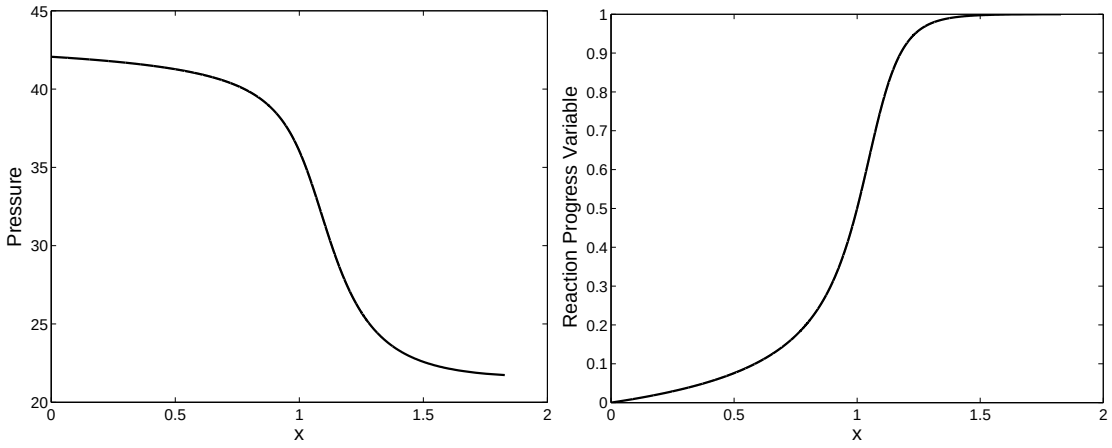

(a) Pressure vs x

(b) Reaction progress variable vs x

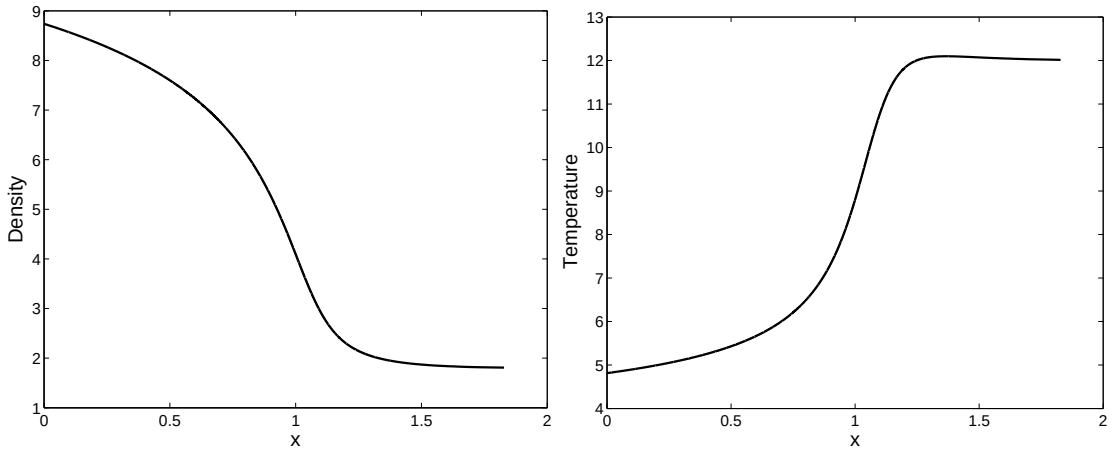

(c) Density vs x

(d) Temperature vs x

Figure 1.6: *Variation of properties behind shock wave for CJ detonation wave.*

of a detonation wave.

The detonation wave instability is of important concern for PDE as it has been shown that when diluted with nitrogen, detonation tends to become more unstable as compared to Argon. These effects will have to be kept in mind while designing the PDE. Neumann pressure varies significantly depending on the stability of detonation wave even when CJ properties are similar. Detonation stability also has an effect on the deflagration to detonation transition of the mixture.

1.1.5 Propagation of a Detonation Wave in a Pipe Closed at One End

In the previous section, we have discussed the general principles of reaction waves in a reacting gas mixture. The case of a tube closed at one end is of particular importance as it forms the basis of pulse detonation engine.

When detonation is initiated in the closed end of the tube, the gas both in front of the detonation wave and near the closed end would be at zero velocity. Since the gas acquires non-zero velocity when the detonation wave passes, the velocity should decrease in the region between the detonation wave and the closed end. As seen in the previous section, the gas velocity relative to the detonation wave at CJ condition would be equal to sound speed on the burnt side. If the condition of the detonation wave does not correspond to the CJ condition and corresponds to the strong detonation, then $v_2 < c_2$. The condition at the closed end, which will have lower density compared to the detonation condition by Rayleigh-Hugoniot relations, can be achieved by either a strong or a weak discontinuity, either of which would be traveling at speed faster than v_2 and will overtake the detonation wave. The only case, where the velocity of the weak discontinuity can match the detonation wave is when $v_2 = c_2$, ie. that corresponding to the CJ condition. This shows that the detonation wave propagated in a pipe, with the gas ignited at the closed end, must correspond to the Chapman-Jouguet point.

Landau and Lifshitz [23] have provided the solution for the unsteady one-dimensional flow which can be applied to the condition of the gas between the closed end and the detonation wave. The salient features of the analysis are reproduced here.

The equations of continuity and momentum for the gas between the closed end and

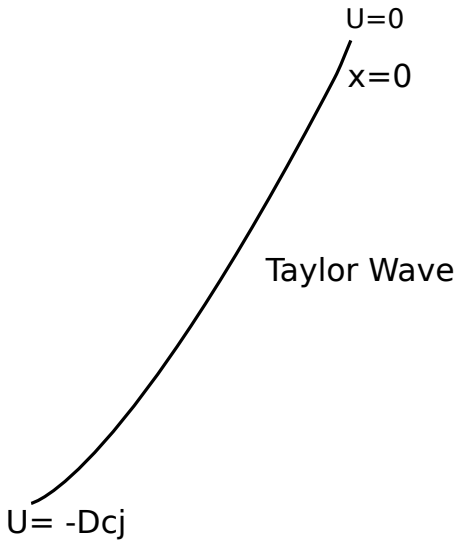

Figure 1.7: *Plot shows the variation of flow velocity in the frame of reference of detonation wave with the tail end of detonation wave moving with -D_{cj}.*

the detonation wave can be written as

$$\rho_t + \rho v_x + v\rho_x = 0 \tag{1.4}$$

$$v_t + vv_x = -\frac{p_x}{\rho} \tag{1.5}$$

We define the similarity variable $\xi = x/t$ and the equations are transformed to ordinary differential equations

$$(v - \xi)\rho' + \rho v' = 0 \tag{1.6}$$

$$(v - \xi)v' = -p'/\rho = -c^2\rho'/\rho \tag{1.7}$$

Constant entropy condition has been used in the second equation above in the form $p' = (\partial p/\partial\rho)_s\rho' = c^2\rho'$. The above equations have either the trivial solution $v =$ constant, $\rho =$ constant or non-trivial solution which can be obtained on the condition $(v - c)^2 = c^2$ or $\xi = v \pm c$. The positive or negative sign has to be taken based on the coordinate system. Considering the coordinate system fixed to the detonation wave, $x = 0$ corresponds to the point where the Mach number is unity Figure 1.7. In this coordinate system, the closed end of the pipe will be moving at a velocity equal to the

detonation velocity away from the CJ plane. Hence at $x = 0$, the conditions of the gas correspond to the CJ condition after detonation. The velocity of the gas relative to the $x = 0$ plane is $c_{CJ} - v_{CJ}$, where c_{CJ} is the speed of sound corresponding to the burnt side and v_{CJ} is the detonation velocity relative to the cold gas. At time $t = 0$, let the detonation wave be at the closed end. The speed of sound at any location between the detonation front and the closed end can be obtained as

$$c - c_{CJ} = \pm \frac{\gamma - 1}{2} |v - c_{CJ}| \tag{1.8}$$

The other variables can be obtained as

$$v = \left(c + \frac{x}{t} \right) \tag{1.9}$$

$$\rho = \rho_{CJ} \left[1 - \frac{\gamma - 1}{2} \frac{|v|}{c_{CJ}} \right]^{2/(\gamma-1)} \tag{1.10}$$

$$p = p_{CJ} \left[1 - \frac{\gamma - 1}{2} \frac{|v|}{c_{CJ}} \right]^{2\gamma/(\gamma-1)} \tag{1.11}$$

Figure 1.8 shows the pressure profile of expansion wave as it moves through the tube closed at one end using Eqn 1.11. The figure has been plotted for the stoichiometric mixture of hydrogen-Air with $P_{cj} = 15.5$ bar. From the figure it can be observed that the final pressure at the end of Taylor wave is almost one-third of CJ value and the tail of wave moves at approximately half of CJ velocity. These results mostly based on one dimensional Euler equations and do not incorporate the loss term. The presence of heat loss will decrease the available pressure at the head end of the tube. In general, with increase in L/D ratio of the detonation tube the heat loss increases and hence an optimum value of L/D has to be chosen so that heat losses are minimum and the length is sufficient for DDT to take place.

1.1.6 Single cycle Impulse of Pulse Detonation Engine (PDE)

The theoretical study of PDE can be used to determine the single cycle impulse of PDE under ideal conditions. Towards this objective two models have been proposed by Wintenberger et al. [1] and Endo and Fujiwara [24]. Both of these models are based on the assumption that the detonation is instantaneously formed in the detonation tube.

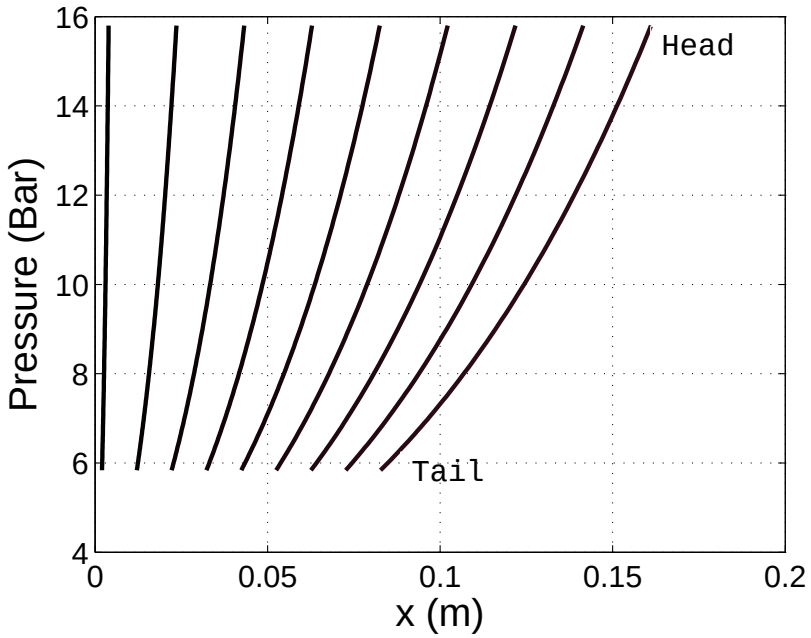

Figure 1.8: *Propagation of Taylor wave from closed to open end in a pipe at different times, showing that tail of Taylor wave propagates close to half of CJ velocity.*

PDE is modeled considering the tube to be closed at one end and open to atmosphere at the other. This condition is similar to the one presented in previous Section 1.1.5. The phase of PDE cycle when detonation propagates inside the tube, the head end pressure can be calculated using the Eqn 1.11. The evolution of pressure at the head end becomes more complicated after the exit of detonation wave from the tube. The calculation of impulse is carried out by integrating the pressure at the closed end of the tube over the single cycle. For this calculation it is important to obtain pressure at the head end of the tube as a function of time. Detonation propagation in PDE is explained in Sec 1.1.7. The impulse of PDE can be written in a general form in terms of the time taken by various processes in PDE as shown in Fig 1.9.

$$I = A(P_2 - P_1)(\Delta t_1 + \Delta t_2 + \Delta t_3) \tag{1.12}$$

Endo and Fujiwara [24] gave a simple model where Δt_1 is the time of travel of detonation wave in the tube. For Δt_2 he assumed the velocity of tail of Taylor wave to be half of detonation velocity and constant for the entire time of travel in tube. The pres-

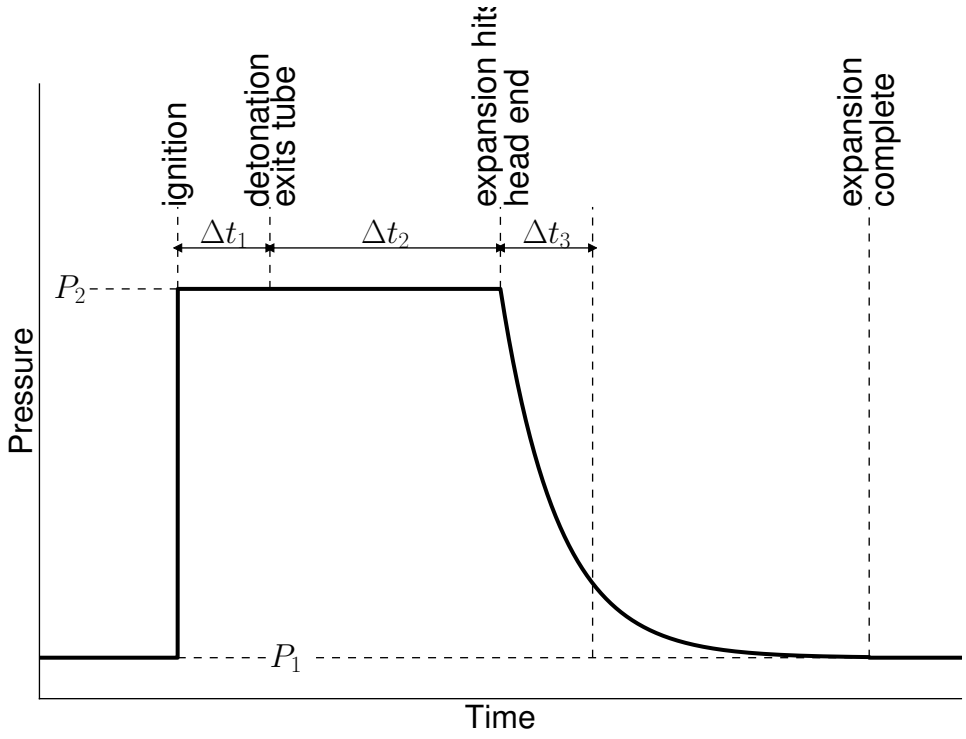

Figure 1.9: *Head end pressure vs time for a single cycle of PDE.*

sure at head end remains constant till the first rarefaction wave hits the head end;this is followed by the blow down which is modeled as self similar process with expansion waves hitting the head end and bringing down head end pressure to the atmospheric values. This was a simple model and in fact simplistic: it over-predicted the experimentally measured specific impulse by 50%.

The model proposed by Wintenberger et al. [1] used the same assumption for Δt_1 where detonation wave travels at constant velocity through out the length of tube. For the second phase, their model considers self similar flow equation with sound velocity behind the detonation as the reference. This equation is solved for appropriate boundary and initial conditions. The phase of motion where expansion wave moves into the static fluid is similar to the Endo-Fujiwar model. The final phase of blow down is modeled empirically in Wintenberger model using information from earlier experiments and numerical simulations.

Endo et al. [2] improved their model by considering interaction of expansion wave

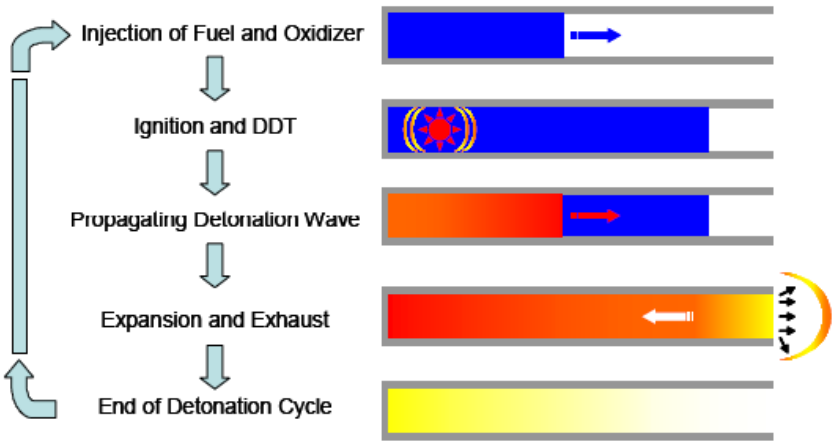

Figure 1.10: *Single cycle of PDE operation.*

with the Taylor wave followed by the motion of expansion wave into the static fluid at the end of Taylor wave.

These models have been extensively tested over the period of time and show good comparisons with the experiments.

1.1.7 PDE Cycle

Figure 1.10 shows the operation cycle of the PDE engine which comprises of the following processes:

- Filling of fuel oxidizer mixture inside the tube.
- Ignition of mixture near the closed end leading to formation of detonation wave and the production of thrust commences from the time retonation wave hits the head end of the tube. Detonation initiation inside the tube is of critical importance in development of PDE.
- Propagation of detonation wave in the tube.
- Detonation wave reaching the open end and expansion wave entering inside the tube.

- Thrust cycle ends once the expansion wave reduces the head end pressure to the ambient.

Till this stage we have examined the basic features of pulse detonation engines. We will now consider a review of the literature relevant to the work presented in this thesis.

1.2 Literature Survey

Many research groups have been working on PDE across the world in Russia, Japan, USA, China and many significant reviews have appeared in literature [25–28]. We divide the literature survey into the following parts

Detonation Initiation related developments is discussed in Section 1.2.1

Choked flames and Quasi Detonation is dealt in Section 1.2.2

Pulse Detonation Engine related developments is first discussed in Section 1.2.3

1.2.1 Initiation

To realize a working PDE, initiation is of critical importance as this process greatly effects the performance of PDE. Transition to detonation can occur by either of the following two techniques:

Direct initiation: In this technique a critical quantity of energy is introduced at a given rate so that the detonation wave is immediately and directly formed.

Deflagration-to-Detonation transition (DDT): In this technique a deflagration wave is generated using conventional methods like spark plug. This wave accelerates through various confinements and finally transits to detonation wave.

The amount of power and energy required for direct initiation is quite large for most of the fuel-air mixtures [29]. This restricts the use of direct initiation for practical engines. Due to this restriction DDT has become the focus of study for initiation of detonation in the PDE.

a) Expermental studies of DDT

The propagation of combustion wave as deflagration or detonation is dependent on various parameters like the ignition energy, confinement and the fuel-air mixture. Under normal conditions, the ignition of these reactants leads mostly to formation of deflagration wave which may go on to transit to detonation wave and this transition is generally referred to as deflagration-to-detonation transition (DDT). This process has been an intense field of research for past century. There are many techniques which were studied in the past for detonation initiation; what follows is a brief survey of these techniques. The experimental work on DDT was started by the pioneering works of Schelekin [30] Oppenheim [31]. Schelekin in the series of experiments laid down the basic criteria for flame acceleration and transition to detonation. From this work he was able to show the effect of turbulence on the acceleration of flame front and the final transition to detonation. The transition was strongly enhanced by the turbulence produced by the interaction of flame with the blockages like spirals and orifice plates and its strong acceleration and final transition. This work was extended by Dorofeev et al. [32] who have given the criteria for the size of obstacle for DDT to take place as $L/\lambda > 7$. In his later works, Dorofeev was able to relate L with the geometrical parameters of the obstacle. This criteria correlates very well with various experimental results with varying parameters [3].

Schauer et al. [33] have used H_2-air mixture for study of thrust produced by PDE's for single and multi cycle operations. They have also studied the effect of using various devices like orifice plates and spirals for enhancing DDT and its effect on the specific impulse.

Sorin et al. [34] have studied the optimization of DDT distance and time for various fuel (H_2,CH_4,C_2H_2,C_3H_8) – air mixtures, using two orifice plates at the head end of the DDT tube. The N_2 dilution was varied for the mixtures to get the same cell size. Their study concluded that L_{DDT} (Length required for transition) is directly proportional to non dimensional activation energy and heat of reaction. They also concluded that time of transition was related to early acceleration of laminar flame in the orifice chamber.

Cooper et al. [35] have studied the effect of increasing the blockage ratio to accelerate DDT on the impulse generated by the PDE and their study concluded that the presence of blockage reduced the PDE impulse up to 25% in cases when transition to detonation took place. It was determined that those regimes in which slow or no

transition to detonation occurred resulted in impulse values 30-50% lower than model predictions. The effect of various extensions on the specific impulse produced by the PDE was also studied. Results of this study showed that irrespective of the shape of attachment the longer attachment produced larger specific impulse. The effect of location of transition point on the specific impulse was studied by [36], [37] for fuel-oxygen mixtures, the general conclusion reached by these authors was that there is no effect of the point of transition on the specific impulse of PDE.

A different methodology was used by Markstein [38] to study the DDT. He studied the shock-flame interaction that leads to development of Ritchmeyer-Meshkov instability and production of turbulence. These processes enhance flame velocity which transits to detonation wave.

The transmission of detonation from smaller to larger tube has also been an important focus of study for long time. Zeldovich et al. [39] proposed the 13λ as the minimum transition tube diameter for detonation to transit from smaller to larger tube. This criterion puts a restriction on using this mechanism for detonation generation. To overcome this restriction, research on using shock diffraction and interaction techniques have been carried out by several researchers. Murray et al. [40] carried out the experimental and numerical simulations to study the importance of initiator tube length and diameter as critical parameters for the successful transmission of detonation from smaller to larger tube. Imploding shock techniques for initiation were also subsequently developed and studied by several authors. Murray et al. [41] were able to reduce the critical diameter for detonation transmission by factor of 2.4 for acetylene-air mixture.

Jackson [42] did extensive study with toroidal initiators using fuel-oxygen mixture with nitrogen dilution for initiation in the toroidal section. He was able to show successful initiation of detonation in main tube with less sensitive mixtures. This method failed to create the detonation wave in propane-air mixture.

Thomas and Jones [43] studied the jet initiation techniques for fuel-oxygen mixture with nitrogen dilution and proposed the formation of localized vorticity pockets leading to the formation of hot spots which transit to detonation wave as the primary mechanism of transition. Lieberman et al. [44] also studied the jet initiation; they conducted experiments with different pressures and varying the nitrogen dilution with propane as the fuel. Their study showed that with jet they were able to detonate the mixtures up to 40% nitrogen dilution beyond which they failed to see the transition to detonation in 75 mm diameter, 1 m long tube. While with obstacles detonation transited for mixture

with 60% nitrogen dilution. The above studies were mostly conducted with fuel-oxygen mixtures with varying N_2/Ar dilution. It can be concluded that for most of the studies the successful detonation was obtained for nitrogen dilution below 40%. The condition for direct initiation with fuel-air mixtures failed in most occasions leading to DDT rather than the direct initiation [45]. The impulse generated by these techniques showed close resemblance with Winthenberger's model [46] for small dilution with nitrogen and reduced to half of the model values as dilution was increased. The comparison of impulse showed that it was higher for the hot jet initiation technique used by Lieberman et al. [44] as compared to that produced by using implosion techniques. In these studies nearly 10% of fuel was used in the early part of chamber to initiate the jet.

b) Numerical study of DDT

The growth in the computational capacity and algorithms over the last few decades led to the beginning of numerical study of DDT. DDT is a very complicated process which requires accurate capturing of large range of scales. The fine scales of chemistry which require mesh sizes of 10-100 μm for capturing the flame. The large scale of the geometry usually having diameter of 1-10 cm and length of 1-2 m. All these scales need to be captured to correctly predict the flame acceleration and transition. This requirement, given the finite computation resources, places a large restriction on the computational domain and making the study of DDT very time consuming. This led to initial studies in this field on multi-step chemistry in one dimension [47] and single step chemistry in two and three dimensions. This work has been put into the correct perspective by Oran and Gamezo [48], in an excellent review paper. Oran and her coworkers have carried an extensive work on DDT [49–51] in which they have simulated various processes leading to transition. Starting with flame shock interaction which gives rise to Ritchmer-Meshkov (RM) instability mechanism. This eventually leads to formation of turbulent flame brush. The accelerating flame brush triggers the formation of hot spots which act like the kernel from which detonation initiates. They were correctly able to predict the detonation in the pre-compressed gas. The transition takes place in presence of temperature gradient mechanism which is in agreement with the work of Zeldovich et al. [39] and the SWACER mechanism of Lee et al. [52]. Kessler et al. [53] has studied the DDT in stoichiometric mixture of Methane-Air using single step chemistry by fitting the parameters in such a way that average flame and detonation properties of mixture

are correctly predicted. They were able to show good comparisons with experiments in tubes with obstacles. The flame acceleration part was correctly predicted for most of the experiments but final points of transition showed much higher velocity for many results and *even predicted DDT for cases where experimentally no transition had occurred*. This anomaly is mostly due to the use of one step chemistry model which fails to predict the detonation failure as has been found by earlier experimental studies [54]. Their numerical studies did not verify the empirical criteria of $D_t/\lambda = 1$ and $L > 7\lambda$ where L is the characteristic length of the geometry. Gamezo et al. [55] studied the effect of blockages on the propagation regimes of detonation wave. They were able to identify three regimes of detonation propagation namely choked regime, quasi detonation and detonation regimes. They were able to correlate this to the blockage spacing. The DDT work carried out by Oran and her work mostly concentrated on single step chemistry which was able to predict several features of DDT process. The study of DDT using multi-step reaction has still not been explored in detail.

In series of papers published by Sivashinsky [18, 56, 57] the importance of hydraulic resistance due to no slip condition at the wall as a critical parameter for DDT transition was highlighted. In their work, a number of one and two dimension simulations were carried out with single specie. His results clearly showed the importance of friction as a central parameter which leads to the heating up of material in the boundary layer which finally triggers the detonation in the boundary layer. This view has also been established in another study carried out by Bychkov et al. [58] in which they developed the model for a flame accelerating in a closed tube with no-slip wall conditions. They were able to show friction as a primary candidate for the acceleration of flame in tubes.

In summary, almost all previous studies have cited no-slip at the wall and turbulence to be the primary mechanisms driving the DDT, though there still remains the question of relative importance on the role of either of the processes.

1.2.2 Choked Flames and Quasi Detonation

The transition process from deflagration to detonation always passes through the intermediate quasi detonation regime. This includes the choked regime of flame propagation and other regimes where detonation travels at sub CJ velocity. These detonations have been extensively reviewed and studied by several authors [15–17, 59]. In this regime the detonation travels as a decoupled shock flame structure. This is known as double

discontinuity structure. The analysis of this structure shows that the combustion wave travels at half Chapman Jouguet velocity in a quasi steady regime. In several experimental works such waves have been observed [11, 34] .

The study of flame acceleration carried out by Lee et al. [13], Peraldi et al. [14] showed the existence of four regimes i.e. quenching, fast flames, quasi detonation and detonation. These regimes were essentially distinguished by the amount of blockage provided to the accelerating flames. For high blockage tubes Lee [11] has suggested that quenching takes place due to mixing time being smaller than chemical time. These studies were performed by placing regular orifice plates along the length of the tube. It was proposed that regular interaction of shocks with the obstacles can sustain the choking regime regularly for indefinite length.

Chao and Lee [60] proposed that the complex shock flame structure can be modeled as a choked deflagration. The presence of obstruction in the path for tubes with larger diameters as compared to the detonation cell sizes can lead to significant velocity deficit due to momentum loss and the detonation propagates as quasi detonation. For tubes with orifice plates larger than 13λ detonation propagates close to CJ values. These results point to some guidelines for the formation of sub CJ regimes but there is no conclusive understanding of the uncertainties involved in the propagation of choked flames in the obstacle laden tubes.

Veser et al. [61] were the first to study the run-up distances to supersonic flames. They studied the minimum run-up distance for the flame acceleration to supersonic combustion regimes in tubes with obstacles both experimentally and numerically. Experiments were conducted in an explosion tube equipped with orifice plate obstacles. Various mixtures of hydrogen were used in the tests. The model assumes that the flame has the shape of a deformed cone, which stretches until the moment when the speed of the flame tip reaches the sound speed with respect to the combustion products. The position of the flame tip at this moment gives an estimate for the run-up distance. Then the flame cone cannot stretch any further and moves down the tube at a quasi-steady velocity. A simple correlation was given relating the various parameters leading to supersonic combustion.

Dorofeev et al. [62] have quantitatively shown that expansion ratio, Zeldovich number and Lewis number for a given air fuel mixture provide the critical information about the acceleration of flames to fast flame modes. By using the H_2-air mixtures with varying dilution they were able to show the critical importance of expansion ratio of mix-

tures. The larger value of expansion ratio makes the flame to act like a fast piston which accelerates the flame at much higher velocity and greatly enhances the transition process.

In an extensive experimental study of H_2-O_2 flame in large tubes, Kuznetsov et al. [63] was able to provide the relation for the acceleration of flame to supersonic speeds for tubes with Blockage Ratio BR<0.1. By fitting the correlations to experimental data they were able to predict the run up distances to within 25% of experimental data.

There is an effect of flame acceleration on the impulse generated. A few earlier experiments [37, 64] have shown that the impulse generated by these quasi detonation regimes is similar to the impulse generated by fully CJ regimes. Roy et al. [26] and Harris et al. [37] have pointed to the fact that it is not conclusive that the specific impulse achieved by using a PDE operating with CJ detonation regime is optimum.

Several studies have concentrated on the geometry of orifice plate and its effect on flame acceleration. The experiments have shown the existence of choked regime even outside of obstacles. In case when obstacle is not of sufficient length as in Sorin et al. [34], it is possible for flame to be accelerated to choked mode and propagate at that velocity. It is to be noted that the presence of excessive obstacles will lead to large momentum loss inside the system.

1.2.3 Pulse Detonation Engines

There are various aspects of this engine which require investigation to optimize its performance, like the design of inlet and outlet, detonation initiation and optimizing the multi cycle operation at system level. The study of PDE is being carried out at various levels, focusing on the various aspects of the engine.

The earliest work on PDE was carried out in Germany by Hoffman [65]. He used the mixture of acetylene/oxygen/water to study the propagation of detonation wave in a tube. Bussing and Pappas [27] have given an excellent survey of earlier work done in this field.

Zeldovich [66] was the first person to study the use of detonation for propulsion. He calculated the efficiency of steady and unsteady device working on the principle of detonation. Though he used approximate values to calculate the efficiency of various systems, his results compare well with those using equilibrium properties and numerical calculations as pointed out by Wintenberger and Shepherd [67]. Zeldovich was first to

estimate the higher efficiency of detonation cycle as compared to Humpry cycle.

Heiser and Pratt [68] have given an exhaustive study of the thermodynamic cyclic analysis of the PDE. The ideal PDE cycle shows performance gains as compared to conventional Brayton cycle for Mach numbers less than 3. At higher Mach numbers, this performance gain is heavily reduced. This study clearly shows that the PDE efficiency is sensitive to the exit design of the engine while it is not much effected by the inlet design.

Wu et al. [69] have carried out the thermodynamic analysis of air breathing PDE with rotary valve and single tube. They have shown the importance of valve close time on the performance of PDE. They were able to show that for multi-cycle operation the PDE performs optimally when operated at 250 Hz. In experimental studies carried out on multi-cycle operation by Schauer et al. [70] using H_2-Air mixtures in tube of 5 cm ID and 92 cm length and operational frequency of 16 and 12 Hz. It was found that the thrust generated at 16 Hz was higher as compared to 12 Hz as expected. The specific impulse generated in case of full fill was 3800 s same for both the tubes while at lower fill fraction it was higher for 16 Hz operation. Authors concluded that the working of PDE are scalable with the frequency of operation. In separate experimental study carried out by [71] with channel of 1.25 cm by 1.9 cm cross section and 20 cm in length. The operating frequency was varied up to 1200 Hz as it was observed that highest specific impulse of 3400 s was obtained at operational frequency of 682 Hz for H_2-Air mixture for $\phi = 0.76$ while for stoichiometric mixture specific impulse of 2950 s was measured. These studies show that high specific impulse close to theoretical values can be achieved in working PDE.

During the past decade there have been several review articles encompassing most aspects of the pulse detonation engines Lam et al. [9], Roy et al. [26], Roy [28], Kailasnath [72]. Kailasnath [72] has summarized the work carried out across US, Canada, Europe and other countries. His paper discusses various aspects of PDE such as Deflagration-to-Detonation Transition (DDT), numerical computations of detonation, performance estimation, enhancement of propulsive performance by partial filling, usage devices such as nozzle, inlets for PDEs, and some applications of PDEs. An overview of the technology of pulse detonation engine is given by Lam et al. [9].

Roy et al. [26] have given a detailed review on the fundamental aspects of PDEs, particularly those related to detonation. The structure of the detonation waves, ignition and initiation of detonation waves, DDT, heterogeneous detonations, impulse obtained

from the detonation tube, and operational constraints of the PDEs have been discussed in detail. This paper also includes a detailed review of the various design concepts proposed for pulse detonation engines such as valve and valveless PDEs, predetonator for inducing detonation in the main tube, stratified charge, etc. for realizing practical PDEs.

Chao et al. [73] have provided a detailed procedure for designing the pulse detonation engine encompassing the various aspects such as specific fuel consumption, limits on the frequency of operation, detonation initiation, liquid fuel handling, drag and flow losses, and the operational envelop of the PDEs. The structural design has also been addressed in this report.

There are also reviews of country wise developments of PDEs by Frolov et al. [74], Hayashi and Fujiwara [75], Qiang et al. [76]. Roy [28] presents an excellent compilation of work, detailing the various aspects of PDE development like DDT, spray detonation, droplet breakup due to impact of shock, dual fuel PDE, laser diagnostics in the study of PDE's, system performance and various other aspects which are relevant to PDE realization. Among various processes of critical importance in developing the working PDE, the formation of detonation wave is of critical importance and the work carried out in this field is discussed in the next section for detonation transmission.

1.3 Summary

The study of previous literature has shown that there is significant understanding about the working of engine using detonation for propulsion. Experimental and theoretical studies on these engines have shown them to give better performance as compared to conventional air breathing engines. Theoretical models have shown [46] PDE's can provide specific impulse of 4200 s under full fill conditions. Experimental studies by Schauer et al. [70] show that these engines provide a specific impulse of approximately 4000 s under full fill condition and can further increase up to 7000 s under partial fill conditions. The acceleration of flames and transmission to DDT have been investigated in earlier studies reviewed by Ciccarelli and Dorofeev [59]. These investigations have not examined the effect of flame acceleration or quasi detonations on the working of PDE. A few earlier studies have shown choked regimes to provide specific impulse magnitude same as in the detonation regime [37, 64] *but these regimes have not been thoroughly investigated for the propulsion applications*. The study of these regimes is

important as they are accompanied with lower pressure as compared to CJ detonation hence are attractive for propulsion applications. Further, most of earlier investigations [59] have concentrated on the symmetrical blockages for the study of DDT. The study of unsymmetrical blockages is not complete and this topic needs further investigation. The numerical studies conducted previously have mostly concentrated on single step chemistry and the use of multistep and multispecie chemistry to study DDT is still in preliminary phase. There are several phases in the process of flame acceleration. Several points of transition between the shock-flame complex have also been found in experiments carried out earlier by Urtiew and Oppenheim [31]. These provide the primary motivation to investigate the flame acceleration and transition to DDT in multidimensional geometry.

Chapter 2

Experiments

As indicated earlier, the review of the previous literature has shown that there have been no detailed studies on the impulse generated by the choked flame. This chapter aims to overcome this inadequacy presenting results of specifically designed experiments. The details of the experimental setup, procedure and results are outlined. First section deals with partial filling experiments that lead to large enhancement in the specific impulse produced by the PDE. Comparison is made between different lengths of tube for the partial-fill cases. It is known that as in case of full-fill tubes where L/D $\approx$ 18-20 gives a maximum impulse while no such condition exists for the case of partial filling. The second part of experiments is regarding the transmission of detonation from smaller to larger tubes and the study of impulse generated by choked regime. Third section deals with experiments carried out in transparent tube and compares the impulse produced by the choked flame and detonation. Last section of this chapter provides the theoretical basis for impulse generated by choked flame. The list of various experimental studies and details are presented in Table **??**

Experiment Sheet				
Experiment/Study	L (m)	ID (mm)	ϕ	BR (%)
Partial Fill	1	42	1.0	42
	2	42	1.0	42
Extension	1	42	1.0	42
	2	42	1.0	42
Extension/Acceleration	1	25	1.0	24-36
Transparent tube	1.5	32	1.0	24-44

Table 2.1: *L=Length, ID=Internal Diameter, ϕ=Equivalance ratio, BR=Blockage Ratio.*

2.1 Experimental studies on partially filled tubes

The first set of experiments deal with study of partial filling. Experiments with partial filing have been conducted previously by various groups. Schauer et al. [70] studied the effects of the pressure relaxation rate upon thrust experimentally by adjusting the amount of detonable mixture in the tube while maintaining the same detonation tube length and significant performance gains were observed. Falempin et al. [77] and Cooper and Shepherd [78] used a ballistic pendulum method to measure single-cycle impulse of Ethylene-Oxygen mixtures in detonation tubes with attached extensions having a constant cylindrical cross section and also with extensions of varying dimensions.

Li and Kailasanath [79] studied the effect of varying the length filled with the detonable mixture in constant cross section tubes. They applied an exponential curve fit to the data relating fuel based specific impulse to the tube length filled with detonable mixture. However no significant study in the past were aimed at measuring the fuel-specific impulse, nor the optimal partial fill as a function of the length of the detonation tube. These parameters are of paramount importance in the realization of a practical PDE, and knowing that partial fills give better fuel-specific impulse makes the need for such a study even more strong. This was the motivation for the following set of experiments.

Figure 2.1 shows schematics of partially filled PDE tube, in which detonable mixture and air share an interface. When the tube is partially filled, the additional tube volume behaves like a straight nozzle delaying the formation of the expansion wave at the exit that propagates back to the closed end. The leading shock wave produced by a traveling detonation can be used to compress a non-combustible mixture. Resulting compressed flow alters the blow down process which is found to lead to higher specific impulse.

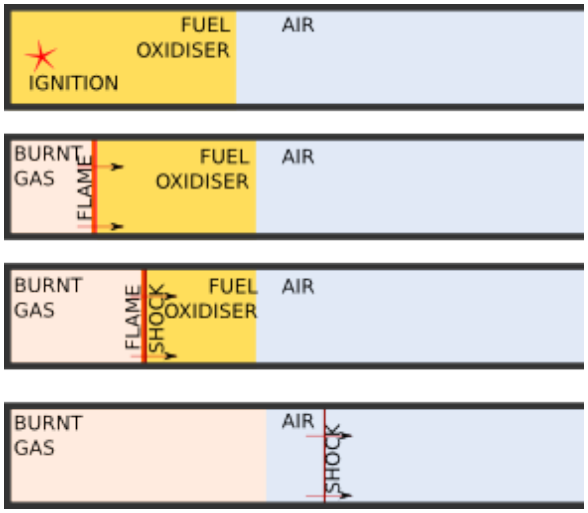

Figure 2.1: *Single cycle working of PDE under partial fill condition.*

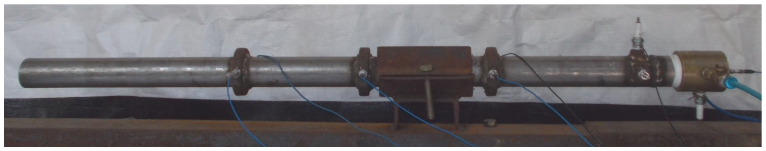

Figure 2.2: *Detonation tube with various attachments. Spark plug, pressure transducers and fuel air inlet.*

2.1.1 Details of setup and Instrumentation

The basic elements of the setup are shown in Fig 2.3.

Detonation Tube and Accessories: Two different detonation tubes were used for the experiments with lengths 2 m and 1 m long respectively. They had the same 42 mm internal diameter (ID). One end of the tube was open to atmosphere and the other end was closed with a threaded brass cap. The brass cap had provision for mounting spark plug, fuel air mixture inlet and pressure transducer (PT). Provision for mounting pressure transducer was also made at distances of 1.22 m and 1.53 m, these were used to measure the detonation pressure and velocity on the 2 m tube. For 1 m tube the transducers were mounted at 50 cm and 70 cm from the head end. The 1 m detonation tube is shown in Fig 2.2.

In this experiment combination of Schelkin spiral and orifice plate was used in order to enhance DDT. From the earlier study using various turbulence enhancement devices

it was found out that this particular configuration gave highest specific impulse [80].

Pressure Data Acquisition: This system includes the following components

The pressure transducers are piezoelectric pressure transducers of PCB make model **PCB-102B04**. They have natural frequency higher than 500 kHz and measuring range from 0.07 bar to 69 bar and 1 μs rise time. Detailed specifications are available at [81].

The signal conditioner PCB make and model number **PCB-482C05** to provide the excitation voltage and also for conditioning the measured signal. Detailed specifications are available at [82].

The digital oscilloscope Oscilloscope used in experiments was of Agilent make, model number **DSO5054A** which samples at 500 MHz, 4 Channels. Detailed specifications are available at [83]

Figure 2.4 shows the oscilloscope connected to the signal conditioner. For all experiments, the data was sampled at 5 Ms/s.

2.1.2 Experimental Procedure

Fill fraction is defined as the fuel/air mixture length (fill length) to tube length. The amount of H_2-Air mixture of equivalence ratio 1 is metered with the suitable rota meters. This metered gas gets mixed in the gas mixer and is passed into the detonation tube. The mixture fraction of gases present in the mixture was independently verified using the Mahek Gas Analyzer which accurately detects the percentage of H_2 and O_2 in the mixture. The solenoid valve was closed after tube was filled with the mixture for the duration corresponding to the fill condition. This was followed by the triggering of spark which simultaneously triggers the oscilloscope which starts the acquisition of data from the pressure transducers. The time interval between the closure of the solenoid valve and spark was $\approx 5[s]$. After the detonation is completed, the detonation tube is purged with the air. All experiments have been conducted at atmospheric pressure which in the present case is 0.9 bar (the ambient pressure at the laboratory, IISc, Bangalore). For these conditions the head end pressure calculated using Eqn 1.11 gives head end pressure of 4.1 bar.

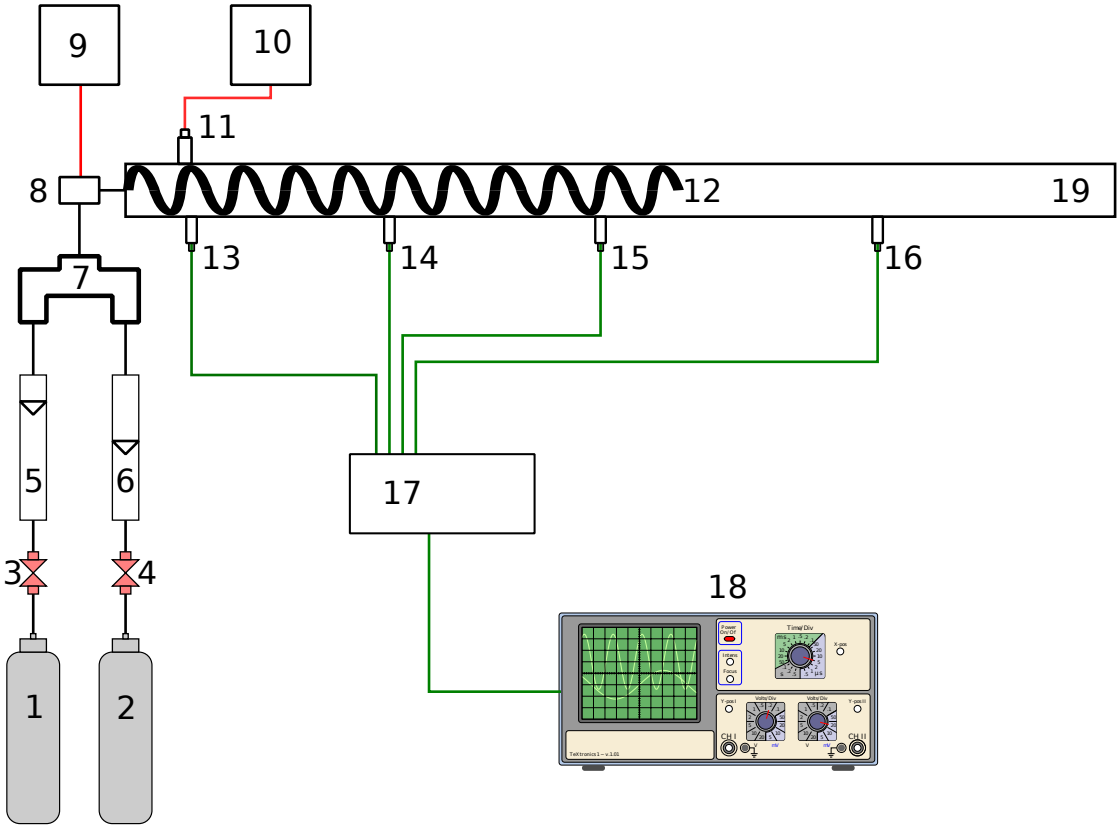

Label	Instrument	Label	Instrument
1	Compressed Air	**9**	Solenoid Controller
2	Hydrogen Cylinder	**10**	Spark Controller
3	Air Control Valve	**11**	Spark Plug
4	Hydrogen Control Valve	**12**	Spiral
5	Air Rotameter	**13-16**	Pressure Transducers
6	Hydrogen Rotameter	**17**	Signal Conditioner
7	Mixing Chamber	**18**	Digital Oscilloscope
8	Solenoid Valve	**19**	Detonation Tube

Figure 2.3: *Schematic Details of Experimental Setup.*

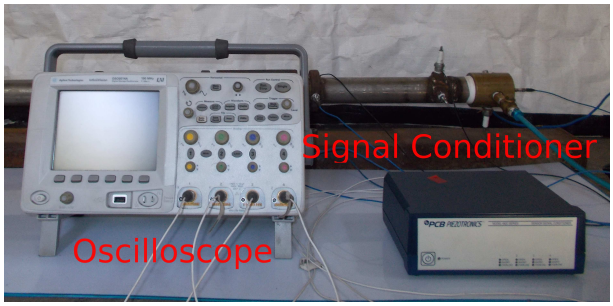

Figure 2.4: *Oscilloscope connected to signal conditioner.*

2.1.3 Results and discussion

These sequence of experiments throw light on many aspects of running PDEs with partial fill. We have analyzed the detonations with the following viewpoints

a) Closed end pressure measurements which show the impulse generating plateau.

b) Impulse measurement and analysis of the impulse generated.

c) Specific impulse which brings out the trends in the fuel-specific impulse with partial fills.

a) Closed end Pressure

In these experiments, the closed end pressure was measured for different fill fractions [0.15-1.0]. Figure 2.5 shows the trends in the closed end pressure for three different partially filled cases. At low fill fractions, the plateau pressure length becomes smaller, while the blow down to atmospheric pressure is slower. This occurs due to the altered expansion regime because of presence of inert gas at the end of fuel-oxidizer mixture.

b) Impulse

Impulse in this experiment is obtained by integrating closed end pressure for different fill fractions. Figure 2.6 shows the variation of single-cycle impulse with fill fraction. This figure shows the results for two different lengths. Three trials were conducted for each point and an maximum variation of 10% was found in the calculated results. For

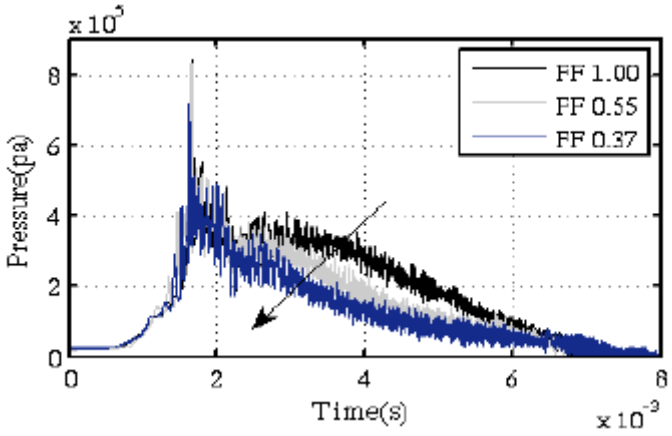

Figure 2.5: *Pressure history at head end for various fill fraction (FF) cases for 2m tube.*

lower fill fractions, the effect of end dilution leads to larger variation in flame acceleration. Flame acceleration has direct effect on the pressure obtained at the thrust wall. Single-cycle impulse increases as fill fraction increases until the maximum impulse is reached at the fill fraction of unity. Impulse and specific impulse for this mixture were compared with the correlations given by Li and Kailasanath [79], Gurney's model mentioned in [78] and Cooper and Shepherd [78]. Expressions used for calculating specific impulse from these correlations are given below:-

- Cooper

$$\frac{I_{sp}}{I_{sp0}} = 0.794 + 0.206\frac{V_0}{V} \tag{2.1}$$

$$0.074 < V/V_0 \leq 1 \tag{2.2}$$

- Kailashnath

$$\frac{I_{sp}}{I_{sp0}} = a - \frac{a-1}{e^{(V_0/V-1)/8}} \tag{2.3}$$

$$a = 3.2 - 3.5 \tag{2.4}$$

- Gruney

$$\frac{I_{sp}}{I_{sp0}} = \frac{2}{\sqrt{3}} \frac{N/C + 1/2}{\sqrt{N/C + 1/3}} \tag{2.5}$$

$$N/C = \left(\frac{V_0}{V} - 1\right)\left(\frac{\rho_a}{\rho_1}\right) \tag{2.6}$$

Where:-

- ρ_a - Density of air
- ρ_1- Density of air/fuel mixture
- N - Mass of air
- C - Mass of air/fuel mixture
- V_0-Volume of tube
- V - Fill volume
- I_{sp}- Specific impulse for partial filling
- I_{sp0}- Specific impulse for full filling

The correlations given by Kailasanath and Cooper have been empirically developed from data obtained by numerical analysis and experiments, while that of Gurney is a theoretical model. Gruney's model predicts the velocity and impulse of a body taking various physical parameters like mass of charge and the temper mass (inert gas) into consideration.

The comparison of our results, shown in Fig 2.6, with these correlations show a better matching for higher fill fraction with those of Gurney's model. At lower fill fraction Gurney model over predicts the impulse. This is because it does not take into consideration the gas dynamic effects which become predominantly important at lower fill fractions. This is confirmed by the fact that at lower fill fractions, our results are closer to other two correlations.

c) Specific Impulse

Figure 2.7 shows the variation of single-cycle specific impulse with fill fraction and fill length. The results are compared with experimental results of Schauer et al. [70]. It is observed that in case of comparing specific impulse based on fill fraction, the results of Schauer show higher value compared to the current experiments for both the tubes as those experiments were carried out at L/D ratio of 18 which gives optimum specific impulse for full-fill condition. But the comparison based on fill length clearly shows

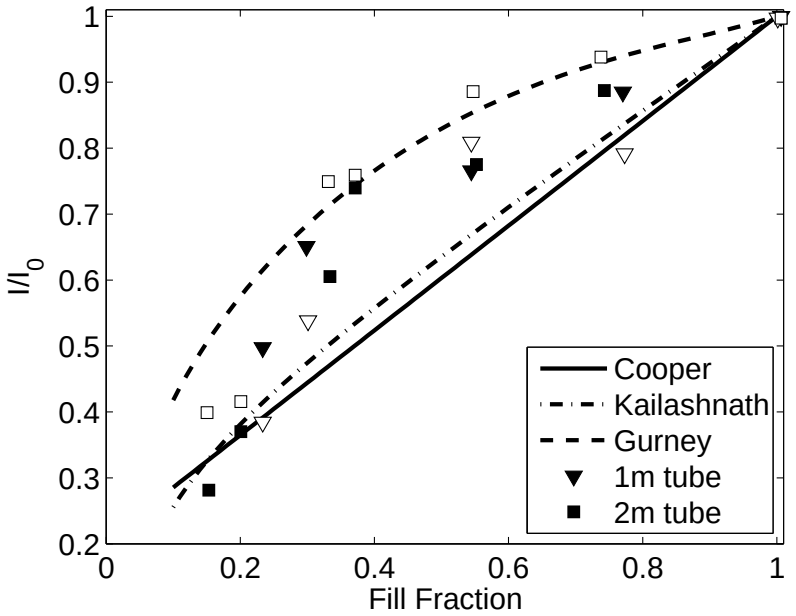

Figure 2.6: *Comparison of impulse with fill fraction for different impulse models; symbols refer to present experiments for two different trials.*

that higher specific impulse is obtained using 2 m tube. From this we can infer that the condition for optimum L/D for full-fill case cannot be extended to partial-fill cases. Fuel based specific impulse declines with fill fraction. It is observed that specific impulse increases as the detonable mixture mass decreases indicating a specific performance gain even though the total impulse decreases. The maximum fuel based specific impulse of 8500 s was obtained for the fill length of 0.25 m. When fill length is less than 0.25 m, the specific impulse drastically decreases. It is observed that even with the fill length of 0.25 m the increase in specific impulse takes place. With tube diameter of 42 mm, 0.5 m is the approximate distance required for transition. This points to the fact that initially accelerated flame is critical for the attainment of higher specific impulse and this point will be further elaborated in the later sections of the thesis.

Specific impulse for the H_2-air mixture was compared with correlation of Gurney, Cooper and Kailasanath in Fig 2.8. The trends in this case are also similar to that of impulse, except that the results show the specific impulse values of 2 m tube to be lower than 1m for full fill. This is due to the fact that the L/D for 1m is close to optimum value of 18 given by Kasahara et al. [84].

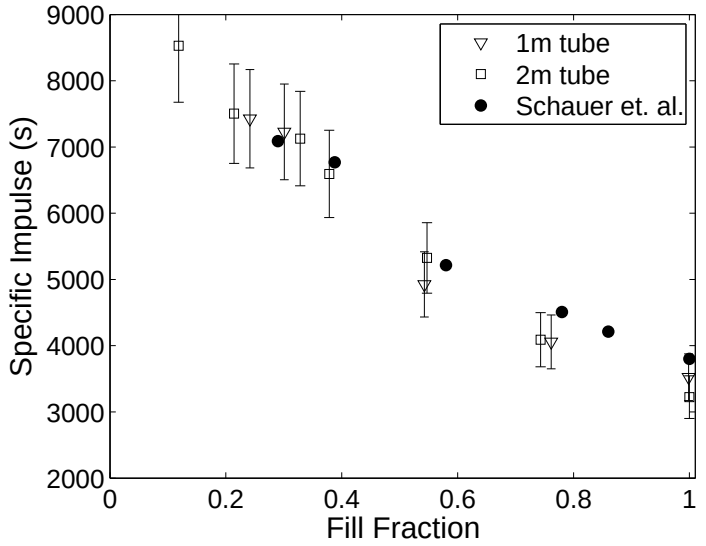

(a)

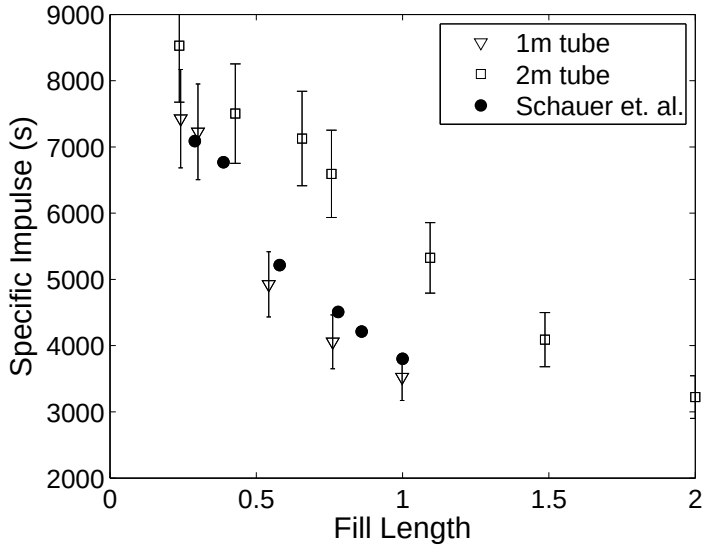

(b)

Figure 2.7: *Variation of specific impulse with the fill fraction (ff) and fill length (fl). Increase in specific impulse with length for the same fill length is clearly seen when comparing with fill length. Values collapse to similar curves when plotted against fill fraction.*

The L/D ratio of a 1 m tube is 24, and that of a 2 m tube is 48. It is seen that the

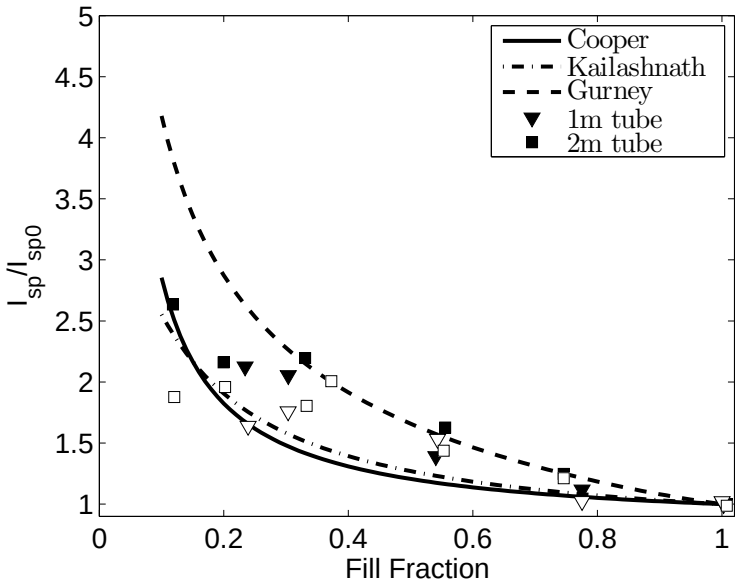

Figure 2.8: *Comparison of the experimental specific impulse data with the results of models on partial-fill condition; symbols are the present experiments, two trials.*

specific impulse of the former is greater than the latter, this is due to the fact that heat loss for larger L/D tube is more as compared to smaller one. The variation of specific impulse with L/D was highlighted by the experimental study of Kasahara et al. [84]. They obtained L/D = 18 as the optimum condition for maximizing specific impulse. This optimal value was experimentally verified by Schauer et al. [33] who obtained a specific impulse of 3800 s using aluminum tube at L/D ratio of 18 which is close to theoretical estimates of $\approx 4200s$.

In the case of partial filling, there are two competing effects which are given below.

Heat loss which decreases the specific impulse with increase in the length of tube, and

Partial filling which causes increase in specific impulse with tube length

The air in case of partial-fill attains a peak temperature of $\approx 600K$ after the passage of shock. In the case of detonation, the fluid behind the wave is at a temperature of $\approx 2500K$. Because of this the effect of heat loss has diminishing effect with increase in the length of tube. Hence the effect of partial-fill in increasing the specific impulse is felt even for very small fill fractions and no saturation can be seen for lower fill fractions. This aspect is also noticed in Figure 2.7 which shows that in the lower fill fraction the

specific impulse calculated using the longer tube is higher compared to the shorter one. The optimization of tube length for maximum specific impulse for partial-fill case shows lesser sensitivity to heat loss.

2.1.4 Brief Summary

In the above section single cycle PDE operation was analyzed. The effect of fill fraction on closed end pressure is determined. Plateau pressure and length increase with fill fraction. Impulse per cycle increases with the fill fraction. The maximum fuel based specific impulse was approximately 7800 s at fill length of 0.25 m. When the fill length was greater than 0.25 m, the specific impulse increases as the partial fill fraction decreases. For fill length less than 0.25 m, the specific impulse decreases sharply. This decrease is due to the short fill length of fuel-air mixture that is not enough for the acceleration of the flame. The comparison of specific impulse obtained for two different lengths of PDE has shown that at partial fill condition, the longer tube performs better. These results also point to the fact that for the smaller fill fractions the length of fill fraction is less than the length required for DDT. Comparison with earlier results of Schauer et al. [33] also points to the same fact. This clearly shows that strongly accelerating flames can also lead to the production of high specific impulse similar to or better than PDE cycle. The results show that partial filling of PDE has significant advantages obtained by limited flame acceleration for lower fill fraction.

2.2 Study of flame acceleration and its effect on Specific impulse

2.2.1 Introduction

To achieve DDT, minimizing both the distance and magnitude of the obstruction are considered important in detonation research. The DDT starts with the formation of flame kernel which develops into flame. As flame propagates from the closed to the open end, it gets elongated and wrinkled leading to its acceleration. As the pressure builds up, it pushes the fluid in front of it, whose motion causes the formation of a boundary layer. As the flame continues to move the flow ahead of it becomes turbulent. Interaction with turbulent boundary layer which is formed ahead of the flame, further accelerates the flame leading to transition [31]. The distance traveled by flame while it accelerates to form detonation wave L_{DDT} is strongly dependent on the geometry, chemical and physical properties of fuel-oxidizer mixture. This length-to-diameter ratio is about 10 – 15 for most of fuel-oxygen mixtures and much larger for fuel-air mixtures. A number of studies have been carried out on DDT in tubes of varying diameters, and it has been generally found that L_{DDT} scales with the diameter of the tube. Larger the tube diameter, longer is the length taken for transition to take place. For practical applications, the smaller this distance is, the more advantageous it is. For this purpose, various geometric obstructions like spirals and orifice plates have been used for reduction of L_{DDT}. The pre-detonator is a device having smaller diameter as compared to the main detonation tube and is filled with fuel-oxygen mixture to create the detonation wave in smaller length and then transmit it to larger tubes. The tubes of smaller diameter will hold very small amount of fuel-oxidizer mixture and if the flame is able to accelerate and undergo transition in this section then the DDT can be achieved effectively with the consumption of very small amount of additional fuel.

The next section gives the overview of experimental setup and procedure, followed by results where the study conducted on various diameters is discussed. This is followed by a brief theoretical overview of choked flames followed by conclusions.

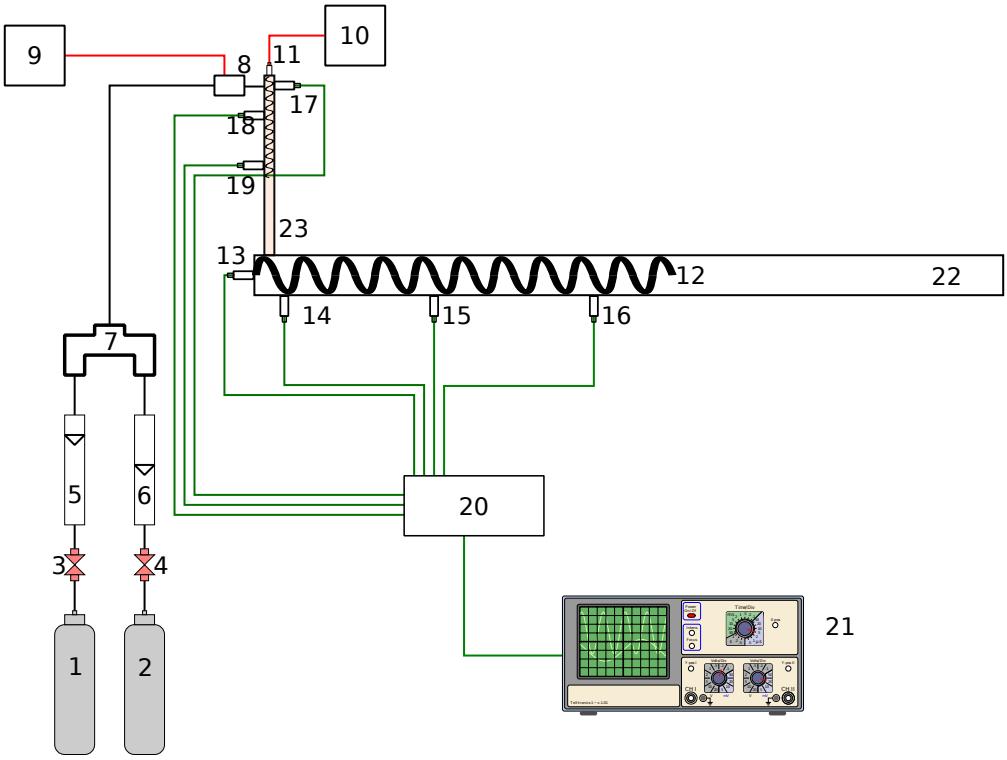

Label	Instrument	Label	Instrument
1	Compressed Air		
2	Hydrogen Cylinder	**10**	Spark Controller
3	Air Control Valve	**11**	Spark Plug
4	Hydrogen Control Valve	**12**	Spiral
5	Air Rotameter	**13-19**	Pressure Transducers
6	Hydrogen Rotameter	**20**	Signal Conditioner
7	Mixing Chamber	**21**	Digital Oscilloscope
8	Solenoid Valve	**22**	Detonation Tube
9	Solenoid Controller	**23**	Extension Tube with Spiral

Figure 2.9: *Schematic Details of Experimental Setup for transmission.*

2.2.2 The Experimental Setup

The experimental setup used is shown in Fig 2.9. The experiment was performed with three tubes, two stainless steel tubes of diameter 42 mm and lengths 1 m and 2 m, and one tube of 25 mm diameter and length 1 m have been used. The tubes have provision for attaching a small diameter tube at the closed end. The 42 mm tube has pressure transducers mounted one at the head end and others at 50 cm and 80 cm from the head end. In the case of 25 mm ID tube the pressure transducers are mounted on the head end and 30 cm, 50 cm and 70 cm from the head end. In this entire study, the reactive mixture is ignited using a conventional automotive spark circuit which provides a spark energy of approximately 25 mJ. This is much lower than the direct initiation energy of detonation. The spark plug and the fuel-air filling attachment are also mounted at the head end of the small tube. The volume of this tube is 1.4 % of the larger tube (of 1 m length). *Hence, it requires very small amount of mixture for initial flame acceleration*. The extension pipe can be attached at the head end of main tube either along the length or perpendicular to it. In both the cases, the smaller tube was aligned along the axis of the larger tube and no artificial swirl is induced. Spirals are used in both tubes to enhance the flame propagation velocity. The use of spiral for the production of detonation wave was first conceived by Schelkin and later this methodology has been extensively used by many groups for studying the transition. It was observed for equivalence ratio of 1 for H_2-air mixture a Schelkin spiral of 42% blockage ratio and 50 cm length was sufficient for detonation transition. This arrangement was found to be insufficient to produce detonation in case of leaner mixtures. For these mixtures, spiral is fitted with additional perforated plate of 58% BR which enhances the DDT as has been studied earlier [85]. Detonation failed to occur in case spiral is removed from either of the tubes.

2.2.3 Experimental Procedure

The experiments are carried out by filling metered quantity of H_2-air mixture of 1 equivalence ratio in the tubes for different time intervals depending on the required fill fraction. The data on pressures at various locations along the length of larger tube are recorded by an oscilloscope and used for further analysis. Impulse and specific impulse are calculated by integrating the pressure at the head end of the main tube. All experiments were repeated at least 3-5 times. In all the cases it was found that due to uncertainty in fill times and slight variation in equivalence ratio, the maximum error

Figure 2.10: *Transmission tube of 5 mm diameter.*

encountered is less than 10% for various trials conducted. The error is highest when the fill fraction is small.

2.2.4 Results and Discussion

a) Propagation of detonation wave in 5 mm tube

The experiments were conducted on the 5 mm dia tube and four pressure transducers were placed at 21, 30, 38 and 46 cm from the closed end of the tube. Figure 2.10 shows the tube with provision for attachment of pressure transducers. The head end of tube has provision of attaching a brass cap on which spark plug and fuel air inlets are mounted.

The fuel-air mixture was ignited at the closed end. The experiments were performed using two spirals of wire thickness of 0.5 mm (Sp1) and 1 mm (Sp2) and both of length 15 cm. Figure 2.11 shows the pressure profile measured in the two cases. With 0.5 mm spiral the flame has already transmitted to quasi-detonation before reaching the first transducer. Here the detonation seems to accelerate on reaching the second transducer but decelerates to decoupled shock and combination wave before reaching the third transducer. With 1 mm spiral the flame is decelerated and reaches the quasi-detonation only at the fourth transducer. The shock velocity was measured in all the cases using the frontal shock where pressure exceeds 3 bar. Five trials were conducted for each configuration and maximum differences of 5 % were noted. This gives a consistent basis for comparison, except for the case when the flame is in the slow acceleration phase and the pressure wave ahead of the flame is more of a compression wave and not a shock wave. In case of smaller diameter tubes, detonation propagates at much lower velocity as compared to CJ detonation. It may propagate as a galloping wave or a decoupled shock flame complex. From the comparison of two cases it is clear that the transition is enhanced for the spiral of 0.5 mm compared to the other two cases. For further studies of transmission Sp1 was used. With Sp1, the propagation of combustion wave was studied with varying equivalence ratio. Table:2.2 shows the variation of shock velocity with

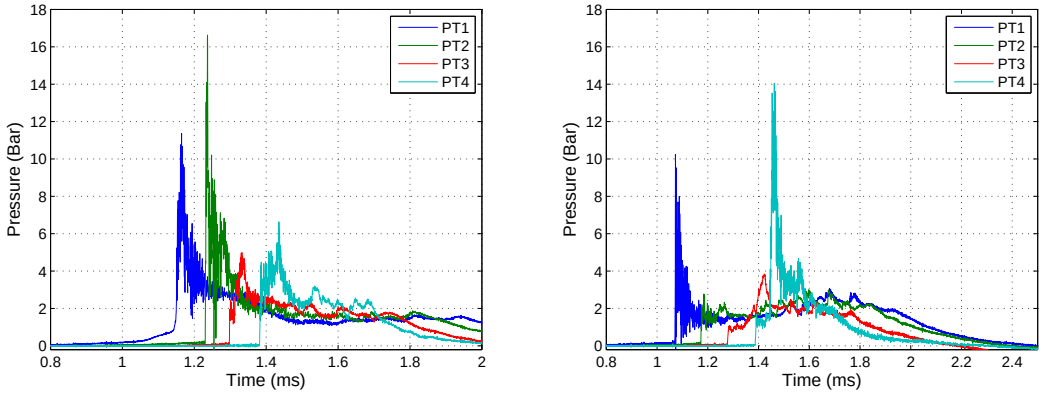

(a) Sp1 **(b)** Sp2

Figure 2.11: *Pressure time data obtained at 4 locations for ϕ =1.*

ϕ	1.1	1.0	0.9	0.8
V1	1100	1000	1000	870
V2	850	800	800	700
V3	900	950	800	600

Table 2.2: *Variation of front shock velocities V1,V2 and V3 (m/s) between transducers with ϕ=Eq Ratio.*

equivalence ratio between the pressure transducers. In all the cases the shock velocity was close to the choked condition for H_2-air mixtures.

b) Transmission of accelerating fast flame normal to the main tube

The transmission of quasi-detonation was studied by placing the smaller tube perpendicular and parallel to the main detonation tube. The axis of transmission was in the same plane for all the studies. The diameter of extension tube is almost half of the cell size of approximately 1 cm for stoichiometric H_2-air mixture, this forces the flame to propagate as a quasi detonation wave or as decoupled shock flame complex. While transmitting out to the larger tube the shock is mostly decoupled from the flame and diffracts into the larger tube with flame following behind it.

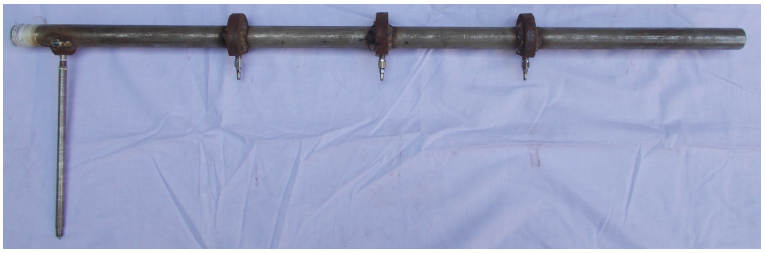

Figure 2.12: *5 mm tube attached perpendicular to the 42 mm tube.*

2.3 Experiments on 42 mm Diameter tube

Figure 2.12 shows the 5 mm tube attached perpendicular to the main tube. Same experiments are repeated with and without the extension tube. Figure 2.13 shows the pressure time data measured in the central locations of the larger tube (at 50 and 70 cm from the head end) for the two cases.

The velocity of shock propagation with attachment is approximately 860 m/s while that without attachment is 1700 m/s. As measurements are made within 1 m the detonation would not have settled into the CJ regime for the case without attachment but the shock pressure of 45 bars at P2 transducer clearly shows that the detonation wave successfully propagates inside the tube. The large pressure spike at P2 is possibly due to proximity of this transducer to the end of the spiral. Also it is well known that H_2-air mixtures tend to travel in quasi regimes before settling down to final CJ value [34]. The comparison of pressure profile clearly shows that the transition to stable detonation has not occurred for the case when detonation is transmitted from smaller to the larger tube. The pressure measurement at transducer P3 is less than 10 bar. The velocity of propagation of this wave is almost half of the propagation speed of CJ detonation, which is close to the choked regime [11]. The wave travels as a decoupled shock wave followed by the combustion front. These waves are metastable and can propagate for long lengths of the order of 100 tube diameters before either decaying to subsonic wave or accelerating to CJ detonation wave [11]. In the present case it is clear that the wave is failing to propagate as detonation wave as it moves along the length of tube. The head end pressures for 1 m and 2 m tubes filled with reactive mixture for a length of 1 m are shown in Fig 2.14 (fill fraction = 1 for 1 m long tube and 0.5 for 2 m tube) and are compared with the case when detonation is initiated in the main tube (1 m) without attachment. In

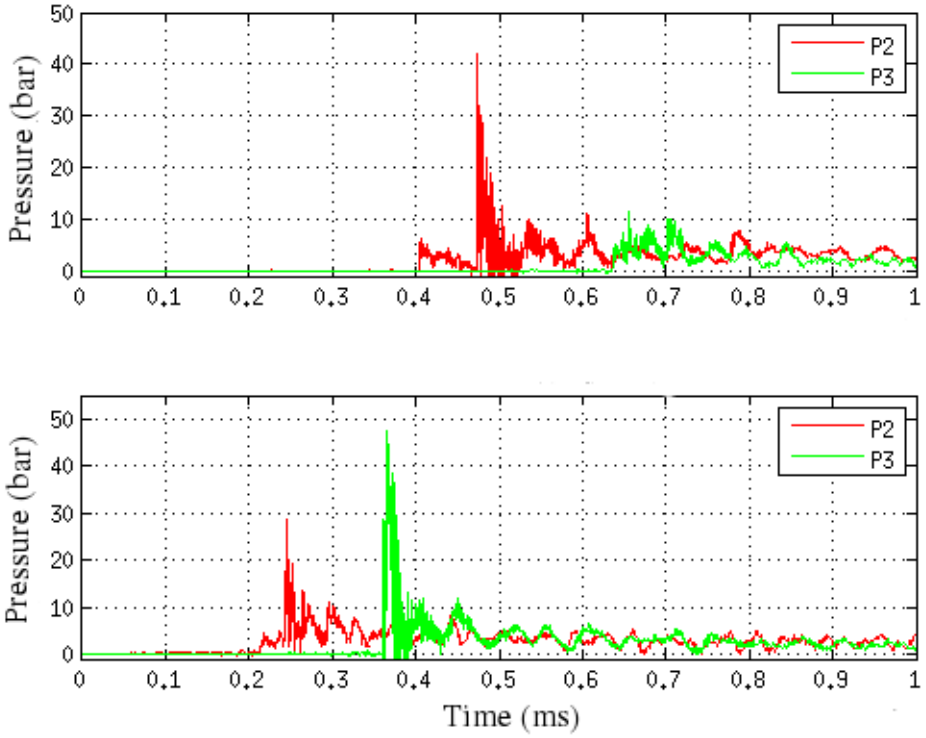

Figure 2.13: *Plots showing the pressure measurements at 50 cm and 70 cm form closed end, with attachment and without attachment.*

case of tubes with attachment, there is an initial pressure spike at the head end which may be due to the decoupled shock wave moving out of the smaller tube ahead of the flame. The pressure at the head end increases to reach a constant mean pressure and then expands to atmospheric pressure. In the normal case (tube without attachment), it takes larger time to attain the constant pressure condition and also this condition is retained for much shorter duration. In this study, the fuel specific impulse calculated using the pressure data from the head end transducer is discussed here; this gives a good relative comparison between different transition methods and modes of propagation of detonation wave. This comparison is pertinent as most of the theoretical models [1, 2] use the single cycle static condition as the ideal state. Specific impulse for the given mixture is a constant value, and so, it forms a consistent basis for comparison of various acceleration mechanisms. Figure 2.15 compares the specific impulse obtained with 1

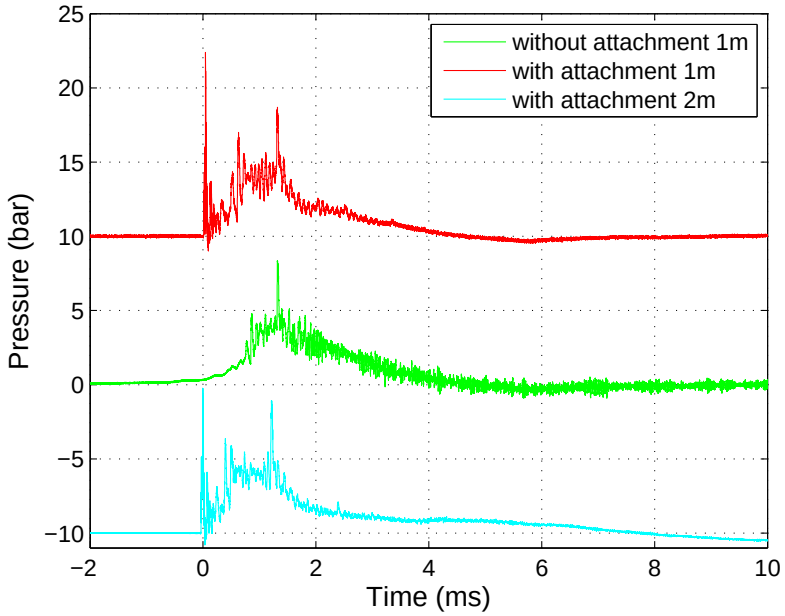

Figure 2.14: *Comparison of pressure profile at head end for same fill length of 1 m. Datum pressure is altered for clear comparison.*

m and 2 m tubes with and without attachment at various fill lengths. Specific impulse obtained with attachment is larger than without attachment. In all these experiments, either with or without attachment, the fill time was kept same. At low fill lengths, specific impulse obtained using tubes with attachment are clearly larger than those without attachment. The reason for this is that at the higher initial velocity, the choked regime would be achieved in relatively short time before transiting to detonation. The attainment of choked regime has been proven to be essential before transition as has been proposed earlier by Sorin et al. [34]. Figure 2.16 shows the clear difference between the head end pressure with and without attachment. The attainment of plateau pressure occurs in much shorter time with attachment. These experiments were repeated with 2 m tube and results were similar, except that at larger fill lengths, difference reduces and at fill lengths greater than 1 m, tube with attachment shows lower specific impulse compared to tube without attachment. In order to examine this behaviour, head end pressures obtained in completely filled 2 m tube with and without attachment are compared in Fig 2.17. This figure shows that the duration of constant pressure and the tail

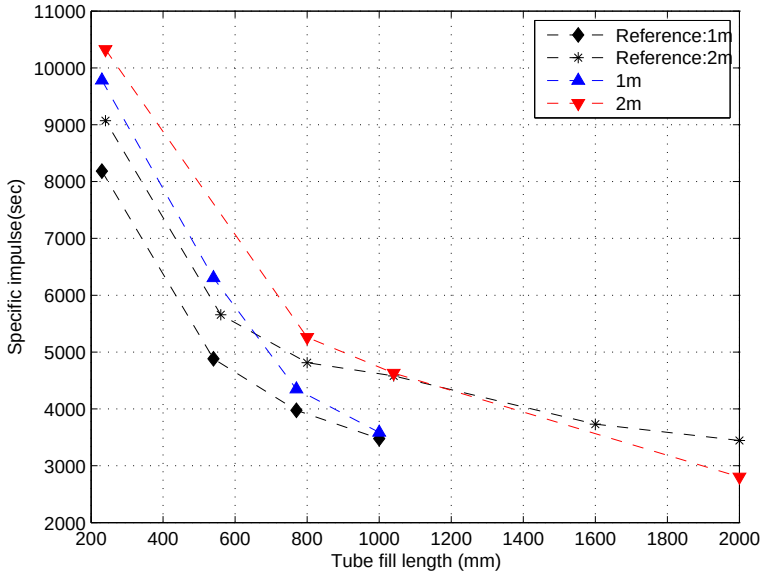

Figure 2.15: *Specific impulse obtained in 1 m and 2 m tubes with and without attachment at various fill lengths.*

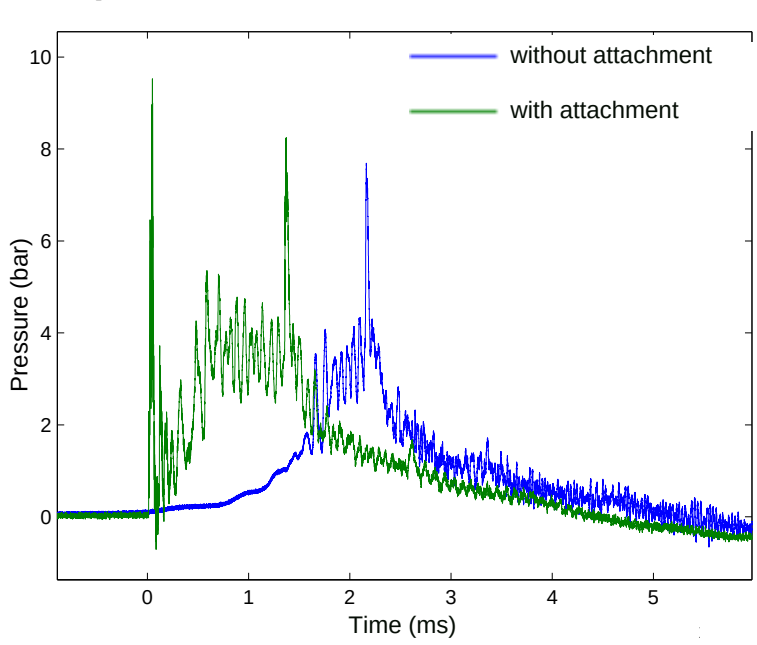

Figure 2.16: *Comparison of head end pressures of 1 m tube with 0.5 fill fraction, with and without small tube attachment.*

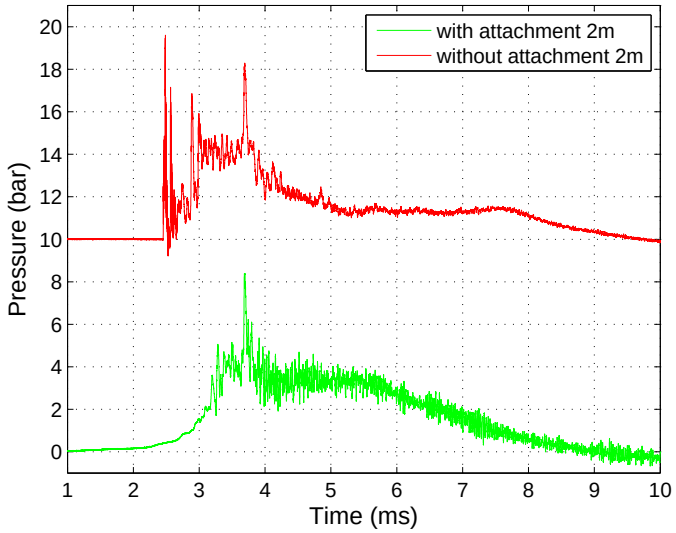

Figure 2.17: *Head end pressure obtained in completely filled 2 m tube without and with extension tube. Datum pressure is altered for clear comparison.*

off are much larger in case of the tube without attachment. The sharp cut off of the head end pressure in the case of tube with attachment indicates the failure of combustion wave at length greater than 1.2 m approximately.

2.3.1 Extension tube length variation

Figure 2.18 shows the trials conducted with the variation of extension tube length. These results show that in case of tube of length of 15 cm, specific impulse decreases for fuel fill fraction of 0.25. From these results, it can be inferred that the length of 25 cm is sufficient for obtaining successful transmission. In case of 2 m long tube, it was observed that in case of wave transmission the detonation which had failed after 1.2 m length got reignited downstream at approximately 1.7 cm from the closed end.

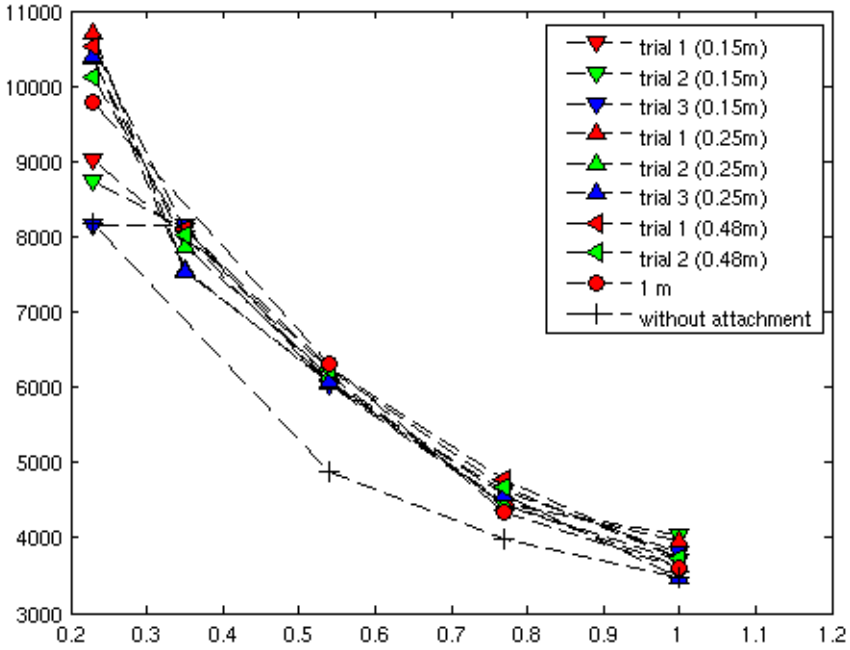

Figure 2.18: *Specific impulse vs fill fraction for different lengths of extension tubes.*

2.3.2 Study of detonation cell structure obtained

To further analyze the difference between the wave structure in case of initiation of detonation inside the tube and using the extension tube, the soot foil methodology was used. Aluminum sheets were coated with soot using kerosene lamp and were inserted inside the tube. The profiles obtained for the two cases are shown in Fig **??**. Comparison of the

soot file structure obtained here clearly shows that in case of transmission, detonation travels as a decoupled shock followed by the deflagration wave, leaving no cell structure. In case of ignition inside the main tube, cell structures are clearly visible. This result further corroborates the inferences made in the earlier section based on measured pressure profiles. The experiments carried out with extension tube leads to formation of decoupled shock and flame structure which fails as it moves along the tube.

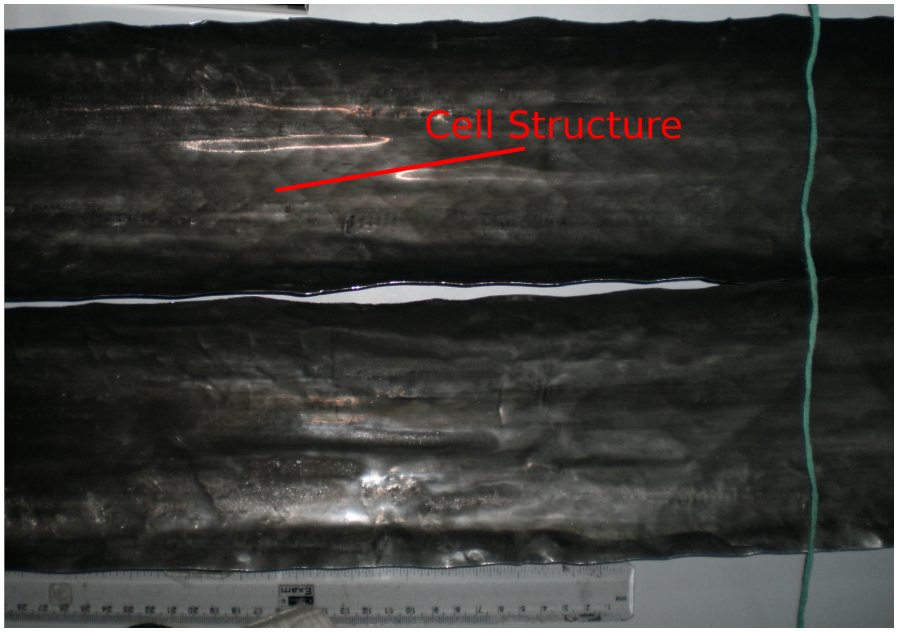

Figure 2.19: *Closed end*

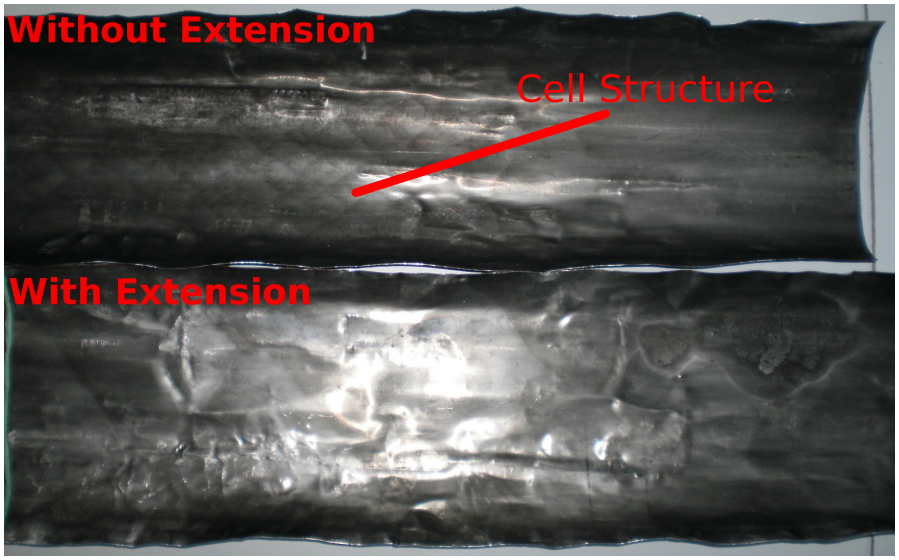

Figure 2.19: *Open end*

Comparison of soot foil records. Upper foil is the case when fuel-air mixture is ignited inside the tube while lower one is with ignition inside the extension tube. The upper foil clearly shows the formation of detonation cell profile while such a record is missing in the lower foil.

2.4 Experiments with 25 mm Diameter tube

SNo	Pitch	Length	Wire thickness
S0	13	300	2
S1	13	600	2
S2	25	600	2
S3	25	600	2.5
S4	25	600	1.5

Table 2.3: *The spirals used in the experiments (dimensions in mm).*

In case of 25 mm diameter tube, Shelikin spirals of various lengths, thickness and pitch are used as shown in Table **??** and Fig 2.20. Main purpose of this set of experiments was to compare the effect of flame acceleration and transition on the specific impulse produced by the tube. In earlier studies by Kiyanda et al. [36] and Harris et al. [37], the general conclusion was that the specific impulse attained in the PDE did not

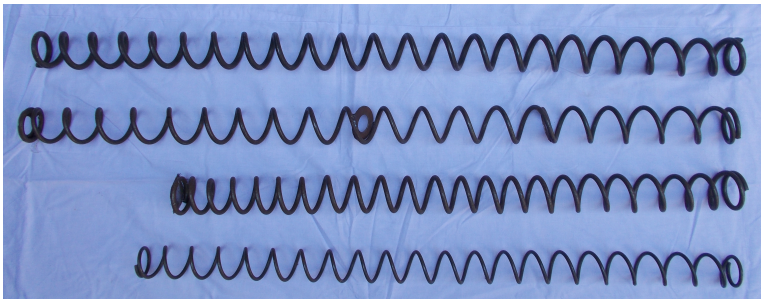

Figure 2.20: *Various spirals used in the experiment.*

depend on the point where DDT is attained till it is sufficiently inside the tube so that no spillage of unreacted mixture occurs from the open end. Recently Takeuchi et al. [86] have carried out the series of experiments for studying the effect of blockage ratio on the velocity and specific impulse produced by the single cycle pulse detonation tube. From their work it is observed that longer and larger blockage ratio will lead to decrease in specific impulse and L_{DDT} effects the specific impulse produced by the detonation tube.The results from the present work further corroborate this observation also pointing out to the importance of achieving the choked state.

The effect of transmission of the detonation wave from smaller to larger tube on the specific impulse for this case was also studied. For 25 mm case it was found that the combination of s0-s0 spirals which was similar to s1 but with higher surface roughness (due to presence of rust on the surface) led to the occurrence of earlier detonation compared to s1. The initial study of detonation transmission similar to the 42 mm tube was conducted. Figure 2.21 shows specific impulse vs fill length for this case. It is observed that in this case also specific impulse attained for the case with attachment was consistently higher than the case without attachment, though the difference is much less compared to the 42 mm tube. The head end pressure in Fig 2.22 for full fill shows that in this case also the pressure rise in case of tube with attachment is faster as compared to the case without attachment. Pressure transducers are placed at 30, 50 and 70 cm from the head end for measurement of shock velocity. The velocity measured between transducer 1-2 is V1 and between 3-4 is V2. The measured V1 velocity for both the cases was nearly same (1100 m/s) while V2 was consistently above 1500 m/s for case without extension and for case with attachment this value remained in between 1000-1500 m/s. To further study effect of flame acceleration on specific impulse various types

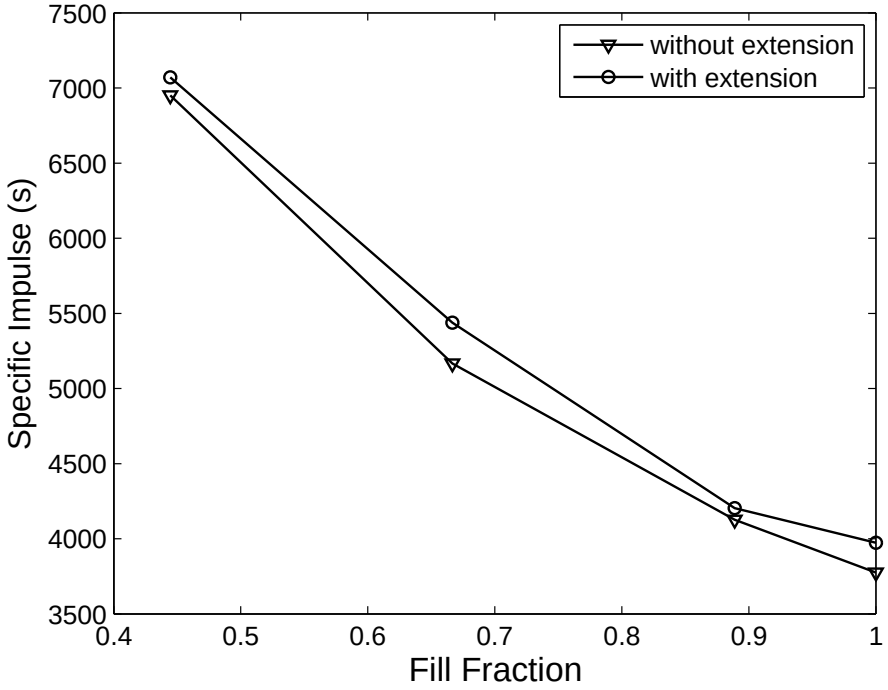

Figure 2.21: *Specific impulse vs fill fraction for 25mm dia 1m tube.*

of blockage combination's were used with length varying from 60-90 cm and blockage ratio varying from 24-36 %. Figure 2.23 gives the plot between the specific impulse and the velocity measured. This graph shows that the initial acceleration of flame is critical for the production of higher specific impulse. The variation of specific impulse with V2 has more scatter. Except for the one point where even after failure specific impulse is higher, the remaining cases show a common trend that failure to accelerate initially leads to decrease in impulse while for all the cases where the shock velocity is above choked velocity of 1100 m/s. The calculated specific impulse is within 10% scatter. Maximum specific impulse obtained is 4100 s which is close to the ideal value of 4200 s given by Endo et al. [2]. It is to be noted that the specific impulse calculated using pressure integration at closed end in this case will not be reproducible in the moving pendulum test as friction due to high blockages effects the impulse. This has been shown also in the work of Cooper et al. [35] where the inclusion of obstacles depending on the blockage ratio was shown to reduce the specific impulse by as much as 25% compared to the theoretical value. This comparison, points to the fact that the

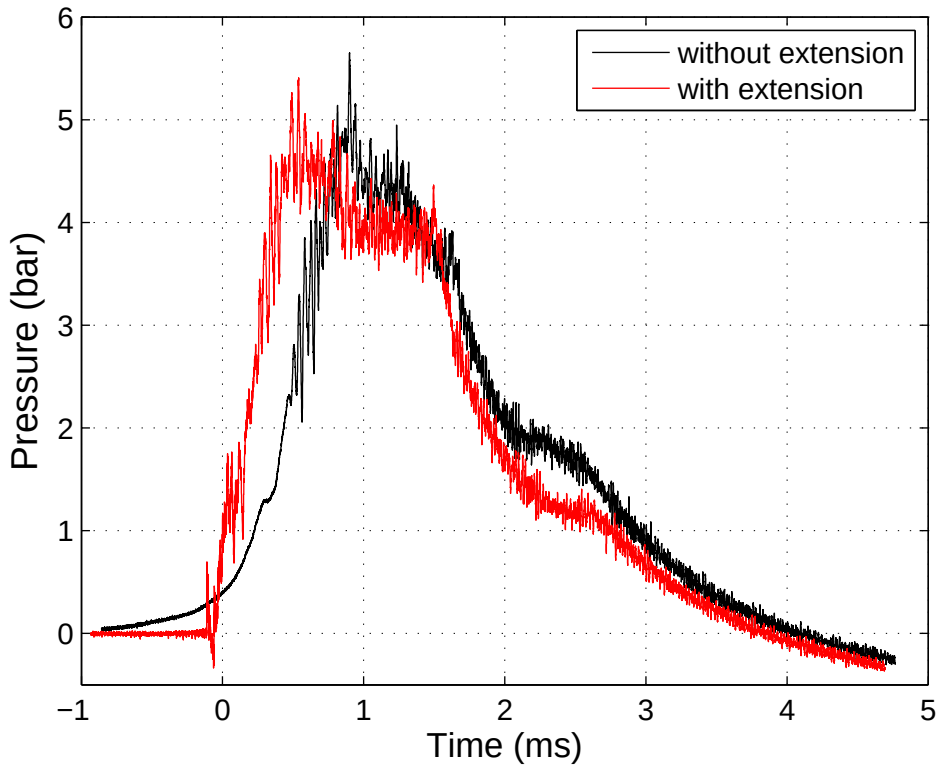

Figure 2.22: *The head end pressure profile with attachment and without attachment.*

specific impulse values calculated from theoretical models based on CJ detonation theory and the current experiments even without achieving CJ detonation are comparable. This points to the fundamental importance of achieving the choked state where the flow comes to rest immediately behind the shock-flame complex propagating close to burnt gas sonic velocity.

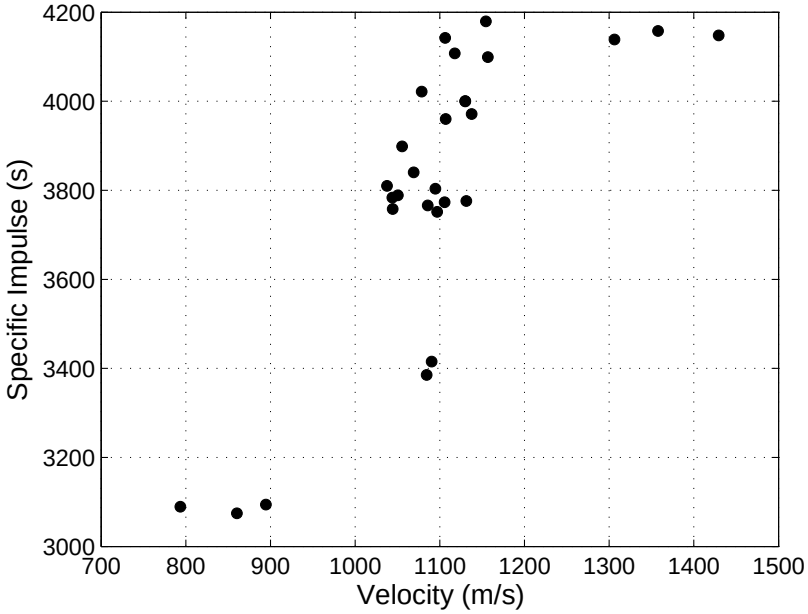

(a) Specific impulse vs V1.

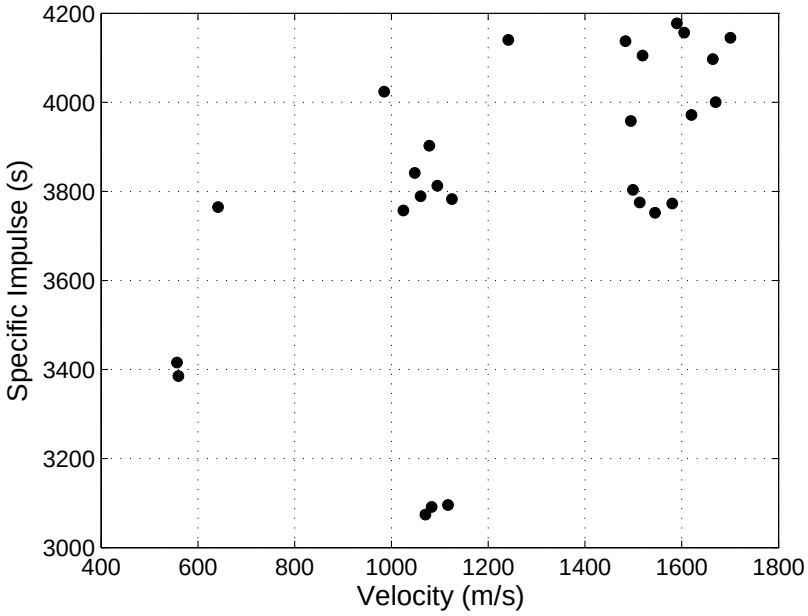

(b) Specific impulse vs V2.

Figure 2.23: *The variation of specific impulse with the shock velocity measured between the three transducers. V1 corresponds to initial velocity while V2 corresponds to later section.*

2.5 Propagation of Detonation in transparent tube

To further investigate the effect of choked flame propagation on the impulse, the propagation of DDT in transparent polycarbonate tubes with different blockages was carried out. These experiments have shown that under conditions of larger blockages the DDT leads to the formation of galloping detonation which continues to stay as a galloping detonation if no external source of disturbance affects the regime as also described by Lee [11].

2.5.1 Experimental setup

The experimental setup used for this work was a transparent polycarbonate tube of 1.5 m length and ID of 32 mm. It is fitted with the brass cap at the closed end and a brass attachment at 1 m distance from the closed end. Both the brass attachments were fitted with dynamic pressure transducers PT-1 on closed end and PT-2 at 1 m from the closed end. The premixed hydrogen and air having fixed equivalence ratio of 1 was filled in the tube from the head end. The mixture was ignited using the automobile spark ignition system. MotionPro Y3 camera was used to acquire the images at 40000 fps with the constant exposure time of 22 μs. For enhancing DDT, following spiral configurations were used in various combination's.

Serial No.	Length (cm)	Thickness (mm)	Diameter (mm)	Pitch (mm)
1	50	2	32	15
2	50	3	32	15
3	50	4	32	15
4	60	3	24	20

Table 2.4: *Specification of various spirals used.*

An orifice plate (O) of diameter 32 mm providing blockage ratio of 50% was also used in some cases for the enhancement of DDT. Results presented here correspond to the following configurations ie. the arrangement of blockages along the length of the tube. The following references will be used in remaining sections:

Name	Configuration
C-1	1 - 3
C-2	1 - 3- 4
C-3	1 - O - 3 - 4
C-4	4

Table 2.5: *Spiral combination's used for the experiments. O refers to orifice plate with blockage ratio of 50 %.*

2.5.2 Results and Discussions

This section presents the observations made from the various experiments. This is followed by the discussion and comparison with the similar other experiments.

a) Pressure

Figure 2.24 gives the pressure profile for the four configurations above. All the cases show similar profiles and the peak pressure at the head end for all cases is nearly 6 bar. The rise time and extent of plateau pressure are different for these cases. The pressure profile shown by transducer PT-2 shows a sub CJ detonation, as first three test cases clearly show the peak pressure achieved is much less than the expected Von-Naumann pressure of 28 bar.

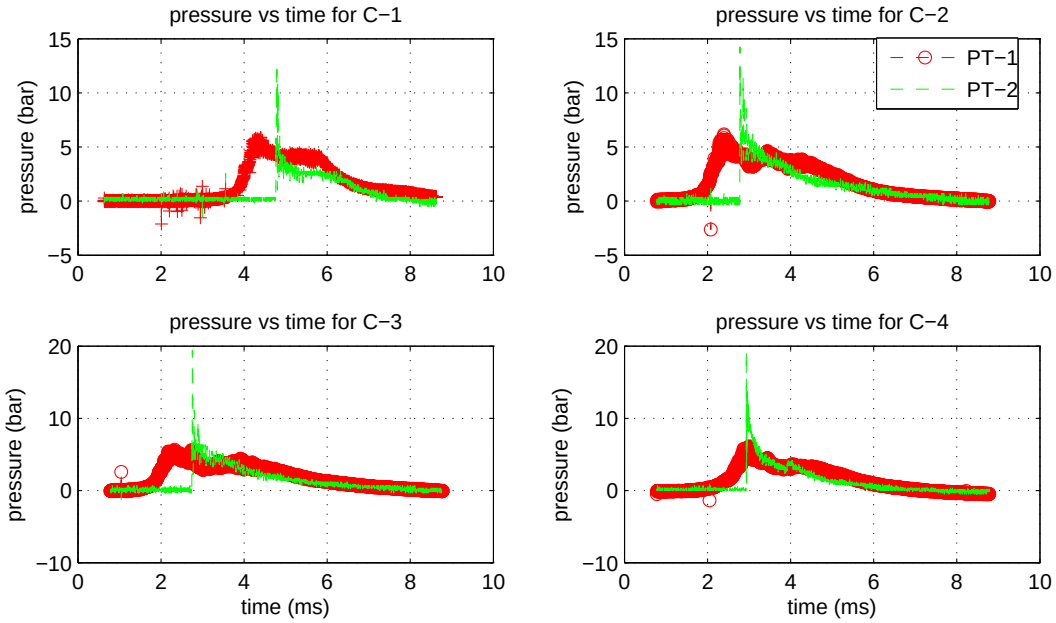

Figure 2.24: *The pressure profiles at head end and at the middle transducer for the four configurations.*

b) Velocity

The next series of Fig 2.25 show the flame motion inside the tube for these cases:- Due to limited light sensitivity of the camera, initial flame formation and acceleration near to the closed end of the tube could not be captured. Figure 2.26 shows the velocity of the front along the length of the tube. From these velocity profiles, it can be clearly inferred that case C-1 propagates very close to the choked regime for the full extent of the tube. Case C-2 and C-3 propagate near to choked regime but do intermittently propagate near to CJ velocity due to the presence of obstacles along the length of the tube. These perturbations lead to transition of metastable wave from choked to CJ regime for short interval. It can be concluded that except for C-4 all other cases propagate as quasi detonation This is a typical case of galloping detonation as reported by [11]. The corresponding effect of these perturbations can be seen in the pressure profiles in Fig 2.24. The impulse for this case was calculated by integrating the head end pressure profile. Table **??** shows the variation of impulse for the four cases. The results clearly show that the impulse obtained in the case of choked condition (C-1) is comparable to that obtained in the CJ case (C-4). Due to the presence of high blockages the value of calculated impulse lies between the values of impulse proposed by Wintenberger et al. [1]

(a) C-1 flame position at 125 (μs) interval

(b) C-2 flame position at 100 (μs) interval

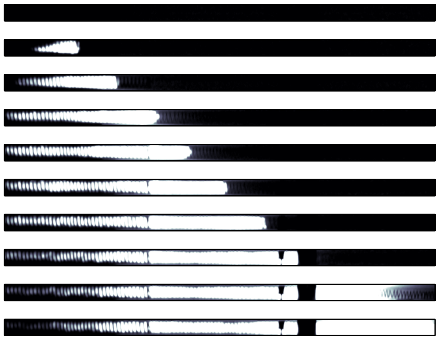

(c) C-3 flame position at 125 (μs) interval

(d) C-4 flame position at 50 (μs) interval

Figure 2.25: *Images of flame motion through the tube captured using high speed camera.*

model and Endo et al. [2] model. The pitch of obstacles used in the present case is close to D/2 which leads to formation of choked waved Gamezo et al. [55]. The impulse generated in the case of C-2 and C-3 is much higher. Due to presence of higher blockage along the length of tube larger drag is produced and hence reduction in the actual thrust will take place.

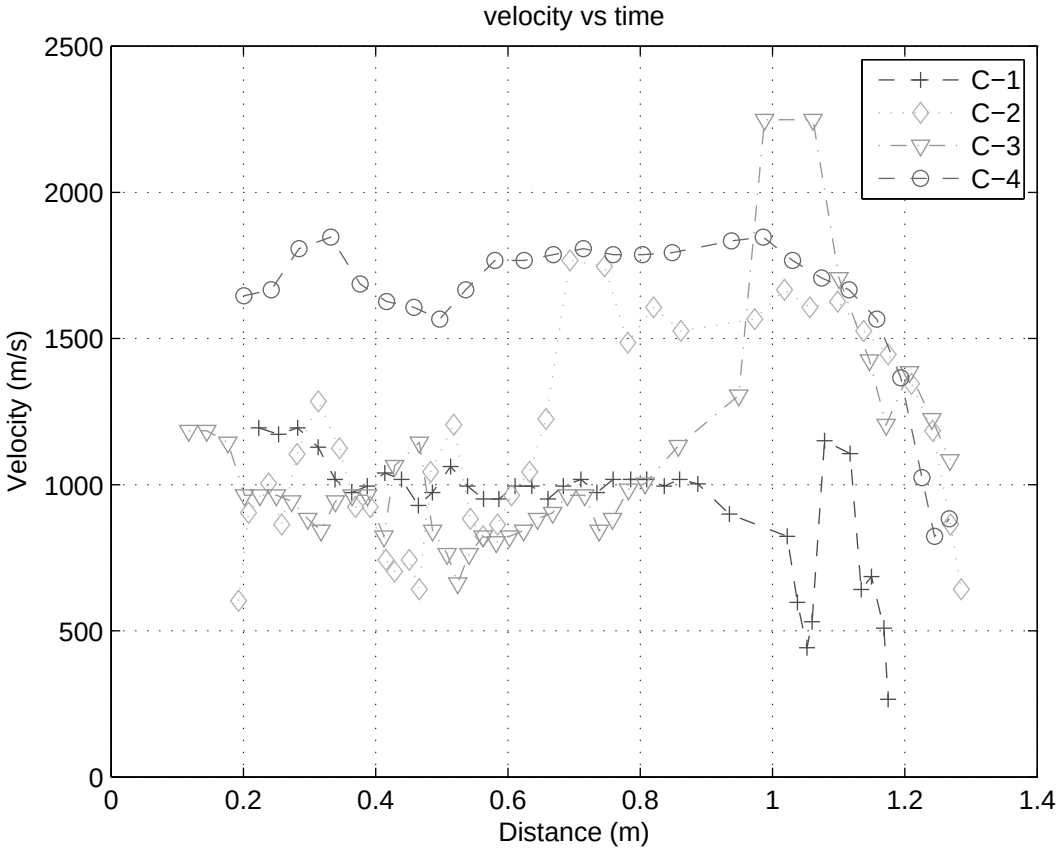

Figure 2.26: *Combustion wave velocity variation along the length of the tube for various cases.*

Config	Impulse(Ns/m^2)	Rise time (ms)
C-1	0.97	0.94
C-2	1.13	0.83
C-3	1.15	0.72
C-4	0.86	0.92

Table 2.6: *Calculated parameters for the four configurations using head end pressure data. For this configuration the theoretical impulse calculated using Wintenberger et al. [1] model is 1.24 Ns/m^2 and Endo et al. [2] model is 1.0Ns/m^2 .*

2.6 Theoretical model for impulse produced by various detonation regimes

The double discontinuity structure can be analyzed by solving the steady state conservation equations across both the discontinuities. The solution of these conservation equations lead to the following expression of choked flames where the flow velocity behind combustion wave is equal to sonic velocity Figure 2.27. We start with conservation equations across shock wave:-

$$\rho_0 U_0 = \rho_1 \left(U_0 - U_1\right) \tag{2.7}$$

$$P_0 + \rho_0 U_0^2 = P_1 + \rho_1 U_1^2 \tag{2.8}$$

$$h_0 + \frac{U_0^2}{2} = h_1 + \frac{U_1^2}{2} \tag{2.9}$$

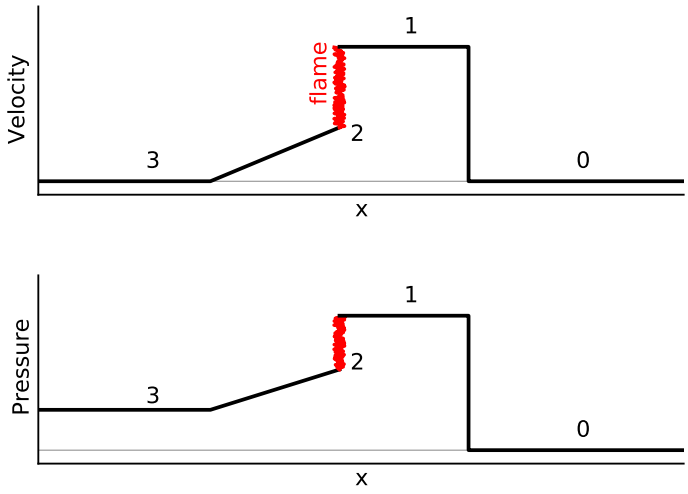

Figure 2.27: *Schematic representation of pressure and velocity variation with distance for the choked state. Various states of mixture are 0: fuel-air mixture, 1: condition after shock, 2: burnt products, 3: state after Taylor wave.*

With some simplification we get

$$\frac{\rho_1}{\rho_0} = \frac{U_0}{U_0 - U_1}$$
$$\frac{P_1}{P - 0} = 1 + \frac{\rho_0}{P_0} U_0 U_1$$
$$\frac{a_0}{\gamma - 1} + \frac{U^2}{2} = \frac{a_1}{\gamma - 1} + \frac{(U_0 - U_1)^2}{2}$$

Conservation equations across flame:-

$$\rho_1 (U_f - U_1) = \rho_2 (U_f - U_2)$$
$$P_1 + \rho_1 (U_f - U_1)^2 = P_2 + \rho_2 (U_f - U_2)^2$$
$$P_1 - P_2 = \rho_1 (U_f - U_1)(U_1 - U_2)$$

We normalize the velocity using a_0 and apply the sonic boundary condition at the burnt end. Algebraic manipulation of this equations lead to the generalized CJ curve also known as Q-curve [15] in literature as shown in Figure 1.4. From this we can get the expression for the flame and the shock mach numbers

$$M_s - \frac{1}{M_s} = \left(\frac{\gamma^2 - 1}{2} \frac{q}{a_0^2} \right)^{\frac{1}{2}} \tag{2.10}$$

Using the relation for CJ detonation the expression for shock Mach number M_s is:

$$M_s = \sqrt{M_{\text{cj}}/4} + \sqrt{M_{\text{cj}}/4 + 1} \tag{2.11}$$

The flame behind this shock propagates at maximum deflagration velocity (D_f) or lower CJ point. Using CJ theory we get

$$M_f = \sqrt{\beta^2 + 1} - \beta \tag{2.12}$$
$$\beta = \sqrt{\frac{(\gamma^2 - 1)}{2\gamma} \frac{q}{RT_s}}$$

The calculated value of Deflagration Mach number can be used to calculate the

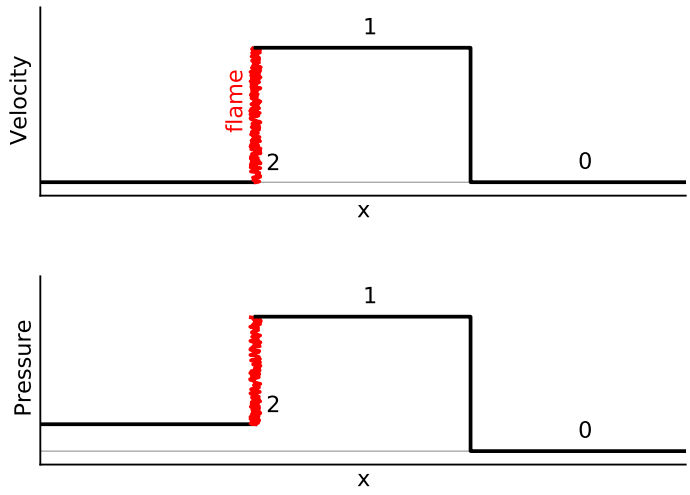

Figure 2.28: *Schematic representation of pressure and velocity variation with distance for the initial acceleration phase.*

pressure ratio across the deflagration wave at the choked condition in the burnt gas.

$$\frac{P_c}{P_1} = \frac{\gamma M_f^2 + 1}{\gamma + 1} \tag{2.13}$$

Using this and the RH condition across the shock wave given by

$$\frac{P_1}{P_0} = \frac{2\gamma M s^2 - (\gamma - 1)}{(\gamma + 1)}; \tag{2.14}$$

the head end pressure can be calculated.

The condition of flame acceleration can be divided into two states. These are one for the initial acceleration of the flame and other state is after the flame gets choked Fig 2.28. The case of initial acceleration can be modeled by assuming final state of combustion products to be at rest hence $U_2 = 0$ in the tube coordinates. Using this

equation the conservation relations can be combined to get:

$$\rho_2 = \frac{\rho_1}{\rho_0}(1 - \frac{U_1}{U0}) \tag{2.15}$$

$$\frac{1}{\gamma - 1}U^2 + U\left[qa_0^2/U_1U_1(\frac{\gamma}{\gamma - 1} - \frac{3}{2})\right] = \left(\frac{a_0^2}{\gamma - 1}\frac{T_2}{T_1} + qa_0^2 + \frac{U_1^2}{2}\right) \tag{2.16}$$

From these equations the density at the end of combustion wave and velocity of combustion wave can be calculated for the given shock velocity. These values are used to calculate the pressure at the end of combustion wave using the relation

$$\frac{P_2}{P_1} = \frac{\left[\chi - \sigma + \frac{2q}{\mu\sigma}\right]}{\chi\sigma - 1} \tag{2.17}$$

where

$$\chi = \frac{\gamma + 1}{\gamma - 1}$$
$$\mu = \frac{P_1}{P_0}$$
$$\sigma = \frac{\rho_1}{\rho_2}$$

Using these relations and RH equations across the shock we can calculate all the relevant properties at the end of combustion wave. Using the relations for property variation across Taylor wave, derived in Sec 1.1.5 is used to calculate the properties at the head end.

For the above two conditions of initial acceleration and the choked state an approximate model for impulse was constructed. After the calculation of head end pressure various times for the motion of waves in the chamber can be approximately calculated as:-

- $t_1 = \frac{L}{U_s}$ time taken by shock to move out of the tube.
- $t_2 = \frac{Lt1}{U_c + U_1 - a_1}$ time taken by incoming expansion wave to hit the combustion wave.
- $t_3 = \frac{L}{a_3}U_c/U_s\left(1 - \frac{U_c}{a_3 + a_2}\right)$ time taken by the expansion wave to hit the end wall.

γ_1 -	1.33
γ_2 -	1.19
q, Mj/kg	2.2
D_{cj}, m/s	1950
P_3, bar	5.1
c_0, m/s	405

Table 2.7: *Parameters of CJ detonation wave used for calculations.*

- $t_4 = \frac{L\beta}{a_3}$ time for head pressure to come back to datum value. β is empirical value taken from Wintenberger et al. [1].

The specific impulse is given using:

$$I_{sp} = P_3 \left(t_1 + t_2 + t_3 + t_4\right) / \rho_1 g L \tag{2.18}$$

These equations were used to calculate the specific impulse of H_2-air mixture with varying shock velocities for initial pressure of 0.9 bar and ϕ=1.0. Various combustion parameters were chosen in such a way that we could reproduce the different parameters for this mixture of H_2-air as given in Tab. 2.7.

Figure 2.29 shows the variation of specific impulse with shock velocity. The calculation of specific impulse is based on two methods using constant and variable γ. For constant γ the resulting specific impulse gets saturated at ∼3900 s as shock velocity increases beyond the choked velocity of 1100 m/s. For variable γ specific impulse grows even beyond the choked regime and final value of ∼4200 is achieved at CJ velocity. The impulse model for CJ detonation can be simply written as

$$I = K \left(\Delta P_3 / D_{cj}\right) V \tag{2.19}$$

where V is the volume of the tube. Here K is a constant, its value has been previously calculated by Wintenberger et al. [1], Endo et al. [2] and Zitoun and Desbordes [87] as 4.8, 4 and 5.4 respectively. While [1] and [2] calculated their value from theoretical model [87] obtained it from experimental curve fit. The present model gives the value of 3.985 for this constant. For the two γ model variation in specific impulse of 25% is seen beyond the choked velocity. This variation does not conform to the variation seen in the experimental value where the specific impulse gets saturated when the wave

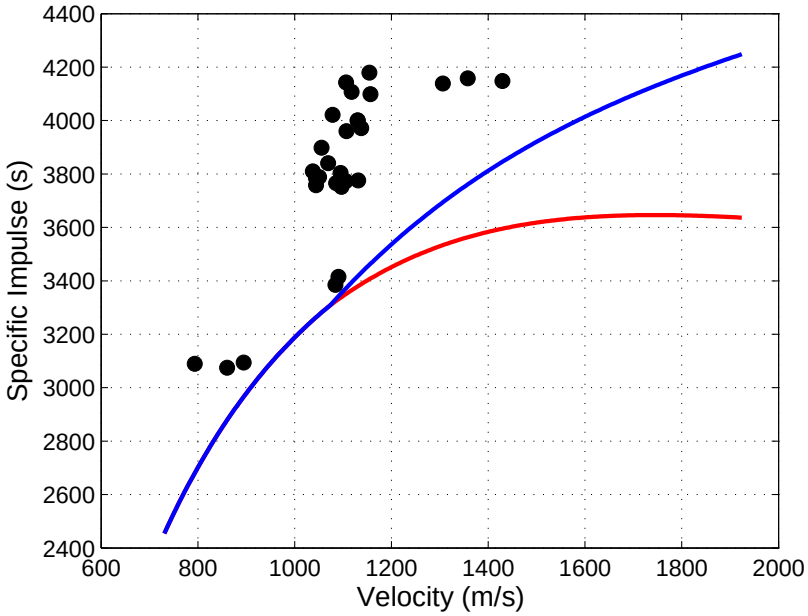

(a)

Figure 2.29: *Variation of theoretical specific impulse Vs shock velocity. Dots are experimental results referring to Fig 2.23.*

accelerates to beyond CJ velocity. This may be due to the complex interaction of shock with the obstructions which leads to the changes in the flow properties behind it. A simple one dimensional model like present one will not be able to captured this dynamics accurately. The complicated wave dynamics associated with interaction of expansion wave, combustion wave and Taylor in presence of obstacles will have to be taken into consideration for such a model to give better comparison with the experiments.

2.7 Summary

In this chapter the study of flame transmission and effect of flame acceleration on the specific impulse produced have been studied. First, a set of experiments were conducted to study the effect of partial filling on the specific impulse for tubes of two different lengths. These results are consistent with results of Schauer et al. [70] . The study of partially filled tubes have shown that longer length tubes lead to the production of higher

specific impulse in comparison to shorter tubes.

Experiments conducted in tubes with detonation initiated using small diameter tube attached at the head end of 42 mm tube has shown that up to 20% improvement in fuel specific impulse can be achieved compared to the normal detonation tubes for the partial-fill cases. Increase in specific impulse is obtained due to the shorter rise time at the head end. This happens in spite of the fact that CJ detonation is not achieved in these cases. The detonation in cases with attachment travel at close to choking regime. However there is a tendency for failure of quasi-detonation wave in tubes of large lengths. In the case of smaller tube of 25 mm diameter, it was observed that the increase in specific impulse with the extension was 5% higher than the case without attachment. This is due to the fact that for smaller tubes, initial flame acceleration is high and therefore, the effect of fast flame transmission is mitigated.

For fuel-air mixture, it has been generally found that direct detonation requires the pre-detonator tube to be of 13λ diameter. For some highly reactive mixtures like ethylene, Thomas et al. [88] were able to reduce the pre-detonator diameter to 5λ approximately. This puts a restriction as extra amount of fuel is consumed in pre-detonator tube. Initial acceleration of flame by using obstacle alone is slow. Use of pre-detonator tube of small diameter and optimized length consumes very less fuel – of the order of 2% and greatly enhances the flame acceleration; a feature that can be noticed from the plateau pressure profiles. Further, this tube can be used in different arrangements like parallel and perpendicular to the main tube providing further flexibility as compared to the introduction of orifice plates [34, 44] inside the tubes to initiate the mixture. Results for all set of experiments emphasize the importance of initial flame acceleration as a critical process for production of higher specific impulse.

In next chapter we will further study the effect of tube attachment on the flame acceleration and transition to detonation using high speed images of flame propagating in transparent tubes.

Chapter 3

Initiation of detonation using extension tube

3.1 Introduction

The effect of initiation of H_2-air mixture using small tube was further studied using the high speed camera. In this study the difference between the flame acceleration when the mixture is ignited inside the tube compared to the ignition using the extension tube could be clearly seen. The study was carried out for different equivalence ratios of H_2-air mixture. Significant advantage can be clearly seen for the equivalence ratio near 1 as there is reduction in DDT distance from 50 cm to 35 cm. For leaner mixtures it was observed that with the use of smaller blockage ratio and orifice plates DDT could be attained within 70 cm of tube while distances as large as 2 m have been reported earlier [60] for similar mixtures.

3.2 Experimental Setup

The experimental setup consists of a transparent polycarbonate tube of 2 m length and 5 cm internal diameter. A pressure transducer is attached at the closed end of the tube. High speed camera of Photron make is used for capturing the images of the flame transition to detonation inside the tube. The head end of tube had also the provision for attachment of extension tube to it which could be attached radially, tangentially and axially. The extension tube was of 5 mm diameter and 25 cm length. Two spirals of

blockage ratio (BR) 0.44 and length of 30 cm (S1) and second with BR of 0.35 and 50 cm length (S2) was used. Spiral S2 is same as that of used for experiments with 42 mm diameter tube. Two orifice plates of blockage ratio 0.53 were used in combination with smaller spiral to enhance the transition. Automobile spark plug was used to initiate the combustion. Pressure transducer was fitted at the head end of the tube. Data acquisition system was coupled in such a way that the ignition of mixture triggered the acquisition of pressure data and images.

3.3 Results and discussion

3.3.1 Experiments with S1

Figure 3.1 show the flame motion for equivalence ratio 1 and spiral S1. The transition takes place near to 35 cm from the closed end with tangential connection of the extension pipe. This clearly shows that the detonation is achieved with extension while it fails without extension. From Fig 3.1 it can be clearly seen that presence of extension tube shortens the time of flame acceleration period which finally leads to transition in case with extension tube. The reason for this can be directly attributed to the ignition of fuel air mixture in the larger tube by a strong jet of accelerating combustion wave from the smaller tube. Figure 3.2 shows the pressure vs time curve for the two cases and the effect of accelerating flame on the head end pressure is also clearly visible.

Figure 3.3 shows the X-t diagram of combustion front for both the cases.

Previously for stoichiometric H_2-air mixtures, DDT length of nearly 1 m was measured [60] for tube of 5 cm diameter. The tube was lined with orifice plates of 0.44 blockage ratio over the length of 3 m. Sorin et al. [34] carried the optimization study for DDT length. They were able to reduce the DDT length to 36 cm for 2.6 cm diameter tube using spiral of BR 0.52 and orifice plates with BR from 0.55 to 0.98. In the current study DDT length of 35 cm is measured when detonation velocity crosses $0.85D_{CJ}$ as shown in Fig 3.1. The criticality of initial flame acceleration has been shown to be significant in the process of DDT. The use of extension tube greatly enhances this process using a small amount of fuel. Transition to detonation using this blockage configuration was seen for mixtures close to stoichiometry. For lower equivalence ratio this blockage configuration failed to produce DDT. Hence configuration with blockages S2 was used.

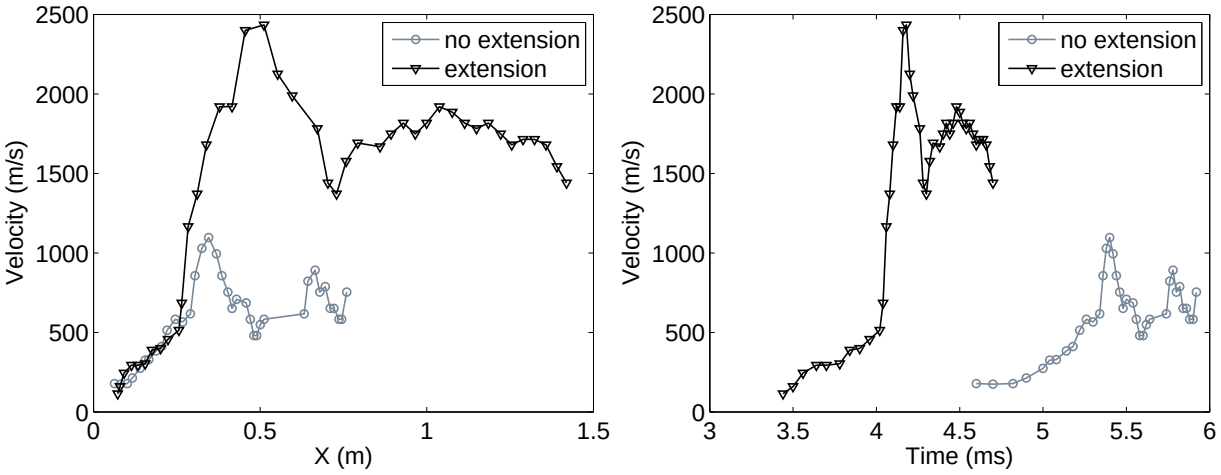

(a) Velocity vs X

(b) Velocity vs Time

Figure 3.1: *Comparison of flame velocity with and without extension tube, as flame propagates through the tube with spiral of BR 44%. Detonation fails to propagate without extension tube, the initial process of flame acceleration is significantly delayed as can be seen from the right figure.*

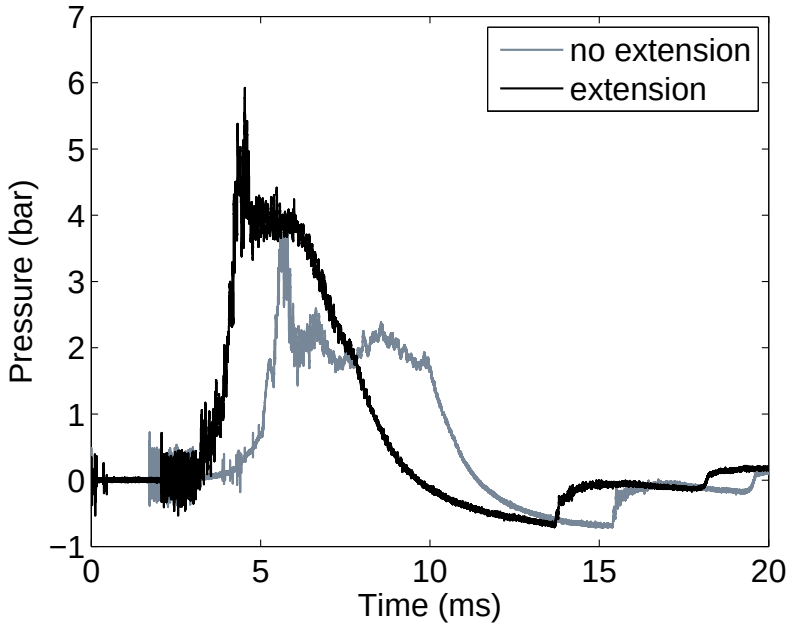

Figure 3.2: *Comparison of head end pressure profile with and without extension tube.*

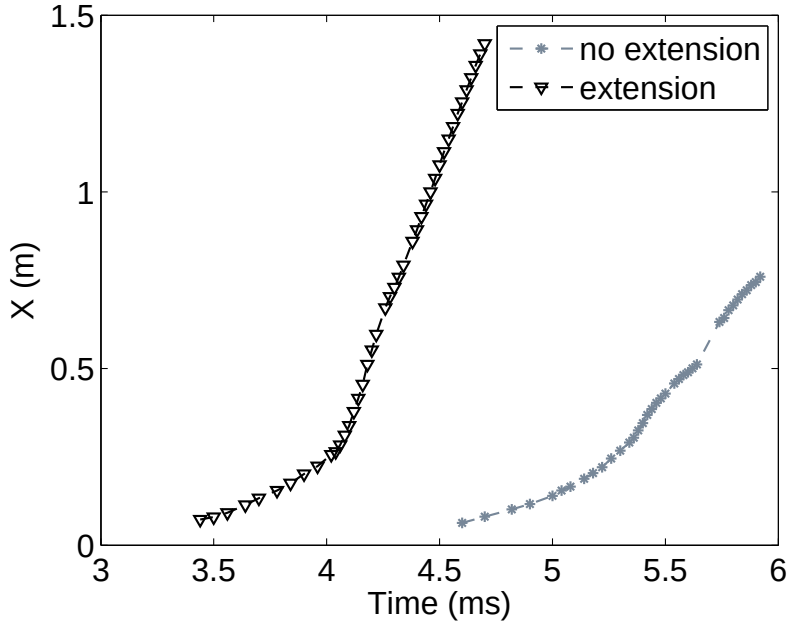

Figure 3.3: *X-t diagram of flame front as it moves through the tube.*

3.3.2 Experiments with S2

For leaner air fuel mixtures, S1 was found to be insufficient for transition to detonation. To overcome this deficiency second spiral of 50 cm length with extra attachment length of 20 cm was used to carry out more experiments. Several experiments with leaner hydrogen mixtures were carried out to study the effect of transmission. Table:3.1 provides the details of the experiments carried out.

From the table it is clear that with a lower blockage ratio of 35% transition could be obtained within 70 cm for majority of the mixtures up to 0.55 equivalence ratio. Of all the arrangements used for transition it was found that the tangential attachment produced the most successful transition with the use of single orifice plate.

Fig 3.4 shows the flame acceleration and transition to detonation for the three different arrangements for ϕ = 0.63. The transition length is approximately 50 cm for all the three cases. In the case of ϕ = 0.55, it was found that no transition could be achieved with axial or radial attachments for all the trials performed. In case of tangential attachment for the 7 experiments conducted 4 produced transition and 3 failed. This may be due to the small variations in the stoichiometry. Figure 3.5 show the velocity and pres-

ϕ	Attachment	S2	Extension	Success	Failure
1.0	A	Y	N	3	None
1.0	T	Y	N	3	None
1.0	R	Y	N	3	None
0.78	A	Y	N	3	None
0.78	T	Y	N	3	None
0.78	R	Y	N	3	None
0.63	A	Y	Y	3	None
0.63	T	Y	Y	3	None
0.63	R	Y	Y	3	None
0.55	A	Y	Y	None	3
0.55	T	Y	Y	4	3
0.55	R	Y	Y	None	3

Table 3.1: *List of experiments conducted showing success and failure for the various cases. T=tangential, A=Axial, R=Radial Attachment.*

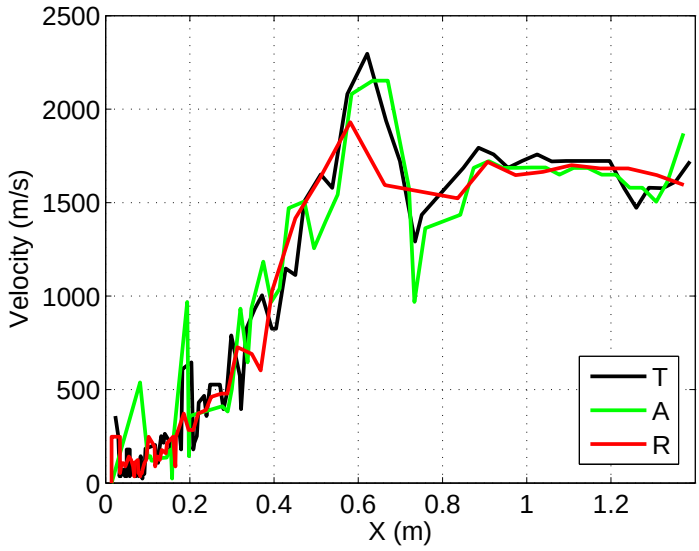

Figure 3.4: *Flame acceleration and transition for the three cases studied for ϕ=0.63. The final velocity is close to D_{cj}=1733 m/s.*

sure plot for one case each of successful and failed transition with tangential attachment for ϕ = 0.55 of the mixture. As DDT is stochastic by nature [55] close to limits such variations are expected. This equivalence ratio is the limit of transition for the tangential configuration as no transition was seen for lower equivalence ratios. This also shows some superiority of tangential transmission as compared to the other two cases.

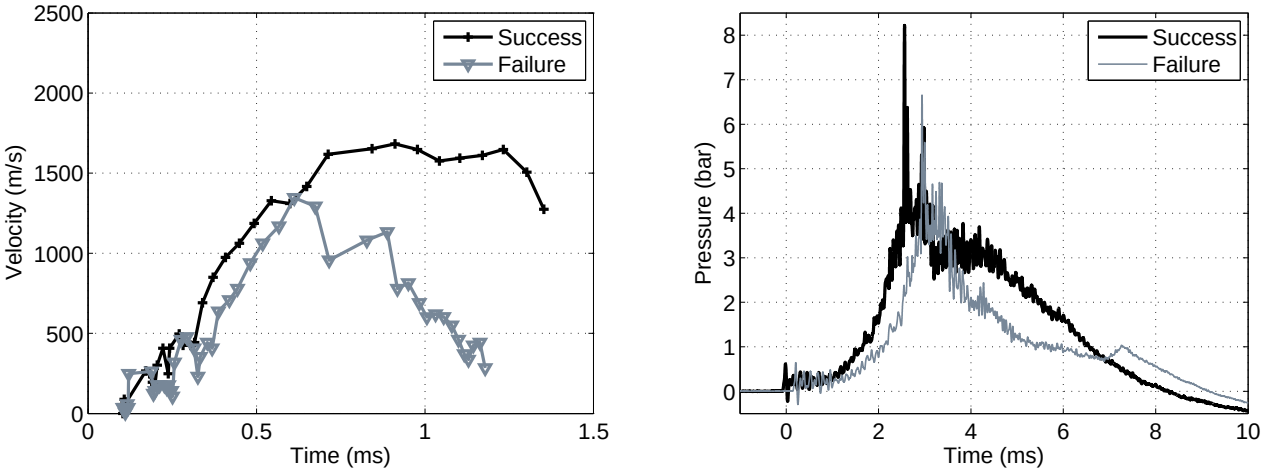

(a) Velocity vs X.

(b) Pressure vs Time.

Figure 3.5: *Pressure and velocity comparison of success and failure cases for ϕ=0.55 using tangential attachment.*

The comparison of two cases clearly show that the initial acceleration is similar in both the cases before it fails for one case when velocity reaches 1300 m/s. The reflection of this can also be seen on the pressure profile as initial pressure after transition is similar for both the cases before it drops quickly for the failed case.

To further study the effect of transition for these cases a second orifice plate was used to tip the flame in its accelerating mode and study the effect of that on transition process. The radial configuration was chosen for this study as it failed to produce DDT for ϕ = 0.55. Figure 3.6 shows the velocity profile as orifice plate is placed farther from the closed end. Placement of orifice plate at 33 cm from the closed end leads to successful transition and this was verified by repeating the experiment 3 times for all the cases.

Most of the earlier studies have treated the transition process using the symmetrical blockages. Study of flame acceleration using unsymmetrical blockages with smaller

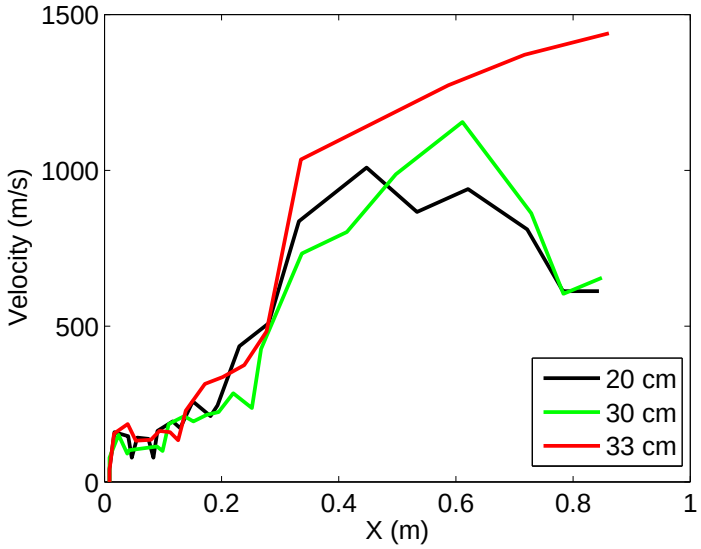

Figure 3.6: *Flame acceleration for different placement of first orifice plate from the closed end of tube for ϕ=0.55.*

blockage ratios and variable placement of orifice plates indicates that it can lead to transition within the given length of tube whereas it fails in the absence of such blockages.

Dorofeev et al. [3] have given the criteria for transition to detonation as a function of the geometry. Their criteria suggests that transition occurs at $L/\lambda > 7$ where L is given by $L = (S + D)/2/(1 - D^*/D)$. This criteria has been shown to be correct for several experimental studies by Ciccarelli and Dorofeev [59]. Table:3.2 presents the comparison of this criteria for the present set of experiments. From these results, it appears that for lower equivalence ratios this criteria is not satisfied. The reason for this can be attributed to the presence of unsymmetrical blockages, as this criteria has been strictly derived for the symmetrical blockages present in the path of accelerating flame. This observation is in line with the theoretical study of DDT in H_2-air mixture by Gamezo et al. [55]. They observed that the staggered blockage configuration resulted in shorter DDT length as compared to symmetrical.

Out of three placements of attachment investigated in this study, it was found that for tangential and radial arrangements the performance of both the configurations was similar. However with ϕ = 0.55, DDT was achieved with the tangential arrangement with single orifice plate but not with the radial arrangement and the axial attachment

ϕ	λ (cm)	L/λ	Success
1.0	1.5	16.6	Y
0.78	2.1	12	Y
0.63	4.5	5.5	Y
0.55	8.9	2.8	Y

Table 3.2: *Values of DDT criteria predicted by Dorofeev et al. [3].*

ϕ	BR	L_{min} (cm)
1.2	0.44	5
1.2	0.38	6

Table 3.3: *Values of minimum distance L from closed end for two blockage ratios, for DDT to be successful.*

was least effective.

3.3.3 Experiments with H_2-O_2 mixtures

To further analyze this perturbation some experiments with single orifice plates in the path of H_2-O_2 flames were also carried out. Blockages were carefully moved along the length of tube, it was found that once flame has achieved some critical velocity a small perturbation leads to transition. Studies were carried out for ϕ = 1.2 using single point blockage. Table:3.3 shows the minimum distance for transition to take place for different blockages for this equivalence ratio.

3.4 Summary

In this chapter study of the effect of extension tube attachment on the process of DDT has been experimentally studied. Three arrangement techniques namely, axial, radial and tangential attachments are examined. It is found that substantial reduction in DDT length and blockage length can be achieved for the stoichiometric H_2-air mixtures using the extension tube. For leaner mixtures it is found that the usage of a tangential entry leads to transition with minimum blockage. The studies carried out have also shown that the placement of blockages at critical distances from the closed end leads to successful

transition. A limited number of studies was also carried out using single point blockages with H_2-O_2 mixture. The results of this study have shown that there is a critical length where the placement of blockages leads to successful detonation transition. This further shows that beyond a critical velocity the presence of obstacles leads to successful transition.

With this background, it is thought appropriate to examine issues of transition problems from one equilibrium state to another. Towards this numerical investigation of the processes is considered and is the subject of the following chapters.

Chapter 4

Numerical Method

4.1 Introduction

The study of deflagration to detonation transition (DDT) has been of great interest to researchers for a long period of time. Starting with the experimental works of [31], [30], [38] lot of work has been carried out in deepening our understanding of the DDT process. The growth in the computational capacity and algorithm over the last few decades led to beginning of numerical study of DDT. The motivation for the present work has come from the series of experimental studies conducted by Ming-hsun Wu [89]. In these experiments, they were able to study the DDT in micro channel tubes of 0.5 to 2 mm. The mixture of H_2-O_2 is chosen for the study as this system has smaller set of species and reaction mechanism amenable to numerical studies. In the present study, flame acceleration and transition to detonation in 2D channel is carried out. The perspective of this work is in understanding the various regimes in the transition process as has been carried out for single reaction case in references [90], [53]. The importance of this work is in exploring the major difference between single step and multi-step reactions for studying DDT. The quantitative comparisons with the actual experimental results and theory will be made wherever possible. Jun-Kai Wang [91] have carried out 3D simulations where they make quantitative comparisons of DDT with the experimental results. Their work clearly shows that the difference between the initial acceleration of flames in 2D and 3D channel which leads to over-prediction of DDT distance in the 2D case. As 3D calculations are computationally intensive these studies were performed with much coarse unstructured meshes which is inadequate in resolving important flow

features like flame and detonation thickness.Fine grids are required to capture the final transition from flame to detonation which occurs through the discontinuous explosion in the unburnt fuel-air mixture. At this point the pressure and temperature values are higher as compared to those in steady state detonation or deflagration wave, hence the correct mesh resolution is required to capture the physics correctly.

4.2 Governing Equations

The generalized Navier Stokes equations in two dimensions with reaction source term and multiple species are given below:

$$\frac{\partial \rho}{\partial t} + \frac{\partial (\rho u)}{\partial x} + \frac{\partial (\rho v)}{\partial y} = 0 \tag{4.1}$$

$$\frac{\partial u}{\partial t} + \frac{\partial (\rho u u)}{\partial x} + \frac{\partial (\rho u v)}{\partial y} + \frac{\partial P}{\partial x} = \frac{\partial \tau_{xx}}{\partial x} + \frac{\partial \tau_{xy}}{\partial x} \tag{4.2}$$

$$\frac{\partial v}{\partial t} + \frac{\partial (\rho v u)}{\partial x} + \frac{\partial (\rho v v)}{\partial y} + \frac{\partial P}{\partial y} = \frac{\partial \tau_{xy}}{\partial y} + \frac{\partial \tau_{yy}}{\partial y} \tag{4.3}$$

$$\frac{\partial e_t}{\partial t} + \frac{\partial (\rho u e_t)}{\partial x} + \frac{\partial (\rho v e_t)}{\partial y} + \frac{\partial (P u)}{\partial x} + \frac{\partial (P v)}{\partial y} = \frac{\partial q}{\partial x} + \frac{\partial q}{\partial y} + \frac{\partial (u \tau_{xx})}{\partial x} + \frac{\partial (v \tau_{xy})}{\partial x} + \frac{\partial (u \tau_{xy})}{\partial y} + \frac{\partial (v \tau_{yy})}{\partial y} \tag{4.4}$$

$$\frac{\partial (\rho Y_i)}{\partial t} + \frac{\partial (\rho u Y_i)}{\partial x} + \frac{\partial (\rho v Y_i)}{\partial y} + \frac{\partial j}{\partial x} + \frac{\partial j}{\partial x} = \dot{\omega_i}''' \tag{4.5}$$

where

$$\tau_{xy} = \tau_{yx} = \mu\left(\frac{\partial u}{\partial y} + \frac{\partial v}{\partial x}\right)$$
$$\tau_{xx} = \lambda\left(\frac{\partial u}{\partial x} + \frac{\partial v}{\partial y}\right) + 2\mu\left(\frac{\partial u}{\partial x}\right)$$
$$\tau_{yy} = \lambda\left(\frac{\partial v}{\partial y} + \frac{\partial v}{\partial y}\right) + 2\mu\left(\frac{\partial v}{\partial y}\right)$$
$$e_t = e + \frac{(u^2 + v^2)}{2}$$
$$q = -k\left(\frac{\partial T}{\partial x} + \frac{\partial T}{\partial y}\right)$$
$$j = D\left(\frac{\partial Y\rho_i}{\partial x} + \frac{\partial Y\rho_i}{\partial y}\right)$$

We make use of stoke's hypothesis which gives

$$\lambda = -\frac{2}{3}\mu$$

the reaction rate is calculated for individual specie as

$$\dot{\omega_i}''' = \sum_{j=1}^{Nr}\left(K_{f_j}\prod_{i=1}^{Ns} C_i^{\nu'_{ji}} - K_{r_j}\prod_{i=1}^{Ns} C_i^{\nu''_{ji}}\right)$$

The transport coefficient of individual gases has been calculated using Sonine polynomial expansion coefficients [92]. Wilks formula is used for the calculation of viscosity and conductivity of the bulk mixture. Equation of state is used to complete the above set of equations.

$$P = \sum_{i=1}^{i=Ns} \rho Y_i RT \tag{4.6}$$

These governing equations are more amenable to treatment if we clearly distinguish between the non diffusive Euler equations and diffusion part separately. The Euler equation for the compressible unsteady flows form a set of coupled hyperbolic partial differential equations. The theory of solution of this set of equations has been extensively developed over the past century with the Method of Characteristics(MOC). These are the curves along which certain properties of the flow remain invariant and across which

the derivatives of the flow variables are discontinuous. Based on extension of these ideas, several numerical and theoretical models have been developed for the solution of this set of equations. In all of these, the central issue is that of handling the shocks and expansion waves. In the present work, we have made use of Roe's approximate Reimann solver with additional fixes to overcome various drawbacks of the scheme. The two major drawbacks of Roe's scheme are in dealing with expansion fan where it produces non-physical (entropy violating) expansion shock and the second is the presence of Carbuncle phenomenon Quirk [93]. This leads to instability of shock in 2 dimensions if the flow is predominantly one dimensional. Both of these can be corrected by using the Local Lax-Fredrich scheme under the H correction framework to add extra dissipation to the scheme. The flux splitting schemes like Van Leer, Harten-Lax-Leer and several of their extensions, though very robust, are more dissipative as compared to the Roe's scheme. The diffusive part is calculated using the conventional central differencing technique. For the present study WENO scheme based on Lax Fredrich scheme was chosen and this scheme is described in next section. It is followed by the test cases solved using this scheme depicting the robustness of this scheme in capturing various complicated flow structures.

4.3 Weighted Essentially Non Oscillatory Scheme (WENO)

4.3.1 Introduction

WENO scheme is an extension of ENO schemes developed by Harten et al. [94] paper. These schemes use the higher order Lagrange interpolation for calculation of higher order flux. The main idea behind these schemes is the way in which we can select the appropriate stencil to carry out the higher order interpolation. While ENO explicitly selects the stencil by checking for the presence of discontinuities, WENO scheme assigns the non-linear weights to the various stencil points and selects the one which does not include any discontinuity for the interpolation. In the present work, WENO schemes have been used for calculating higher order fluxes. WENO scheme can be developed to any order of accuracy, and several extensions of these have been developed for different set of problems. WENO schemes are used in the framework of compressible Navier-

Strokes flows with flow speed varying from low subsonic to supersonic speeds in the presence of very strong shocks. This scheme has been utilized for real gas flows with additional chemical kinetics and multi-component diffusion. While WENO is used for the Euler part of equation the diffusion derivatives are calculated using 4th order central derivatives. Chemical kinetics is treated using implicit Crank-Nicholson.

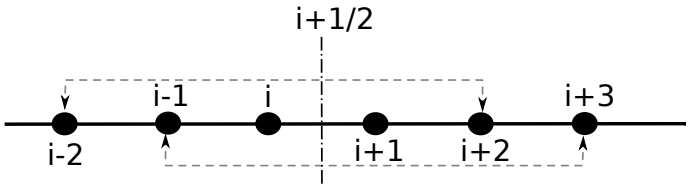

Figure 4.1: *Forward and backward stencil spread over 6 points used for the interpolation of fluxes.*

Fig 4.1 shows the six point stencil used for WENO interpolation. We assume a variable over the finite difference stencil of WENO. The stencil for the current cell i+1/2 extends from i-2 to i+3. First we compute the eigenvalues for the Euler equations which are well known to be u-a, u and u+a. The right and left Eigen-vectors of Euler equations are computed at the face i+1/2 using the density weighted average of cells i and i+1 as was proposed by Roe [95]. The work of Fedkiw et al. [96] and Dieterding [5] gives an extensive description about the efficient way of calculating and implementation of these average states for multi-specie reactive flows. In the present study we compute the following averages $\bar{\rho}$,
$baru, \bar{e}, \bar{Y_i}$. From these variables, first temperature is calculated using Newton-Raphson method and then other properties like $p, p_e, p_{\rho_i}, \bar{a}$ are calculated. These variables are used in the computation of $R_{i+1/2}$ and $L_{i+1/2}$ which are right and left eigenvectors of generalized Euler equations. This algorithm is one-dimensional by nature and the similar procedure in other dimensions can be carried out for multidimensional studies.

The general procedure of solution is

- Use reaction solver to update the reaction.
- Calculate viscous fluxes over the stencil.
- Compute Euler fluxes using RF-LLF scheme.
- Update in time using TVD RK-3 time stepping.

The eigenvalues at the interface are calculated based on the H correction principle.

The non-linear WENO weights which get the information about the presence of discontinuity in the given stencil and selects the appropriate stencil for the calculation of the gradient are first calculated.

$$\beta_1 = \frac{13}{12}((f(i-2) - 2f(i-1) + f(i))^2 + 1/4(f(i-2) - 4f(i-1) + 3f(i))^2 \quad (4.7)$$

$$\beta_2 = \frac{13}{12}((f(i-1) - 2f(i) + f(i+1))^2 + 1/4(f(i-2) - 4f(i-1) + 3f(i))^2 \quad (4.8)$$

$$\beta_3 = \frac{13}{12}((f(i) - 2f(i+1) + f(i+2))^2 + 1/4(f(i) - 4f(i+1) + 3f(i+2))^2 \quad (4.9)$$

$\gamma_1 = \frac{1}{10}$, $\gamma_2 = \frac{6}{f}10$, $\gamma_3 = \frac{3}{10}$

$$r_k = \frac{\gamma_k}{(\epsilon + \beta_k)^2} \quad (4.10)$$

$$\omega_k = \frac{r_k}{\sum_{k=1}^{3} r_k}$$

The three third order derivatives are calculated as below

$$f^1_{i+1/2} = \frac{1}{3}f(i-2) - \frac{7}{6}f(j-1) + \frac{11}{6}f(j) \quad (4.11)$$

$$f^2_{i+1/2} = \frac{-1}{6}f(i-1) - \frac{5}{6}f(j) + \frac{1}{3}f(j+1) \quad (4.12)$$

$$f^3_{i+1/2} = \frac{1}{3}f(i) + \frac{5}{6}f(j+1) - \frac{1}{6}f(j+2) \quad (4.13)$$

and combined using the formula

$$f_{i+1/2} = \omega_1 * f^1_{i+1/2} + \omega_2 * f^2_{i+1/2} + \omega_3 * f^3_{i+1/2} \quad (4.14)$$

to calculate the left flux $f_{i+1/2}$. The right flux is symmetrically calculated using the stencil which is right biased. Under the ideal conditions (implying the absence of discontinuity within the given stencil) the final flux of fifth order accuracy is obtained. This procedure is directly applied to the characteristic flux variables to get the final flux in case of RF.

As stated above, the positive reconstruction for f_{cp} and negative reconstruction for f_{cm} are applied to compute the positive and negative contributions to flux and finally

added at (i+1/2) to get the final flux.
The calculated flux is left multiplied by right eigenvector to get the flux and the above procedure is repeated. In the above equation the use of ϵ is made in eq (5) so that the denominator does not become zero. This value was originally given as 10^{-6} by Shu et al. [97]. This value is in dimensional terms and it is appropriate to make this quantity dimensionless as per Henrick et al. [98]. Such a modification has been incorporated into the code.

4.3.2 Boundary Conditions

The calculation of fluxes at the boundary is done by reducing the order to third and second as we move closer to the boundaries. This is done by using the 3rd order counterpart of 5th order WENO and directly calculating the second order flux on the face adjacent to the wall. It should be noted here that this is done without applying any limiter. Other option is to use ghost cells on either side of domain and compute the interpolation using the fifth order WENO on all the faces. The different types of boundary conditions used are:-

a) Adiabatic wall

$$
\begin{aligned}
u_n &= 0 \\
u_{||} &= 0 \\
\frac{\partial C_i}{\partial n} &= 0 \\
\frac{\partial T}{\partial n} &= 0
\end{aligned}
$$

b) Opening

The opening boundary condition is simply incorporated by extrapolating the values from inside of the domain on to the nodes lying on the face of boundary.

	x≤0.03(m)	x>0.03(m)
ρ (kg/m^3)	1.1	0.25
P (kPa)	110	10
U (m/s)	270	170

Table 4.1: *Initial state of the gas across the discontinuity.*

4.4 Test Cases

4.4.1 Real gas test case

The first test case demonstrates the working of code for the real gas shock tube problem [5]. The tube is filled up with oxygen and the initial condition:

The domain is of 0.1 m length which is equally divided into 200 parts. Table 4.1 gives the initial state of the gas. The results of the calculations are plotted at 80 μs shown in Fig 4.2. The figures clearly show the strength of WENO algorithm in capturing shock and contact discontinuity accurately.

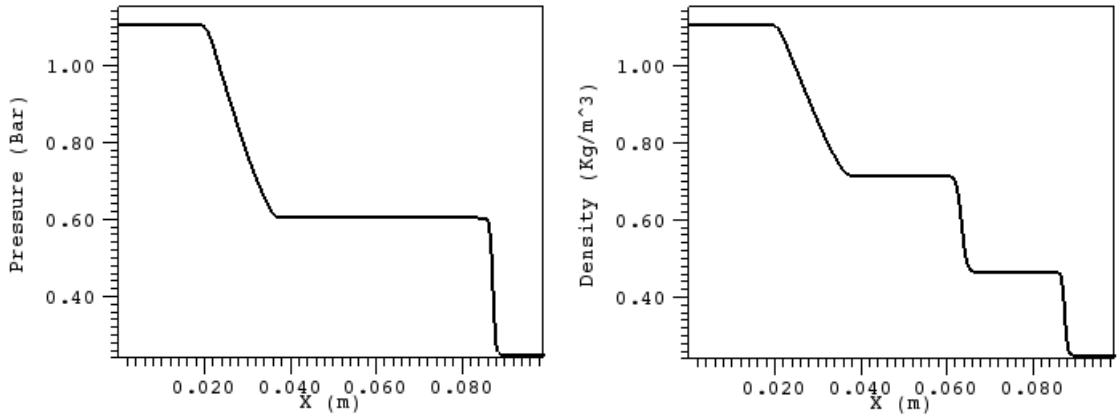

(a) Pressure vs X. **(b)** Density vs X.

Figure 4.2: *Real gas test case with O_2 as test gas; results at 80μs.*

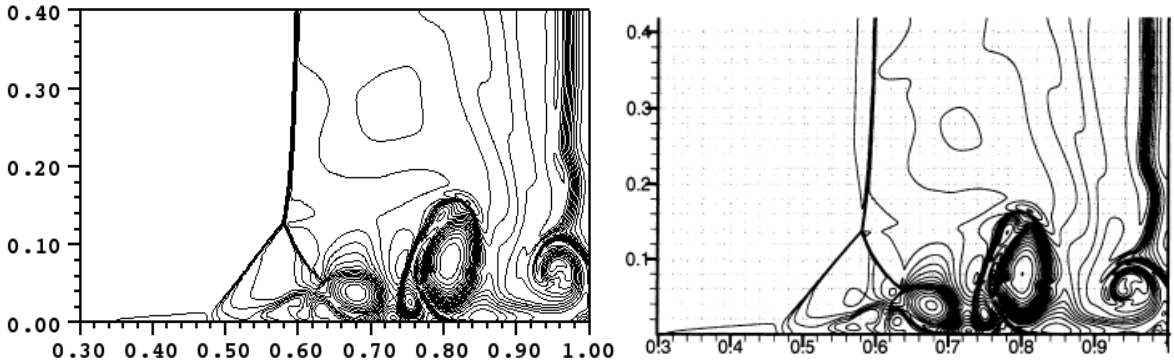

(a) Current scheme **(b)** Ref Daru and Tenaud [99]

Figure 4.3: *Density contours at 1s. Shows the accurate capturing of vortex structure behind the reflected shock. The height of the triple point and secondary vortex is also correctly captured.*

4.4.2 Shock BL interaction

This is a viscous test case which shows the strength of algorithm in capturing the interaction of shock with viscous boundary layer Daru and Tenaud [99]. The test case is set in a domain of 1x1 with 501x501 mesh. This test case is set in a non-dimensional framework with following initial conditions:- The Reynolds number is 200 and Prandlt

	$x \leq 0.5$	$x > 0.5$
ρ	120	1.2
P	$120/\gamma$	$1.2/\gamma$
U	0	0

Table 4.2: *Initial conditions.*

number is 0.73. Fig 4.3 shows the comparison of results with earlier results. They display close resemblance of the vortex structure behind the reflected shock. The height of the triple point and vortex is same in both the figures. Fig 4.4 shows the comparison of density along the wall with the reference computations.

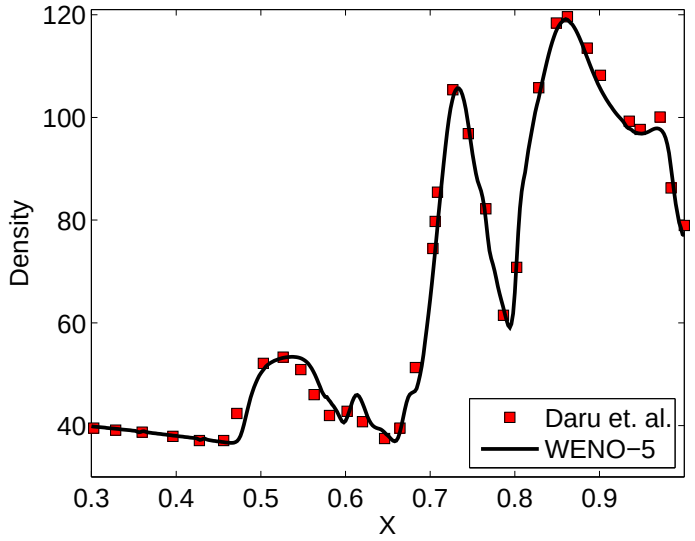

Figure 4.4: *Comparison of density profile along the wall at 1 s after the initial state.*

4.4.3 Detonation 2D structure

This test case shows the development of triple structure of detonation wave for H_2-O_2 mixture diluted by 70% Argon and initial pressure set to 6.667 KPa and temperature of 298 K. It shows the accurate capturing of 2D detonation wave with complex interaction and structures. For this test case Euler equations are solved with the source term for reactions. The flow is initialized by providing the one dimensional detonation structure behind which a small region with high pressure and temperature is kept which explodes forming a single triple wave. As the wave progresses in time it becomes unstable due to development of inflection point near the wall and the second triple shock is formed and detonation propagates at the mean velocity of 1667 m/s . For this reactive mixture, the 1D induction zone thickness is 1.4 mm approximately, and for this test case a resolution of 22 mesh points in the induction zone was chosen. Figure 4.5 and Fig 4.6 shows the comparison of temperature and density gradient profiles between the current scheme and that used by Dieterding [5]. The reference cases shown are computed with 22 cells within induction zone for temperature case and 44 cells for density gradient. The pictures given below clearly depicts the superiority of current scheme in capturing the fine structure behind the detonation front more sharply as compared to the reference. These results are in line with the study of Richtmyer–Meshkov instabilit by Latini et al. [100]

where the authors have clearly shown the better capturing of instability in mushroom structure using WENO scheme.

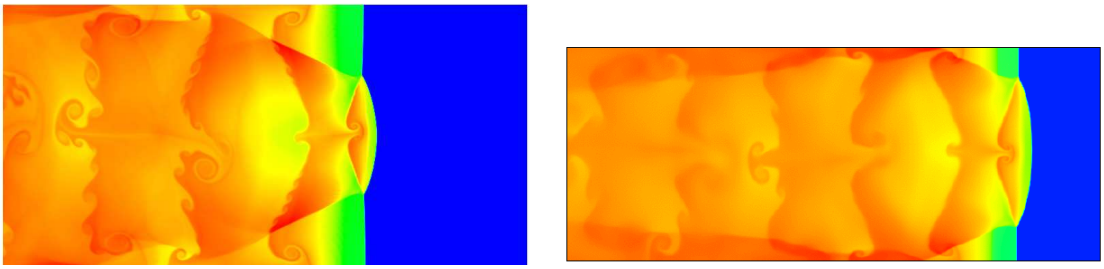

(a) Current scheme **(b)** Ref [5]

Figure 4.5: *Temperature profile of 2D H_2-O_2-Ar detonation. The fine instability structures seen developing behind the detonation front have been very accurately captured using the current scheme while they are diffused in the reference case.*

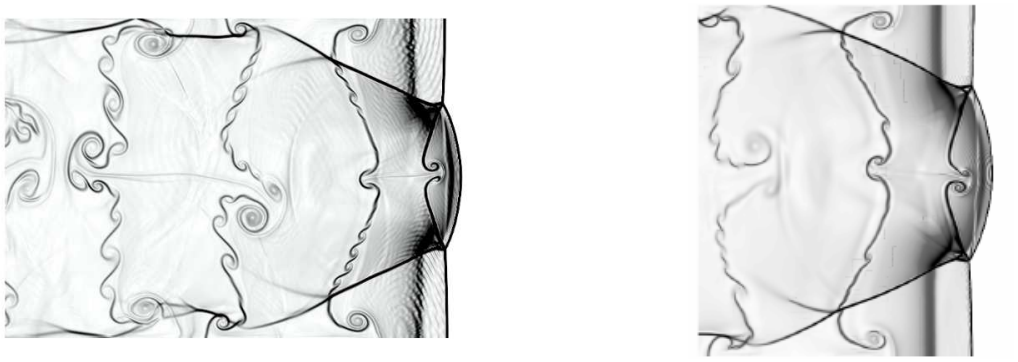

(a) Current scheme **(b)** Ref [5]

Figure 4.6: *Numerical schlieren of 2D H_2-O_2-Ar detonation. We can see the fine structures behind the detonation front using 22 points in induction zone which are clearly visible using WENO5 while they are diffused in reference test case even after using 44 point in the induction zone.*

4.4.4 One dimensional H_2-O_2 flame structure

This test case represents the one dimensional flame propagation. This test case is initiated by giving central ignition and flame propagates to either end ;as flame propagates it leads to rise in pressure ahead of flame which reduces the flame velocity. In this simulation initial flame velocity of 11 m/s was measured which reduces to 8 m/s as flame propagates through the domain. Figure 4.7 and Fig 4.8 show the variation of various properties across the flame. For this test case a mesh of 10 μm was selected. As can be seen from the figures below this mesh size captures most of the features accurately.

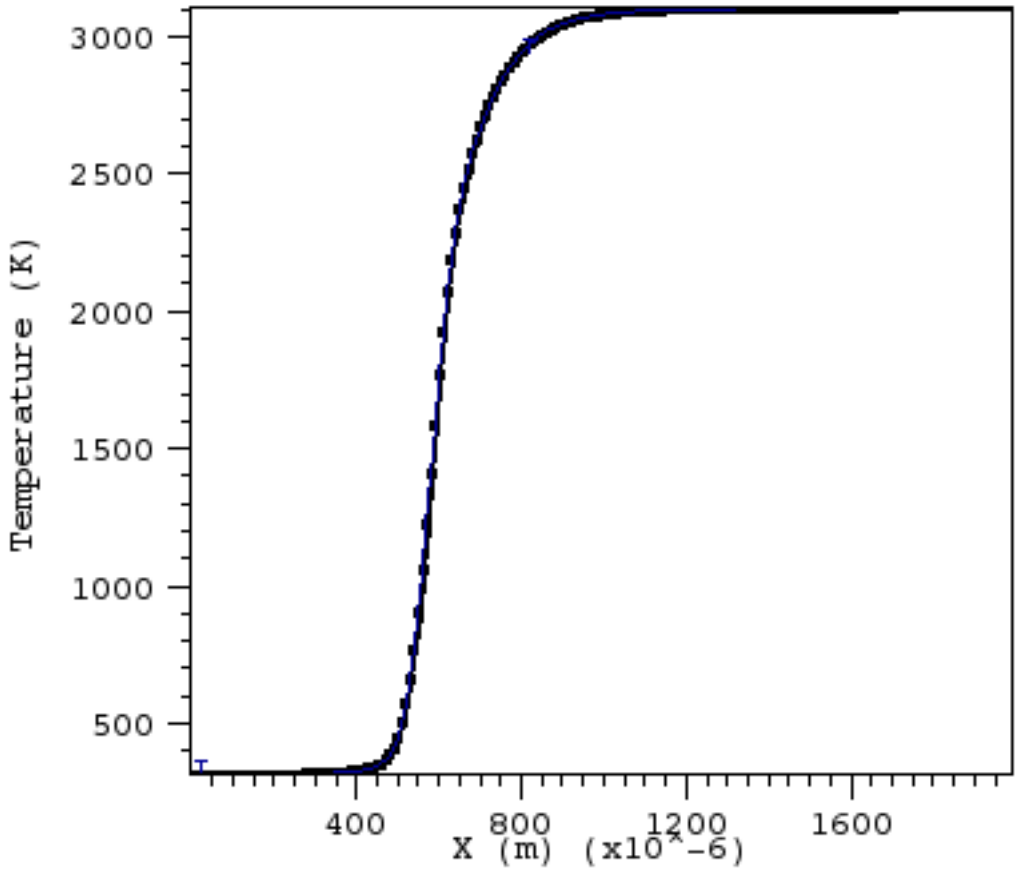

Figure 4.7: *Temperature distribution across H_2-O_2 flame. CEA gives value of temperature of 3086 K.*

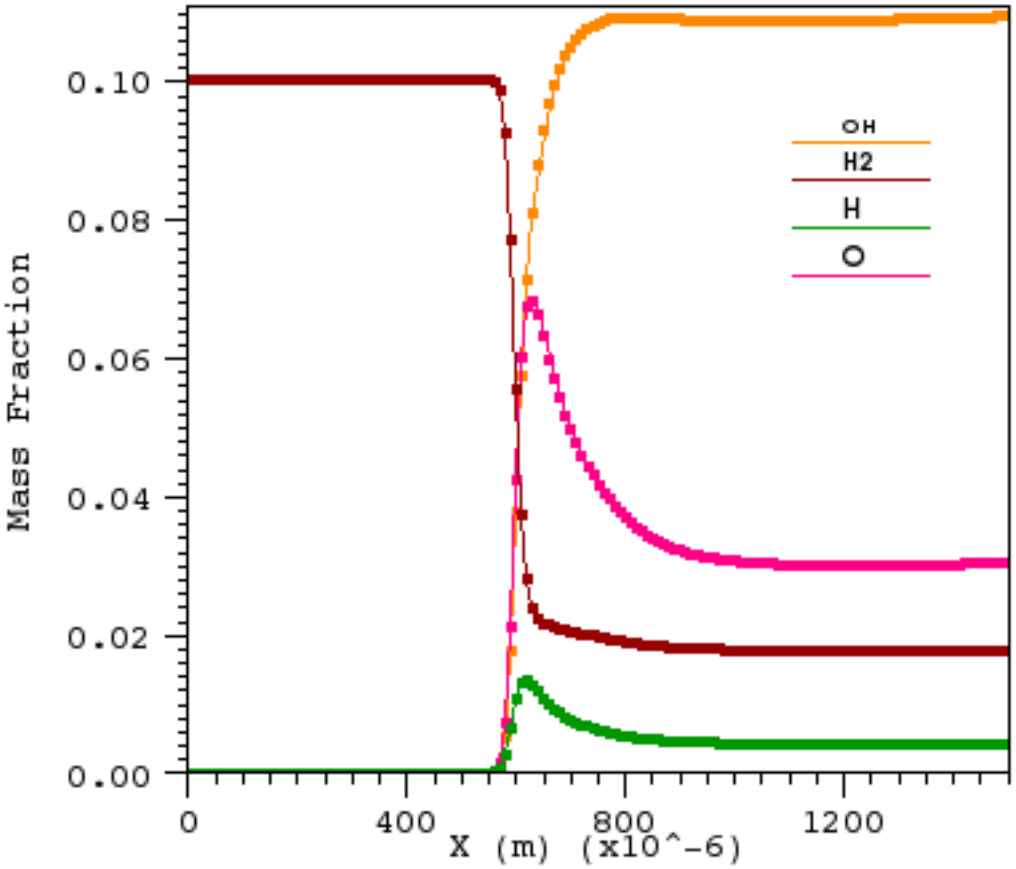

Figure 4.8: *Mass fraction of species across flame. CEA values for various species are OH=0.13, H_2=0.019, H=0.005, O=0.034.*

4.5 Summary

In this chapter a brief description of the WENO-5 algorithm was provided. Various reactive and non reactive test cases have been tested using this numerical scheme. The results gave reasonably good comparison with respect to the earlier test cases. In the next chapter these numerical schemes will be used to study the DDT and interaction between flame and shock.

Chapter 5

Numerical study of DDT

5.1 Study of DDT in micro channel with stoichiometric H_2-O_2

This chapter describes the problem setup and the results from the study of DDT in micro channels using the scheme developed in the previous chapter. M. A. Liberman [101] and Aikun et al. [102] have conducted studies in micro channels. While Liberman's work is around two dimensional channels, the calculations of Aikun are three-dimensional.

5.2 Numerical setup and domain

In the present study the numerical domain used was a rectangular channel with closed wall on three sides and open on one side. The whole domain is filled with stoichiometric H_2-O_2 mixture. From the previous study it was known that mesh size of 10μm was found to be accurate enough to capture the correct flame speed for stoichiometric H_2-O_2 mixture. As flame accelerates thorough the channel there is increase in pressure and temperature in front of flame which eventually will lead to decrease in flame thickness. Taking this point into consideration for this study, the uniform mesh size of 5 μm was used. From the mesh refinement study it was found that for most part of propagation regime both mesh sizes resulted in same acceleration profile. The mesh was moved along the flame shock interface in such a way that the resolution within the interface was not effected. The Courant number of 0.3 was used for most part of simulation

except for the final transition part where the Courant number less than 0.1 was used. The flame is initiated in the simulation by placing a uniformly hot mixture of H_2-O_2 at 1500 K in small region of 0.5 mm near the closed end of the tube.

5.3 Results and discussion

The initial set of experiments were conducted with pure stoichiometric H_2-O_2 mixture. The computer simulations were performed in tubes of 0.5, 0.25, 0.2 mm diameter. For all simulations 19 step reaction mechanism proposed by Jachimowski [4] presented in Table **??** was used. These mechanisms have been previously used for studying detonation in H_2-air mixtures for different equivalence ratios given by Yungster and Radhakrishnan [103].

Figure 5.1 shows the pressure profile as the flame accelerates through the tube. In the initial phase of flame acceleration up to 83.7 μs maximum pressure is 10 bar but it picks up to 40 bar by 86.1 μs and finally the transition takes place within 0.2 μs.

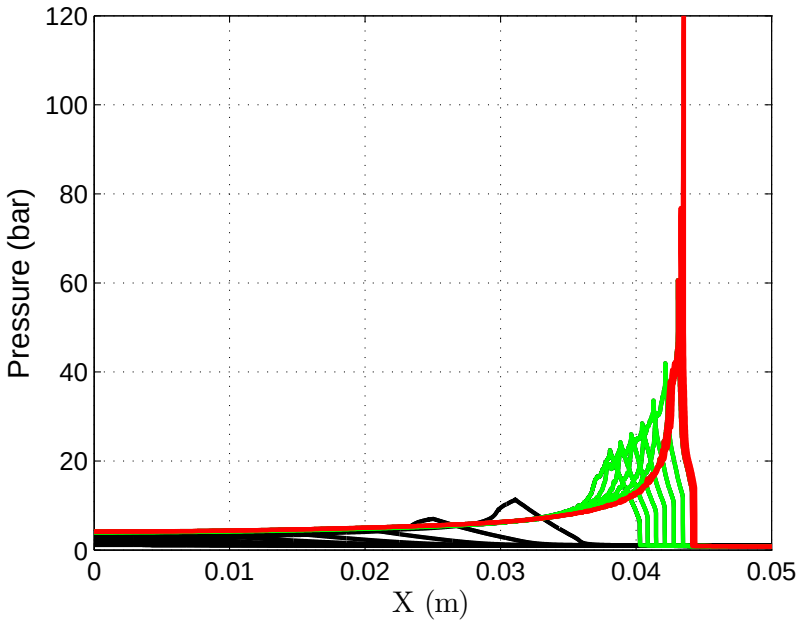

Figure 5.1: *The variation of pressure with x for different times. Black: time up to 83.72 μs, Green: time up to 86.07 μs, Red: time up to 86.20 μs. There is a strong exponential growth prior to final transition.*

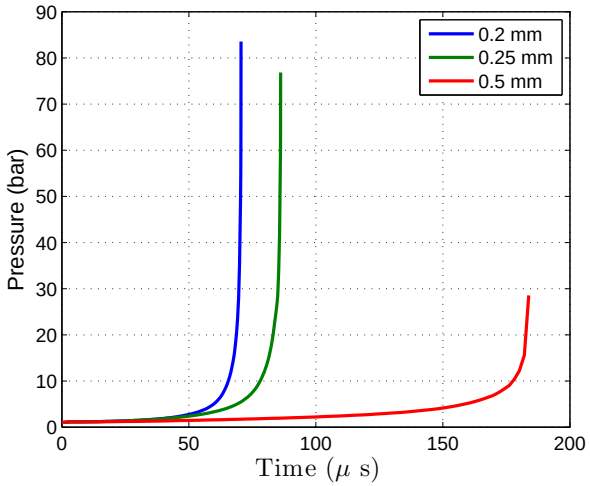

Figure 5.2: *The variation of peak pressure inside the domain with time.*

Fig 5.2 shows the variation of maximum pressure in the domain for all the cases. From the trends it is clear that there is an exponential growth of pressure in front of the flame as it accelerates through the tube before transiting to detonation. This is in accordance with the flame acceleration law M. A. Libermann [90] where:

$$V = \frac{dx}{dt} = Aexp(kt)$$
$$k \approx \frac{A}{R}, A \approx \Theta U_f, \Theta = \frac{\rho_u}{\rho_b}$$

Here, V is the flame velocity and U_f is the laminar flame velocity and Θ is the density ratio across the laminar flame. The three cases of flame acceleration and transition shown above are set out with this relation and the results are presented in Fig 5.3. The value of A used in the present case was 13 for 0.2mm,14 for 0.25mm and 15 for 0.5 mm channel. The value reported in M. Kuznetsov [104] is 70 for stoichiometric mixture of H_2-O_2 with initial pressure of 1 bar. This discrepancy is due to the fact that simulations are performed in 2D channel where the initial flame acceleration will be much lower. The case of 0.2 mm closely follows the theoretical curve. In case of 0.25 mm initial acceleration of flame is higher than theoretical curve, this is because same initial high temperature zone is provided over the same width which leads to faster initial acceleration. For the case of 0.5 mm channel theoretical curve differs from the computational result (see the right most two curves in the Figure Fig 5.3) as boundary layer is not fully

developed in this case and a weak shock is formed in front of the flame. Above relation is derived from the linear theory and is limited in validity as this relation is valid for the case where boundary layer is fully developed and no shock is present in front of the flame. This is primarily due to neglecting the gas-dynamic effects by the theoretical model and variation in laminar flame velocity is also neglected. Dynamics of flame acceleration in presence of the shock is completely different as shock itself derives the energy from the accelerating flame and there is a dynamic coupling between the shock strength and the temperature and pressure of gas in front of flame. This is a non-linear coupling which is not considered in the simple theoretical models of flame acceleration in tube using above relation. Further if the flow is turbulent, flame acceleration becomes more complicated. In recent work Kessler et al. [53] performed 2D simulation in large channels with obstacles and single step chemistry for methane air DDT and were able to reproduce experimental results for DDT. This further shows that for larger channels the effect of turbulence and shock dynamics are very important and both of these play most critical part in flame acceleration to detonation. These effects cannot be captured using the simple flame acceleration models.

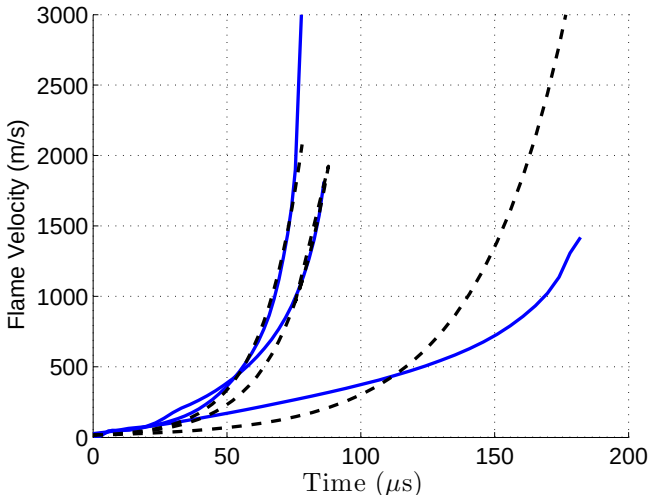

Figure 5.3: *Comparison of flame acceleration for three channels with the theory. Value of coefficient A used for the three cases is 13, 14 and 15 for 0.2, 0.25 and 0.5 mm respectively (left to right). Dash lines are curve fits, Solid lines for the three channels respectively.*

5.3.1 Grid dependence study

The study of grid dependence was carried out for 0.25 and 0.5 mm channel case. The simulation were carried out using 10 μ and 5 μ mesh size. Figure 5.4 compares the velocity profile of the flame for the two cases. It shows less than 2% variation between the two cases.

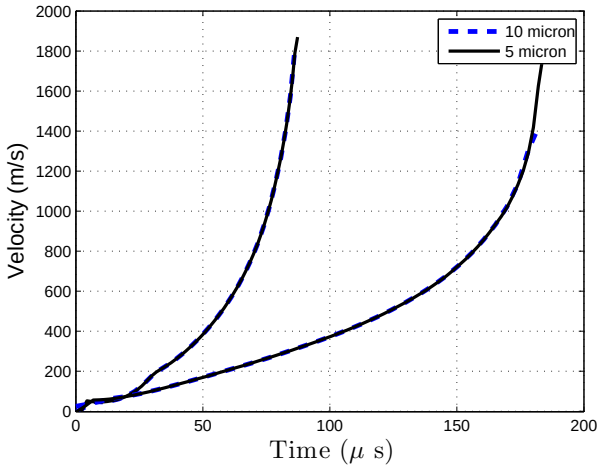

Figure 5.4: *Comparison of velocity variation with time for 0.25 and 0.5 mm cases using 5 μ and 10 μ mesh. Net variation of less than 3 % has been observed*

5.3.2 Effect of reaction mechanism

As there are several reaction mechanisms available for H_2-O_2 system. For comparison simulations were conducted with Westbrooks 34 step chemistry Table **??** (see Dieterding [5]). Figure 5.5 shows the comparison of flame velocity for the two reaction mechanisms. Flame acceleration for both the cases till 150 μs is similar. In the later phase Jachimowski's reaction mechanism shows faster acceleration compared to Westbrook's. The reason for this deviation can be accounted for by the fact that as the velocity of flame increases there is increase in pressure and temperature ahead of the flame affecting the third body reactions for the two cases.

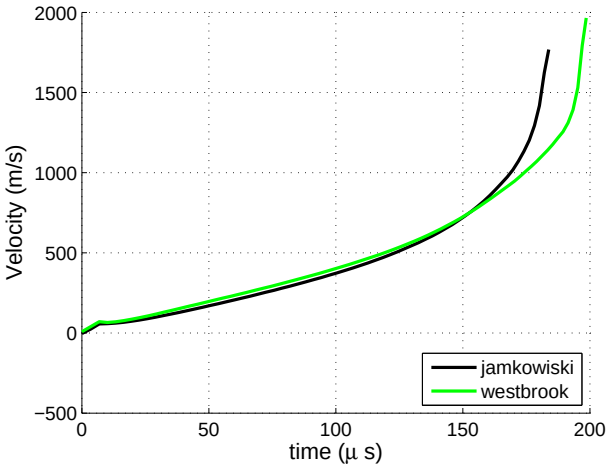

Figure 5.5: *Comparison of Flame velocity vs time for the two reaction mechanisms.*

5.3.3 Flame length variation and transition

Figure 5.6 and Fig 5.7 show the variation of flame length with time for three channels. Flame length was measured as length of 2000 K isothermal contour. For all the three cases the peak value of normalized flame length was close to 10. As the flame is accelerated along the length of the tube it gets stretched due to no slip condition at the wall which leads to increase in flame surface and velocity. Due to continuous production of pressure wave ahead of flame strong shock waves start developing very close to the flame front. Due to the increase in pressure the flame length starts decreasing and front becomes thinner this makes the flame more unstable this is triggered by Ritchmayer-Meshkov instability. Flame becomes corrugated and pressure waves developing at the flame front start interacting with each other which triggers closer to the flame front. Figure 5.8 and Figure 5.9 show the profile of temperature, pressure and species variation close to the flame front.

Recently published results by M. A. Liberman [101] are in similar lines with the present work. They were able to capture the transition at the flame tip which is similar to what was observed in our studies. The algorithm used in their study was of first to second order accuracy which is diffusive in nature. This leads to over prediction of flame and boundary layer thickness due to which the flow ahead of flame gets altered. The critical channel thickness of 0.5 mm obtained by them is higher than 0.2 mm predicted by present work. Aikun et al. [102] conducted 3D DNS study, using spectral schemes

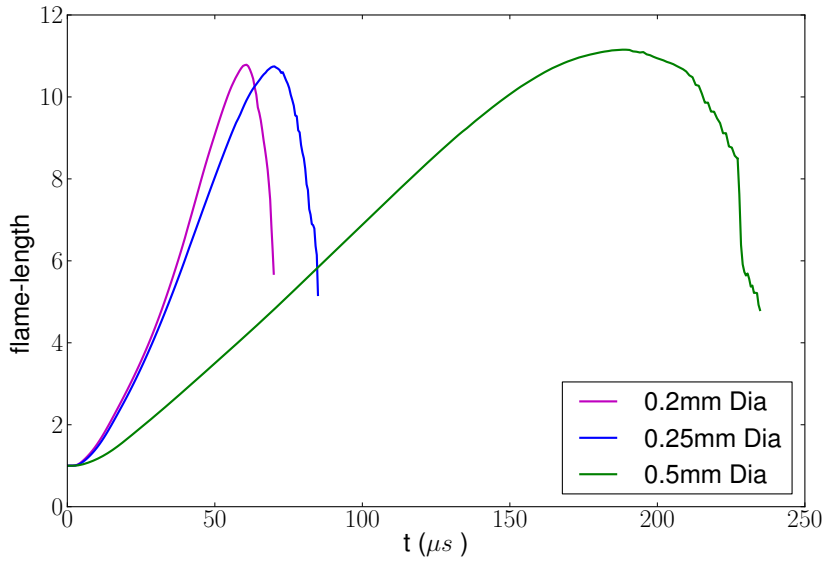

Figure 5.6: *Variation of flame length (normalized by channel width) with time.*

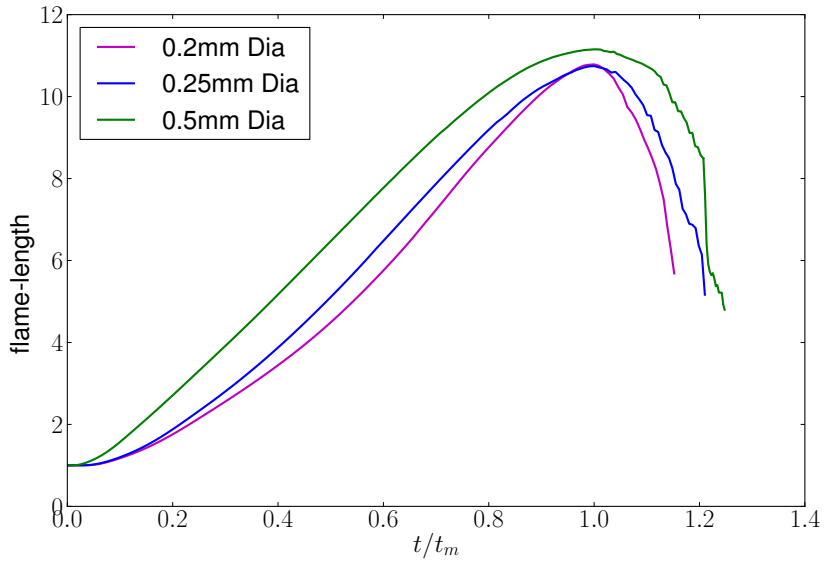

Figure 5.7: *Variation of flame length (normalized by channel width) vs time normalized with respect to time at maximum flame length.*

for studying H_2-O_2 flames in micro channels, it was concluded that flame propagated in the parabolic form for channels up to 0.2 mm in thickness though with much reduced

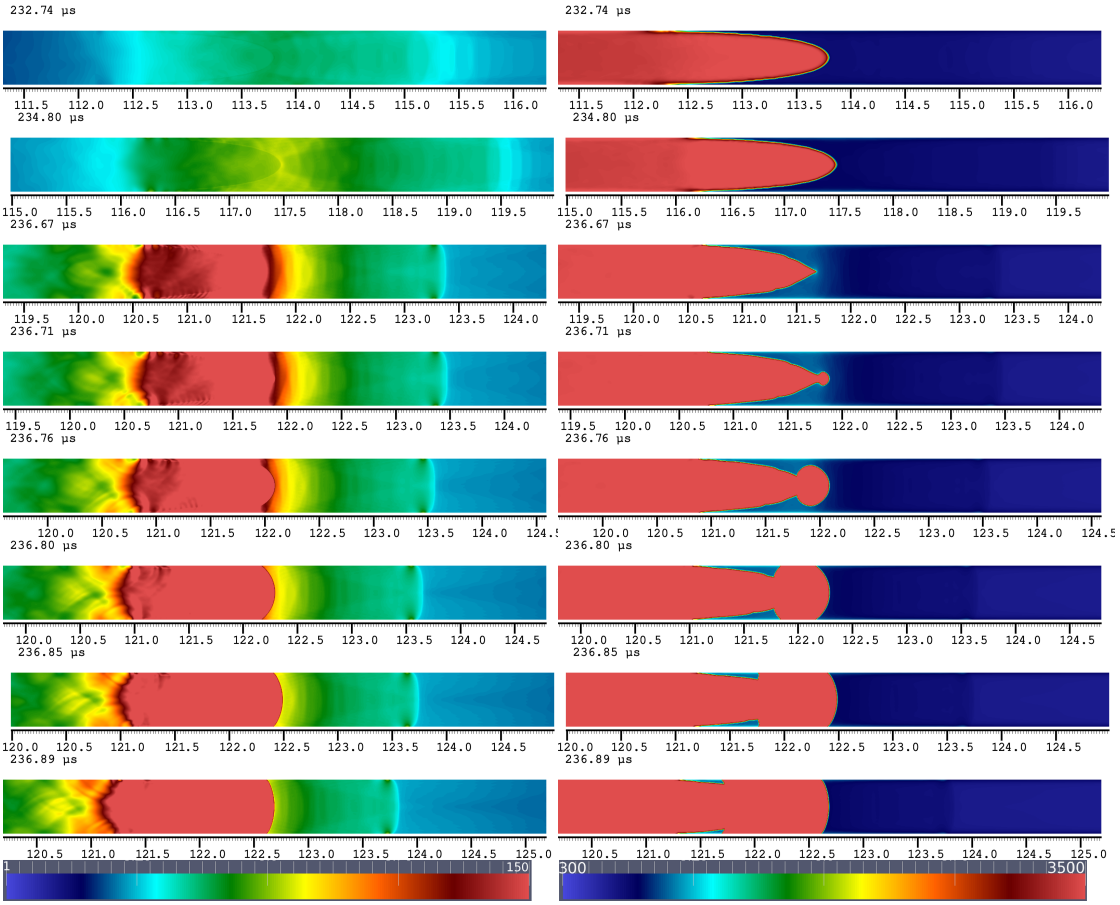

(a) Pressure (bar) **(b)** Temperature (K)

Figure 5.8: *Pressure and temperature profiles 0.5 mm channel. [As flame propagates through the tube it gets elongated. Close to the transtion the shock develops close to the flame which decreases the flame length and final transition takes place at the tip of the flame.]*

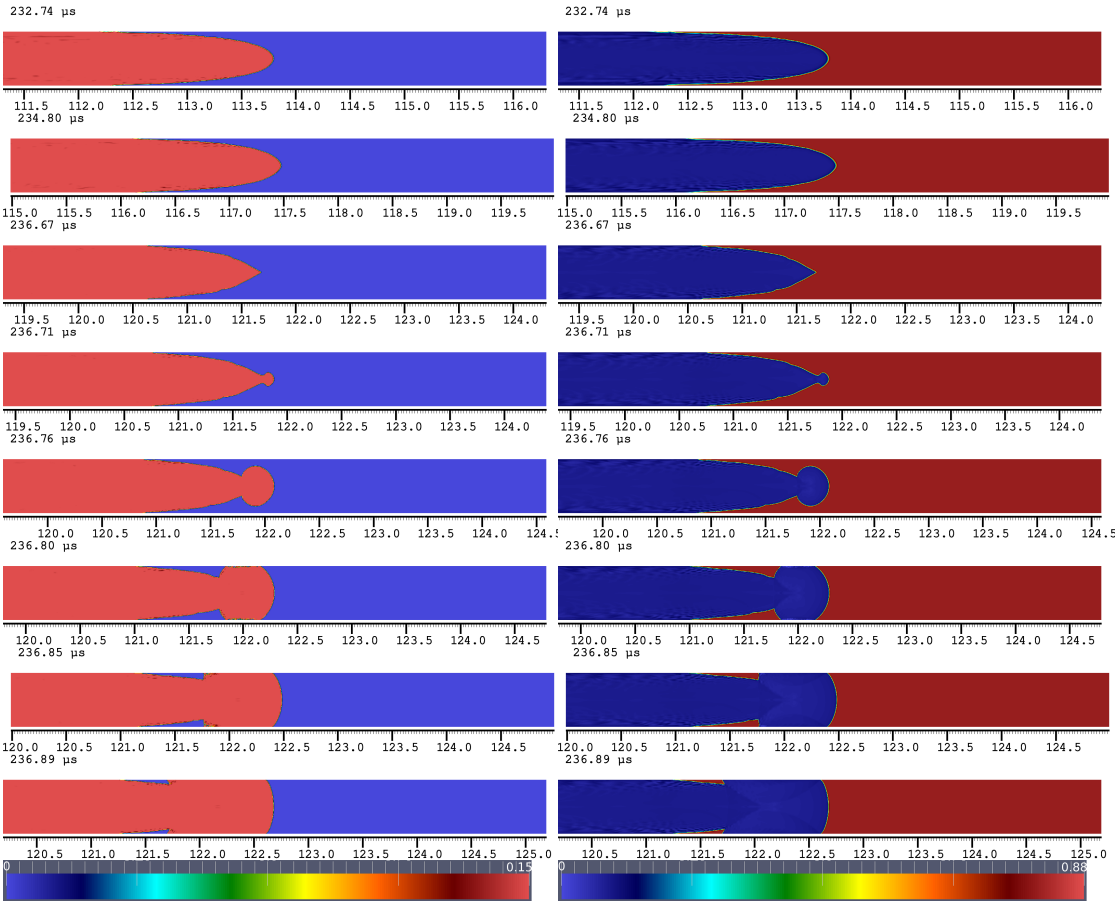

(a) OH **(b)** O2

Figure 5.9: *Profiles of species mass fraction as flame accelerates through the channel of 0.5 mm width.*

length as compared to 0.5 mm channels.

5.4 Initial condition variation

The above simulations were repeated with change in initial conditions. For this set of simulation higher energy was introduced in the smaller initial portion of the channel with temperature of 3500 K as compared to 1500 K in the earlier simulations. These simulations were carried out only in the domain of 0.5 mm channel width. The results exhibited some fundamental variation as compared to the earlier results.

5.4.1 Initial flame acceleration

The acceleration of flame and final transition to detonation are shown in Fig 5.10. The flame accelerates from the close end of the tube towards the open end of the tube with the formation of a weak discontinuity in front of it. This wave propagates at a sonic speed with respect to the unburnt mixture ahead of it followed by the accelerating flame behind it. The accelerating flame gradually gains speed till it becomes greater than the shock. This is simultaneously coupled by the gradual build up of pressure behind the constant velocity pressure wave, and this leads to the gradual build up of shock strength

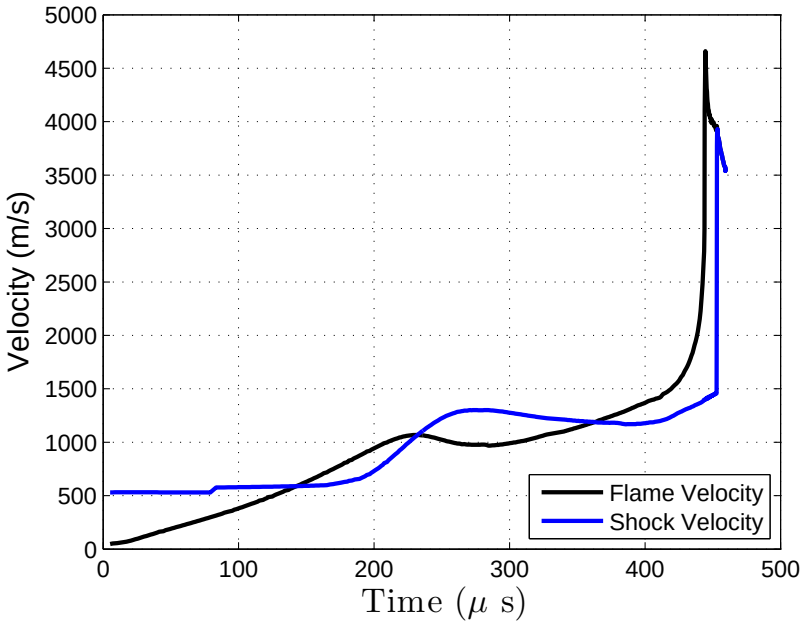

Figure 5.10: *Flame and shock velocity vs time.*

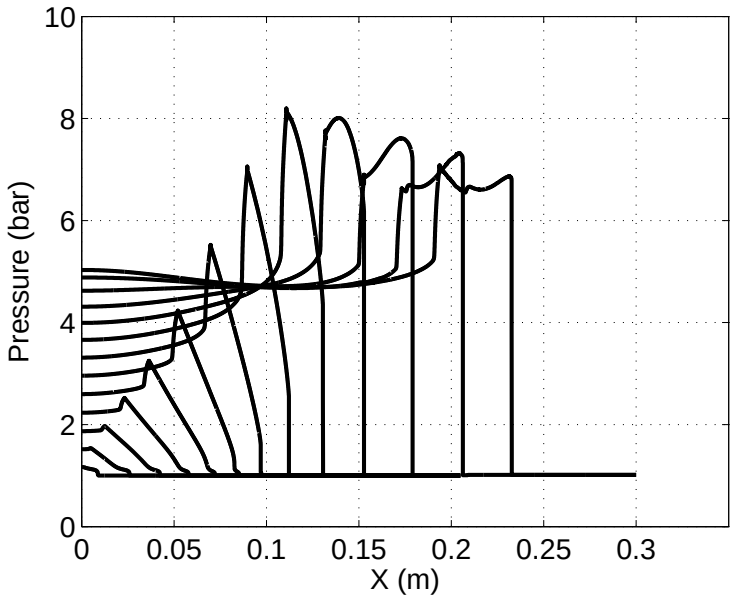

Figure 5.11: *Pressure profile at different times.*

as the flame is constantly pushing the flow ahead of it like a piston. Close to the flame there is build up of pressure that increases in strength as the flame accelerates which is similar to earlier cases.

5.4.2 Flame deceleration

This is followed by the phase of deceleration of flame similar to the observations in the experiments carried out by Ming-hsun Wu [89]. The method of ignition used in the present study leads to production of weak compression wave ahead of the flame which seems to move just ahead of the accelerating flame. The accelerating flame produces the compression waves ahead of it which at around $t = 200\mu$s coalesces with this forward moving compression wave and a build up of shock formation can be observed. M. Kuznetsov [104] has recently performed experiments in millimeter scale tubes and such coalescing of compression waves leading to build up of shock are observed in his work.

Figure 5.11 shows the formation and build up of shock in front of accelerating flame. The build up of pressure behind the shock wave, decelerates the flow at around 0.23 ms hence the flame speed with reference to fixed coordinates also decreases. This period

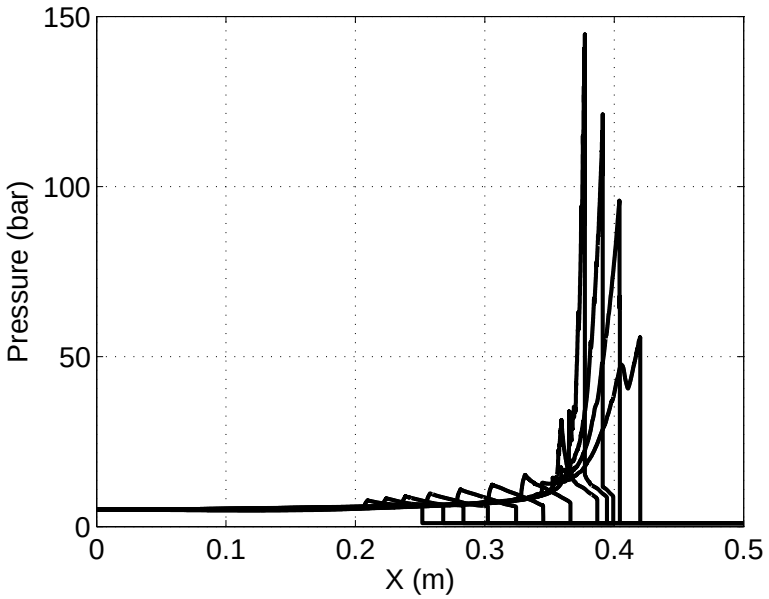

Figure 5.12: *Pressure build up in front of flame leading to transition*

is significant due to the pressure build behind the shock the initial build up of pressure near the flame front gets affected. Ming-hsun Wu [89] have cited the heat loss to be one reason for such deceleration in their experiments. Such deceleration is not observed in the work of Jun-Kai Wang [91] since they used either adiabatic or isothermal wall conditions to study DDT. The dynamics of build up of pressure in front of accelerating flame is the reason for this deceleration.

5.4.3 Second phase of acceleration

This small deceleration front is followed by the reaccleration of the flame and in this second phase the flame accelerates continuously behind the shock. The pressure again starts to build up at the flame front as shown in Fig 5.12. The experimental results of Urtiew and Oppenheim [31] have indicated that the precursor shock traveled at around Mach no 2-3 producing a pressure of 5-6 bar in front of the flame. In the present simulation the pressure ratio of around 6 bar is obtained. Flame accelerates to speeds between 1000-1500 m/s before transiting to detonation.

5.4.4 Transition to detonation

The formation of detonation wave is shown in the series of density gradient, Schelerin plots below. The flame propagates without any wrinkles for major part of the flow and then starts developing wrinkles around 400 μs and then, in a very short time transits to detonation. The appearance of wrinkles on the flame front is like the points of density gradients which are not aligned and this can lead to production of Richtmyer-Meshkov instability at the flame front. The cusp of this wrinkled flame acts as a source of pressure wave getting concentrated at the front of the flame and continuing to amplify with the passage of accelerating flame. As in the previous case flame develops corrugations which leads to pressure waves interacting within themselves and the flame itself. These waves appear to get accumulated at the tip of the flame leading to the formation of a bow shock at the front. After this, the pressure starts to increase rapidly behind the tip of accelerating flame and this finally causes transition to detonation. The final phase of transition to detonation takes place at the flame tip where a strong explosion wave propagates in the shocked gas due to the build up of pressure. The pressure obtained in these results was very high around 200 bars which corresponds to the ratio of 50 approximately. From simple calculation a detonation wave propagating at Mach 5.2 into H_2-O_2 mixture at 6 bar pressure should lead to pressure ratio of 25 but the present ratio seems to be very large as compared to that. This discrepancy may be due to the 2D nature of the calculation which does not produce relaxation in the third direction. The rise time for this whole process is very small which may be one of the reason for the attainment of such large pressure ratio in short period of time which is less than 5 mus. This peak pressure seems to be over predicted but as per Urtiew and Oppenheim [31] they measured the peak pressure of over 80 atm in their study. This was interpreted by authors to have occurred due to very short rise time of pressure at the shock front. As the final transition period is of very short duration it is practically difficult to get the correct value of peak pressure during transition.

5.4.5 The strength of precursor shock

The present study deals with the importance of refining the region between the flame and the shock so that the build up of shock wave from the coalescing of weak compression wave can be correctly captured. The importance of this can be inferred from Fig 5.15 that show the pressure profiles of accelerating flame and the flame speed respectively.

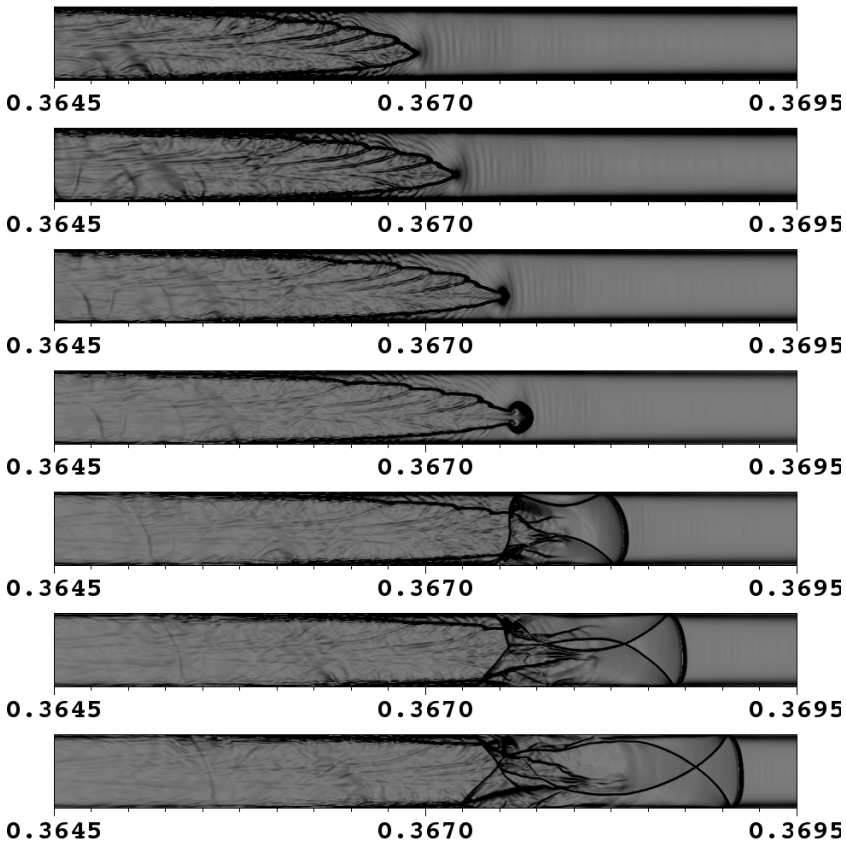

Figure 5.13: *Density gradient images of final phase of flame propagation prior to transition.*

This computation was carried out with a mesh size of 20μm. The delay in the build up of shock in front of the flame leads to inhibited growth of flame leading to the formation of detonation wave. This simulations points to the fact that if the build up of shock in front of flame can be avoided it may lead to a very short transition lengths at least for the case of highly reactive mixtures like H_2-O_2.

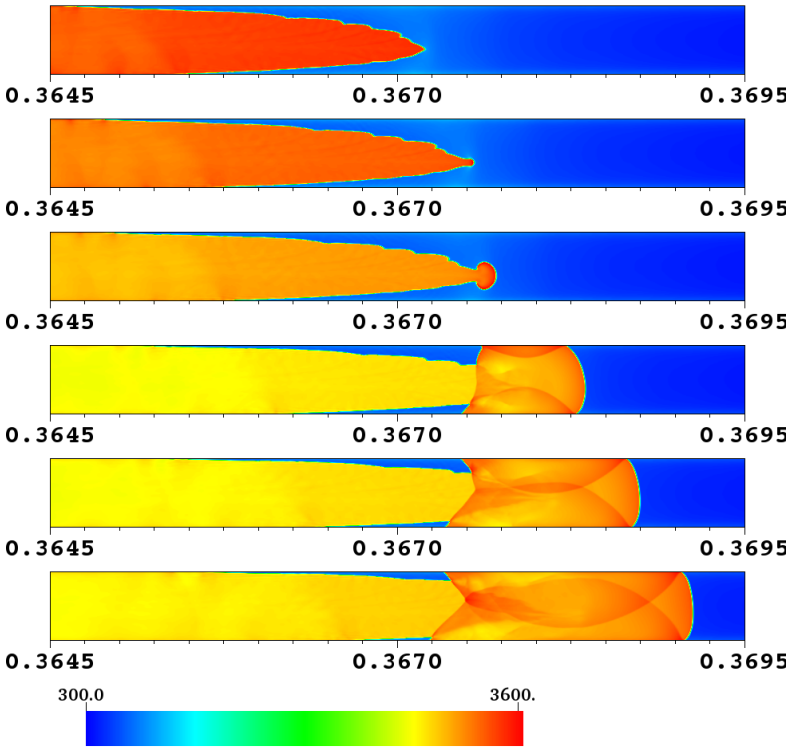

Figure 5.14: *Temperatures profile of flame propagation close to transition. Images show the transition in the duration of 1μs before transtion.*

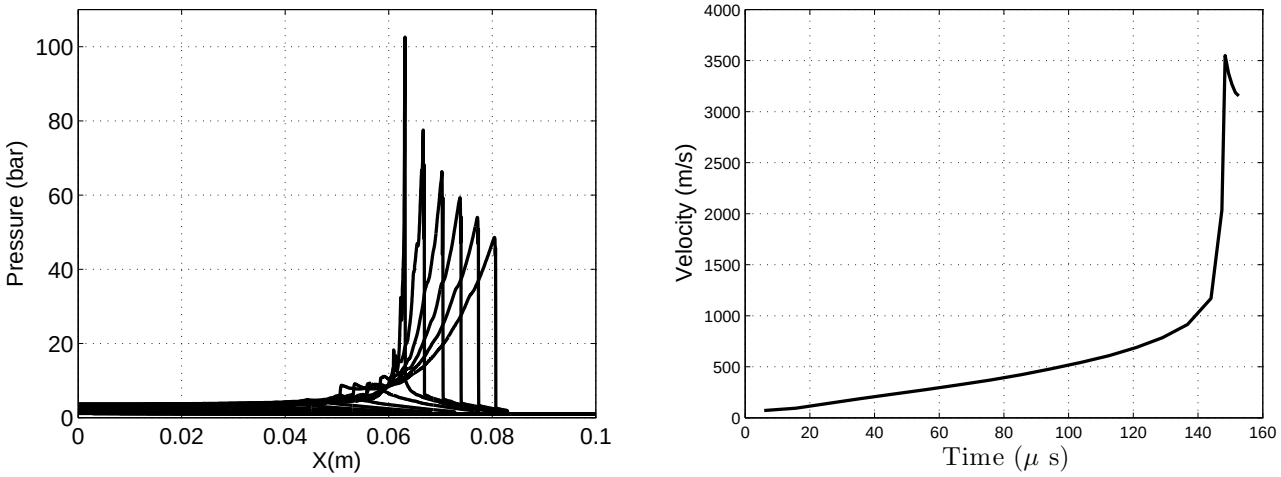

(a) Pressure Profile at various time steps.

(b) Velocity Vs time for coarse mesh.

Figure 5.15: *Simulation with coarse mesh.*

5.5 Strong Initiation

In this section a brief study of the effect of wrinkling of flame surface on the DDT is presented. Initial condition for the test case was set as temperature of 2000 K and pressure of 50 bar in the small region of 0.5 mm near the closed end of the channel of 1 mm width. Figure 5.16 show the pressure and temperature plots at various times. Figure 5.17 shows the pressure and temperature profiles in 2D and transition to detonation clearly takes place between the flame and the shock. Flame propagates behind the shock and due to no slip condition at the wall the flame close to wall propagates faster and this wrinkles the planar flame. This wrinkled flame acts as a source of pressure waves which interact with the forward propagating shock and this leads to formation of hot spots between the shock and flame which eventually triggers the transition to detonation.

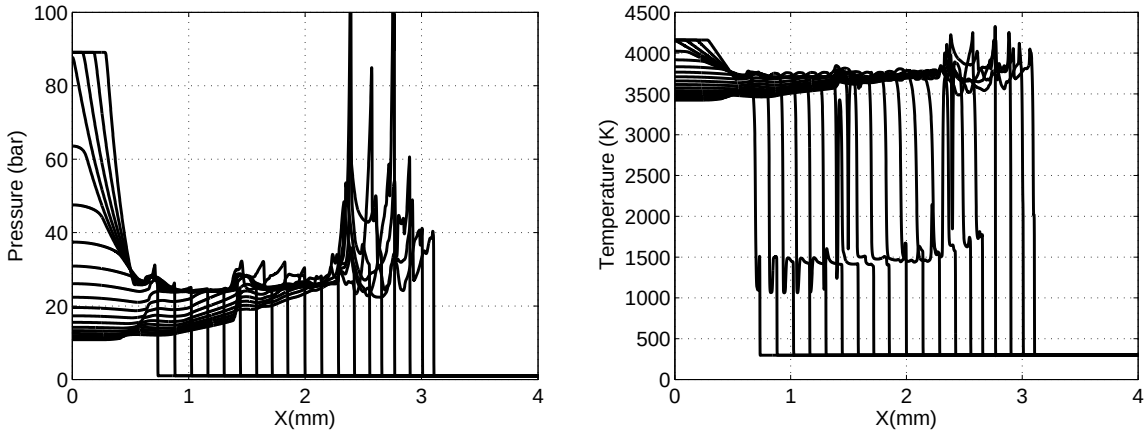

(a) Pressure vs X

(b) Temperature vs Time

Figure 5.16: *1-D plots of pressure and temperature for different times for wrinkled initiation with slip condition. In this case explosion takes place between the flame and shock and final transition to detonation occurs.*

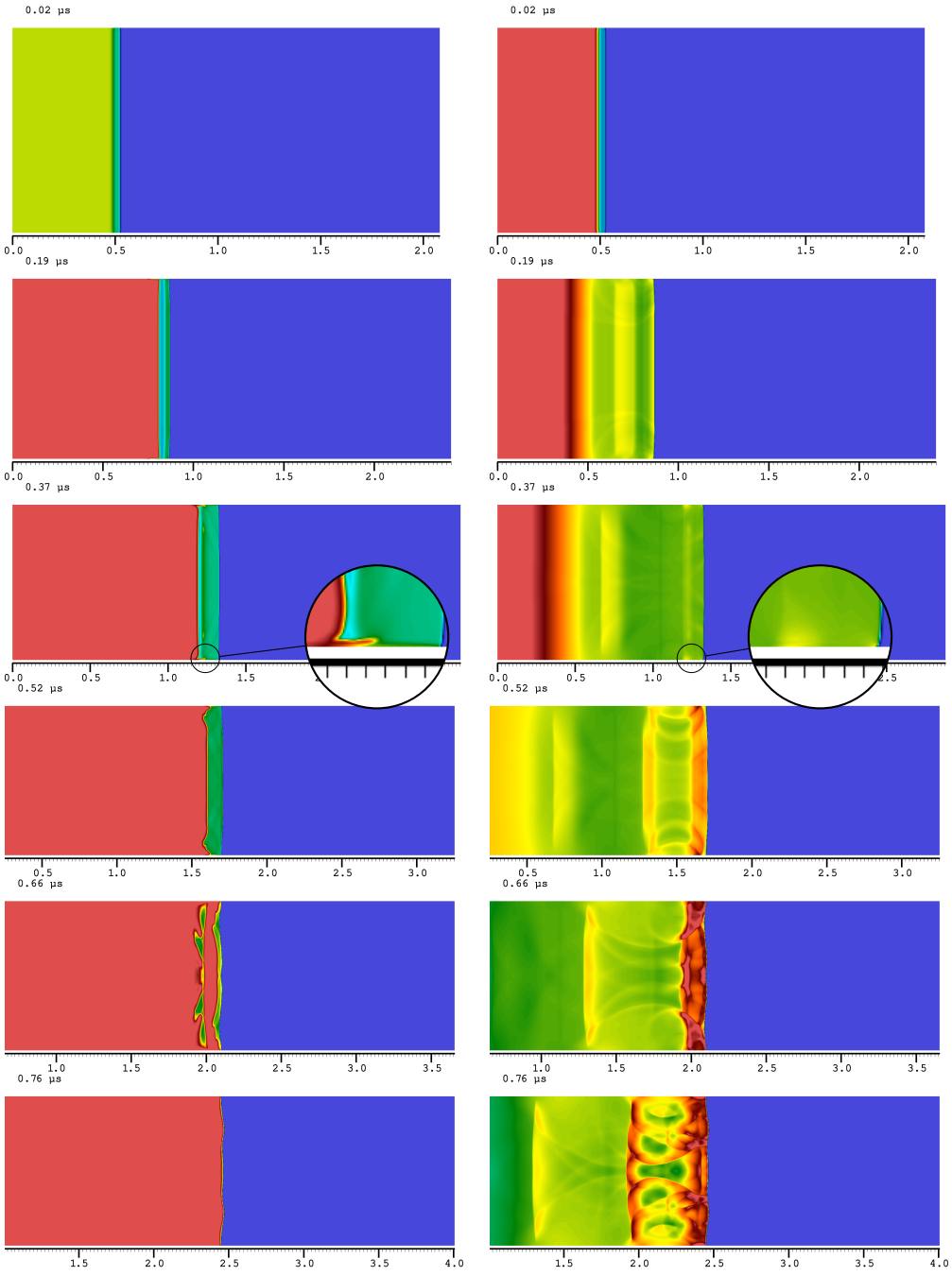

Figure 5.17: *Pressure and temperature variation in domain for strong initiation with no slip condition at the wall.*

5.6 Summary

In this chapter the study of the process of the formation of detonation is delineated through careful numerical simulations. Simulation of DDT in micro channels show increase in DDT length with the increase in width of channel. Flame gets elongated as it moves along the channel width. This leads to increase in flame surface area leading to higher consumption of fuel which further increases the flame velocity. Increase in velocity ahead of flame leads to increase in flame length. With the build up of pressure, shock waves move closer to the flame leading to decrease in flame length and flame thickness. This leads to development of instability and final transition to detonation is close to the region where flame length reaches its maximum value. Normalization of flame length with time profiles show the data collapsing to similar profiles.

Simulation carried out with changed initial condition using Westbrook's reaction mechanism shows a different mode of flame acceleration and transition to detonation. The initiation at the closed end is done by giving high temperature of 3500 K at the closed end. This leads to small pressure wave which moves ahead of the flame. As the shock wave moving ahead of flame catches up with this pressure, the shock wave is triggered to increased strength leading to formation of strong shock ahead of the flame. This also leads to a slow down of the accelerating flame.

In the final section effect of flame wrinkling is studied using strong initiation at the closed end. High pressure and temperature is provided at the closed end with planar initiation. No slip condition with planar initiation leads to faster flame propagation near the wall which leads to the flame becoming wrinkled and final transition takes place between the wrinkled flame and the planar shock moving ahead of the flame.

Chapter 6

Conclusions and future work

6.1 Conclusions

This thesis has dealt with the study of experimental and numerical study of acceleration and transition of a deflagration wave to detonation wave. In the experimental section, the main focus of this work has been to study the effect of flame acceleration on the impulse produced by the PDE. Impulse in the PDE is generated by the action of pressure generated by detonation wave on the head end of the tube. The results show that optimum specific impulse generated inside the PDE is regulated by the heat loss and the initial flame acceleration before DDT takes place. Further enhancement can be caused by using the pressure behind the detonation wave at the end of propagation regime by partially filling the detonation tube. Earlier studies have shown that L/D ratio can be optimized to get maximum specific impulse using full fill. The studies carried out in the current thesis using two tubes of different lengths but with the same diameter show that higher specific impulse can be obtained with longer tube (larger L/D ratio) in comparison to the optimum value. These results show that the impulse continues to be enhanced without saturation with increase in the length of tube beyond the presence of the combustible mixture.

The study of initial flame acceleration before transition to detonation was carried out in three different experimental setups using different flame acceleration mechanisms like spirals and orifice plate. In the first configuration, the flame is accelerated in smaller tube and this leads to the attainment of a quasi-detonation with velocity near 1100 m/s. This is achieved in smaller length of tube and in lesser time. The transmission of this

quasi-detonation in the larger tube further enhances the flame acceleration leading to reduction of length and time of DDT. The study of transmission for different equivalence ratio has shown enhancement in transition with DDT length of 70 cm for mixtures up to $\phi = 0.55$.

The use of extension tube with larger tube of 42 mm diameter with lengths of 1 and 2 m leads to transmission of decoupled shock and flame inside the tube. The placement of spiral attached with orifice plate at its end in the path of transmitted flame leads to production of decoupled shock flame configuration which travels close to choked flame velocity. It is observed that the impulse generated with this configuration is similar to one produced by ignition at head end leading to the formation of CJ detonation wave with similar blockage configuration. The impulse generated under partial fill condition for both the cases show higher impulse generated with the attachment tube as compared to ignition inside the larger tube. This is inferred to be due to faster acceleration of the flame inside the smaller tube which leads to faster rise of pressure at the head end of the tube.

The second configuration tested is of 25 mm diameter and 1 m length. In this case the effect of attachment tube is diminished as faster acceleration of flame is achieved even in the smaller tube diameter. With the same tube, several experiments were conducted using different lengths and sizes of blockage ratios. The results of this study show a strong dependence of shock velocity on the impulse generated. These results show that there is a sharp increase in specific impulse as the shock velocity crosses the choked flame condition. In fact, the impulse gets saturated and further increase in velocity of shock wave does not increase the specific impulse for cases where the shock velocity is above the choked velocity.

The third set of experiments was conducted in a transparent tube. The results from these study shows that higher impulse is obtained with larger blockage when flame travels close to choked condition as compared to the case when it travels close to CJ detonation.

Numerical simulation of flame acceleration in micro-channels with multi-step reaction mechanism has been studied. 2D Navier stokes code utilizing WENO scheme for multi-step reaction has been developed by the author specifically. The study of different non-reactive and reactive test cases has shown the robustness of code in capturing flow structures like vortices and shocks. The study of flame acceleration and transition to detonation has shown that the transition takes place close to the tip of the accelerating

flame. The build up of pressure in front of accelerating flame leads to the decrease in flame thickness. Thin flames being more prone to instability lend themselves to the development of corrugation on the surface which further leads to generation of pressure waves due to Ritchmeyer-Meshkov instability. Interaction of these waves behind the shock compressed gas helps in enhancing the transition process.

6.2 Future work

The experiments from the current study have shown that detonation propagating at velocity closer to choked condition has the ability to produce impulse similar to that in CJ regime. To translate this into actual engine, the study of multi-cycle PDE has to be carried out using optimum blockage configuration. This study can be further extended to include different hydrocarbon fuels. The numerical simulations can be carried out for realistic geometry for H_2-air mixtures.

Bibliography

[1] E. Wintenberger, JM Austin, M. Cooper, S. Jackson, and JE Shepherd. Analytical model for the impulse of single-cycle pulse detonation tube. *Journal of Propulsion and Power*, 19(1):22–38, 2003.

[2] T. Endo, J. Kasahara, A. MATSUO, K. IBANA, S. SATO, and T. FUJIWARA. Pressure history at the thrust wall of a simplified pulse detonation engine. *AIAA journal*, 42(9):1921–1930, 2004.

[3] SB Dorofeev, VP Sidorov, MS Kuznetsov, ID Matsukov, and VI Alekseev. Effect of scale on the onset of detonations. *Shock Waves*, 10(2):137–149, 2000.

[4] C.J. Jachimowski. Analytical study of the hydrogen-air reaction mechanism with application to scramjet combustion. Technical report, National Aeronautics and Space Administration, Hampton, VA (USA). Langley Research Center, 1988.

[5] Ralf Dieterding. Parallel adaptive simulation of multi-dimensional detonation structures. Technical report, 2003.

[6] M. Berthelot and P. Vielle. On the velocity of propagation of explosive processes in gases. *C. R. Hebd. Sceances Acad. Sci.*, 93:18–21, 1881.

[7] E. Mallard and H. Le Chaterlier. On the propagation velocity of burning in gases explosive mixture. *C. R. Hebd. Sceances Acad. Sci.*, 93:145–148, 1881.

[8] Larine Barr. Pulsed detonation engine flies into history. URL `http://www.afmc.af.mil/news/story_print.asp?id=123098900`.

[9] Matthew Lam, Daniel Tillie, Timothy Leaver, and Brian McFadden. Pulse detonation engine technology: An overview. Applied Science 201, The University of British Columbia, 2001.

[10] Sivatai Amit Kumar. Parametric and performance analysis of a hybrid pulse detonation/turbofan engine. Applied science, The University of Texas at Arlington, 2011.

[11] J.H.S. Lee. The detonation phenomenon. *The Detonation Phenomenon, by John HS Lee. Cambridge: Cambridge University Press, 2008.*, 1, 2008.

[12] W. Fickett and W.C. Davis. *Detonation: theory and experiment*. Dover Pubns, 2011.

[13] JH Lee, R. Knystautas, and CK Chan. Turbulent flame propagation in obstacle-filled tubes. In *Symposium (International) on Combustion*, volume 20, pages 1663–1672. Elsevier, 1985.

[14] O. Peraldi, R. Knystautas, and JH Lee. Criteria for transition to detonation in tubes. In *Symposium (International) on Combustion*, volume 21, pages 1629–1637. Elsevier, 1988.

[15] AK Oppenheim. Fourth symposium (international) on combustion, 1953.

[16] GK Adams and DC Pack. Some observations on the problem of transition between deflagration and detonation. In *Symposium (International) on Combustion*, volume 7, pages 812–819. Elsevier, 1958.

[17] JF Clarke. Fast flames, waves and detonation. *Progress in energy and combustion science*, 15(3):241–271, 1989.

[18] I. Brailovskya and G. Sivashinsky. Hydraulic resistance and multiplicity of detonation regimes. *Combustion and flame*, 122(1-2):130–138, 2000.

[19] J.H.S. Lee and I.O. Moen. The mechans of transition from deflagration to detonation in vapor cloud explosions. *Prog. Energy Combust. Sci.*, 6:359âĂŞ389, 1978.

[20] J.J. Erpenbeck. Stability of idealized one-reaction detonations. *Physics of Fluids*, 7:684, 1964.

[21] M. Short and D.S. Stewart. Cellular detonation stability. part 1. a normal-mode linear analysis. *Journal of Fluid Mechanics*, 368:229–262, 1998.

[22] HI Lee, D.S. Stewart, University of Illinois at Urbana-Champaign. Dept. of Theoretical, and Applied Mechanics. Calculation of linear detonation instability: one-dimensional instability of plane detonation. *Journal of Fluid Mechanics*, 216:103–132, 1990.

[23] L. D. Landau and E. M . Lifshitz. *Fluid Mechanics*, volume 6 of *Course in Theoretical Physics*. Pergamon Press, Oxford, U.K., 1987.

[24] T. Endo and T. Fujiwara. A simplified analysis on a pulse detonation engine model. *Transactions of the Japan Society for Aeronautical and Space Sciences*, 44(146):217–222, 2002.

[25] K. Kailasanath. A review of research on pulse detonation engine nozzles. *AIAA Paper*, (2001-3932), 2001.

[26] G. D. Roy, S. M. Frolov, A. A. Borisov, and D. W. Netzer. Pulse detonation propulsion: challenges, current status, and future perspective. *Progress in Energy and Combustion Science*, 30:545–672, 2004.

[27] T. Bussing and G. Pappas. Pulse detonation engine theory and concepts. *Developments in high-speed-vehicle propulsion systems(A 97-15029 02-07), Reston, VA, American Institute of Aeronautics and Astronautics, Inc.(Progress in Astronautics and Aeronautics.*, 165:421–472, 1996.

[28] G.D. Roy. *Combustion processes in propulsion: control, noise, and pulse detonation*. Butterworth-Heinemann, 2006.

[29] J.H. Lee and K. Ramamurthi. On the concept of the critical size of a detonation kernel. *Combustion and Flame*, 27:331–340, 1976.

[30] K. I. Shchelkin. *Gas Dynamics of Combustion*. Mono Book Corp, 1965.

[31] P. A Urtiew and A. K Oppenheim. Experimental observations of the transition to detonation in an explosive gas. *Proceedings of the Royal Society of London. Series A, Mathematical and Physical Sciences*, 295:13, 1966.

[32] SB Dorofeev, VP Sidorov, AE Dvoinishnikov, and W. Breitung. Deflagration to detonation transition in large confined volume of lean hydrogen-air mixtures. *Combustion and flame*, 104(1):95–110, 1996.

[33] F. R. Schauer, R. P. Bradley, and J. L. Hoke. Detonation initiation of hydrocarbon-air in a pulsed detonation engine. *AIAA Paper*, (2001-1129), 2002.

[34] R. Sorin, R. Zitoun, and D. Desbordes. Optimization of the deflagration to detonation transition: reduction of length and time of transition. *Shock Waves*, 15(2): 137–145, 2006.

[35] M. Cooper, S. Jackson, J. Austin, E. Wintenberger, and JE Shepherd. Direct experimental impulse measurements for detonations and deflagrations. *Journal of propulsion and power*, 18(5):1033–1041, 2002.

[36] C.B Kiyanda, V Tanguay, A.J Higgins, and J.H.S Lee. Effect of transient gasdynamic processes on the impulse of pulse detonation engines. *Journal of propulsion and power*, 18(5):1033–1041, 2002.

[37] P. G. Harris, R. Farinaccio, R. A. Stowe, Higgins, P. A. Thibault, and J. P. Laviolette. The effect of DDT distance on impulse in a detonation tube. *AIAA Paper*, (2001-3467), 2001.

[38] G.H. Markstein. *Nonsteady Flame Propagation*. Macmillan, New York, 1964.

[39] Ya. B. Zeldovich, V. B. Librovich, G. M. Makhviladze, and G.I. Sivashinskil. On the onset of detonation in a nonuniformly heated gas. *Astron. Acta*, 15:313, 1970.

[40] SB Murray, F. Zhang, and KB Gerrard. Critical parameters for pulse detonation engine pre-detonator tubes. In *International Colloquium on the Dynamics of Explosions and Reactive Systems, Hakone, Japan*, volume 27, 2003.

[41] SB Murray, PA Thibault, F. Zhang, D. Bjerketvedt, A. Sulmistras, GO Thomas, A. Jenssen, and IO Moen. The role of energy distribution on the transmission of detonation. *Fundamentals and Control, Roy, GD, Frolov, SM, Netzer, DW and Borisov, AA, eds., Elex-KM Publishers, Moscow*, pages 139–162, 2001.

[42] S.I. Jackson. *Gaseous detonation initiation via wave implosion*. 2005.

[43] GO Thomas and A. Jones. Some observations of the jet initiation of detonation. *Combustion and flame*, 120(3):392–398, 2000.

[44] DH Lieberman, KL Parkin, and JE Shepherd. Detonation initiation by a hot turbulent jet for use in pulse detonation engines. In *Proceedings of the AIAA/ASME/SAE/ASEE 38th Joint Propulsion Conference, AIAA Paper*, volume 3909, page 2002, 2002.

[45] JE Shepherd. Pulse detonation engines: initiation, propagation and performance. *GALCIT Report FM2005*, 2, 2005.

[46] E. Wintenberger, JM Austin, M. Cooper, S. Jackson, and JE Shepherd. Analytical model for the impulse of single-cycle pulse detonation tube. *Journal of Propulsion and Power*, 19(1):22–38, 2003.

[47] I. F. Castro-Ruiz M. T. Parra-Santos. Numerical simulation of the deflagration to detonation transition. *Combustion, Explosion, and Shock Waves*, 41(2):215, 2005.

[48] Elaine S. Oran and Vadim N. Gamezo. Origins of the deflagration-to-detonation transition in gas-phase combustion. *Combustion and Flame*, 148:4–47, 2007.

[49] AM Khokhlov, ES Oran, and GO Thomas. Numerical simulation of deflagration-to-detonation transition: the role of shock–flame interactions in turbulent flames. *Combustion and flame*, 117(1):323–339, 1999.

[50] A.M. Khokhlov and E.S. Oran. Numerical simulation of detonation initiation in a flame brush: the role of hot spots. *Combustion and Flame*, 119(4):400–416, 1999.

[51] A.M. Khokhlov, E.S. Oran, and J.C. Wheeler. A theory of deflagration-to-detonation transition in unconfined flames. *Combustion and Flame*, 108(4):503–517, 1997.

[52] J.H.S. Lee, R. Knustautas, and N. Yoshikawa. Photochemical initiation of gaseous detonations. *Astron. Acta*, 5:971, 1978.

[53] DA Kessler, VN Gamezo, and ES Oran. Simulations of flame acceleration and deflagration-to-detonation transitions in methane–air systems. *Combustion and Flame*, 157(11):2063–2077, 2010.

[54] M Kuznetsov, G Ciccarelli, S Dorofeev, V Alekseev, Yu Yankin, and TH Kim. Ddt in methane-air mixtures. *Shock Waves*, 12(3):215–220, 2002.

[55] Vadim N Gamezo, Takanobu Ogawa, and Elaine S Oran. Flame acceleration and ddt in channels with obstacles: Effect of obstacle spacing. *Combustion and Flame*, 155(1):302–315, 2008.

[56] L. Kagan and G. Sivashinsky. The transition from deflagration to detonation in thin channels. *Combustion and flame*, 134(4):389–397, 2003.

[57] I. Brailovsky and G.I. Sivashinsky. Hydraulic resistance as a mechanism for deflagration-to-detonation transition. *Combustion and flame*, 122(4):492–499, 2000.

[58] Vitaly Bychkov, Arkady Petchenko, V yacheslav Akkerman, and Lars-Erik Eriksson. Theory and modelling of acclerating flames in tubes. *Physical Review E*, 72, 2005.

[59] G. Ciccarelli and S. Dorofeev. Flame acceleration and transition to detonation in ducts. *Progress in energy and combustion science*, 34(4):499–550, 2008.

[60] J. Chao and JHS Lee. The propagation mechanism of high speed turbulent deflagrations. *Shock Waves*, 12(4):277–289, 2003.

[61] A. Veser, W. Breitung, and SB Dorofeev. Run-up distances to supersonic flames in obstacle-laden tubes. In *Journal de Physique IV (Proceedings)*, volume 12, pages 333–340, 2002.

[62] SB Dorofeev, MS Kuznetsov, VI Alekseev, AA Efimenko, and W. Breitung. Evaluation of limits for effective flame acceleration in hydrogen mixtures. *Journal of loss prevention in the process industries*, 14(6):583–589, 2001.

[63] M. Kuznetsov, V. Alekseev, I. Matsukov, and S. Dorofeev. Ddt in a smooth tube filled with a hydrogen–oxygen mixture. *Shock Waves*, 14(3):205–215, 2005.

[64] J. L. Hoke, R. P. Bradley, and F. R. Schauer. Impact of ddt mechanism, combustion wave speed, temperature and charge quality on pulsed detonation engine performance. *AIAA Paper*, pages 2005–1342, 2005.

[65] E. Hoffman. Reaction propulsion by intermittent detonative combustion. *German Ministry of Supply, Volkenrode Translation*, 1940.

[66] Y.B. Zeldovich. The question about energetic use of detonation combustion. *Journal of Technical Physics*, 10(17):1453–1461, 1940.

[67] E. Wintenberger and JE Shepherd. Introduction to âĂIJto the question of energy use of detonation combustionâĂİ by ya. b. zeldovich. *Journal of Propulsion and Power*, 22(3):586–587, 2006.

[68] W.H. Heiser and D.T. Pratt. Thermodynamic cycle analysis of pulse detonation engines. *Journal of Propulsion and Power*, 18(1):68–76, 2002.

[69] Y. Wu, F. Ma, and V. Yang. System performance and thermodynamic cycle analysis of airbreathing pulse detonation engines. *Journal of Propulsion and Power*, 19(4):556–567, 2003.

[70] F. Schauer, J. Stutrud, and R. Bradley. Detonation initiation studies and performance results for pulsed detonation engine applications. Technical report, DTIC Document, 2001.

[71] N. Nguyen and A.D. Cutler. Pressure and thrust measurements of a high-frequency pulsed detonation tube. *AIAA*, 2008.

[72] K. Kailasnath. Recent developments in the research on pulse detonation engines. *40th AIAA Aerospace Sciences Meeting & Exhibit*, (AIAA 2002-0470), January 2002.

[73] T.W. Chao, E. Wintenberger, and J.E. Shepherd. On the design of pulse detonation engines. GALCIT Report FM 00-7, California Institute of Technology, Pasadena, CA 91125, 2001.

[74] S. M. Frolov, V. S. Aksenov, and V. Ya. Basevich. Air-breathing liquid-fueled pulse detonation engine demonstrator. *Doklady Physical Chemistry*, 402:93–95, 2005.

[75] A. K. Hayashi and T. Fujiwara. Recent progress of japanese PDE research. *40th Aerospace Science Meeting & Exhibit*, (AIAA 2002-0475), 2002.

[76] LI Qiang, FAN Wei, YAN Chuan-jun, HU Cheng-qi, and YE Bin. Experimental investigation on performance of pulse detonation rocket engine model. *Chinese Journal of Aeronautics*, 20:9–14, 2007.

[77] F. Falempin, D. Bouchaud, B. Forrat, D. Desbordes, and E. Daniau. Pulsed detonation engine possible application to low cost tactical missile and to space launcher. *AIAA paper*, 3815, 2001.

[78] M. Cooper and JE Shepherd. The effect of nozzles and extensions on detonation tube performance. *AIAA paper*, 3628, 2002.

[79] C. Li and K. Kailasanath. Partial fuel filling in pulse detonation engines. *Journal of propulsion and power*, 19(5):908–916, 2003.

[80] Harish.N, Abhishek bhat, P.J.Paul, and N.Shanmugapriya. Comparative study of impulse generated by detonation for two different blockage configurations. In *Proc. of 21th NCICEC, Davangere, India, pp. 593-600*, 2009.

[81] PCB. Product specifications: Model: 102b04, . URL http://www.pcb.com/products.aspx?m=102B04.

[82] PCB. Product specifications: Model: 482c05, . URL http://www.pcb.com/products.aspx?m=482C05.

[83] Agilent. Dso5054a 5000 series oscilloscope: 500 mhz, 4 channels. URL http://www.home.agilent.com/en/pd-1087127-pn-DSO5054A.

[84] J. Kasahara, Y. Tanahashi, T. Numata, A. Matsuo, and T. Endo. Experimental studies on l/d ratio and heat transfer in pulse detonation. In *th International Colloquium on the Dynamics of explosions and Reactive Systems, Hakone, Japan, Jul*, 2003.

[85] N Harish, Abhishek Bhat, and P. J. Paul. Experimental study of partial filling on performance of PDE. In *8^{th} Asia-Pacific Conference on Combustion*, 2010.

[86] Sho Takeuchi, Doi Naoki, and Jiro Kashahara. Effect of ddt process on impulse of diaphragm-less pulse detonation tube. *ASPACC-2010*, 8:487–492, 2010.

[87] R Zitoun and D. Desbordes. Propulsive performances of pulsed detonations. *Combustion Science & Technology*, 144(1):93–114, 1999.

[88] GO Thomas, SM Ward, R.L. Williams, and RJ Bambrey. On critical conditions for detonation initiation by shock reflection from obstacles. *Shock Waves*, 12(2): 111–119, 2002.

[89] S.F. Son-R.A. Yetter Ming-hsun Wu, M.P. Burke. Flame acceleration and the transition to detonation of stoichiometric ethylene/oxygen in microscale tubes. *Proceedings of the Combustion Institute*, 31:2429, 2007.

[90] A. Ivanov-I. Matsukov M. A. Libermann, M. Kuznetsov. Formation of the pre-heated zone ahead of a propagating flame and the mechanishm underlying the ddt. *Physics Letters A*, 373:501, 2009.

[91] Ming-Hsun Wu Jun-Kai Wang. A numerical study on deflagration-to-detonation transition of hydrogen-oxygen mixtures in small tubes. *ASPACC 2010*, page 1165, 2007.

[92] JO Hirshfelder, C.F. Curtis, and R.B. Bird. Molecular theory of gases and liquids, 1964.

[93] James J Quirk. A contribution to the great riemann solver debate. *International Journal for Numerical Methods in Fluids*, 18(6):555–574, 2005.

[94] Ami Harten, Stanley Osher, Björn Engquist, and Sukumar R Chakravarthy. Some results on uniformly high-order accurate essentially nonoscillatory schemes. *Applied Numerical Mathematics*, 2(3):347–377, 1986.

[95] PL Roe. Characteristic-based schemes for the euler equations. *Annual review of fluid mechanics*, 18(1):337–365, 1986.

[96] Ronald P Fedkiw, Tariq Aslam, Barry Merriman, and Stanley Osher. A non-oscillatory eulerian approach to interfaces in multimaterial flows (the ghost fluid method). *Journal of Computational Physics*, 152(2):457–492, 1999.

[97] Chi Wang Shu, Oleg Schilling, and Wai Sun Don. Weno flux schemes. *Journal of Computational Physics*, 70(2):805–836, 1995.

[98] Andrew K Henrick, Tariq D Aslam, and Joseph M Powers. Mapped weighted essentially non-oscillatory schemes: achieving optimal order near critical points. *Journal of Computational Physics*, 207(2):542–567, 2005.

[99] V. Daru and C. Tenaud. Evaluation of tvd high resolution schemes for unsteady viscous shocked flows. *Computers & fluids*, 30(1):89–113, 2000.

[100] Marco Latini, Oleg Schilling, and Wai Sun Don. Effects of weno flux reconstruction order and spatial resolution on reshocked two-dimensional richtmyer–meshkov instability. *Journal of Computational Physics*, 221(2):805–836, 2007.

[101] M. F. Ivanov3-A. D. Kiverin3 M. S. Kuznetsov4 A. A. Chukalovsky2 T. V. Rakhimova M. A. Liberman, 2. Deflagration-to-detonation transition in highly reactive combustible mixtures. *ICDERS*, (23), ICDERS.

[102] T. Aikun, P. Jianfeng, S. Xia, and X. Hong. Numerical simulation study of premixed hydrogen-oxygen combustion process in micro-scale rectangular channel. In *Computer Distributed Control and Intelligent Environmental Monitoring (CDCIEM), 2011 International Conference on*, pages 520–524. IEEE, 2011.

[103] Shaye Yungster and Krishnan Radhakrishnan. Pulsating one-dimensional detonations in hydrogen–air mixtures. *Combustion Theory and Modelling*, 8(4): 745–770, 2004.

[104] I. Matsukov M. Kuznetsov, J. Grune. Effects of shock waves, boundary layer and turbulence on flame acceleration and ddt in highly reactive mixtures. *ICDERS*, 2011.

Appendix A

Reaction Mechanisms

Reactions	A	B	E_a (kj/kmol)
$H_2 + O_2 \rightarrow HO_2 + H$	1.0E+14	0.0	5.6e+04
$H + O_2 \rightarrow OH + O$	2.6E+14	0.0	1.68e+04
$HO_2 + H \rightarrow OH + OH$	1.4E+14	0.0	1.08e+03
$H_2 + O \rightarrow OH + H$	1.8E+10	1.0	8.90e+03
$H_2 + OH \rightarrow H + H_2O$	2.2E+13	0.0	5.15e+03
$OH + OH \rightarrow O + H_2O$	6.3E+12	0.0	1.09e+03
$HO_2 + H \rightarrow H_2O + O$	1.0E+13	0.0	1.08e+03
$HO_2 + O \rightarrow O_2 + OH$	1.5E+13	0.0	9.50e+02
$HO_2 + OH \rightarrow H_2O + O_2$	8.0E+12	0.0	0.00e+00
$HO_2 + HO_2 \rightarrow H_2O_2 + O_2$	2.0E+12	0.0	0.00e+00
$H + H_2O_2 \rightarrow H_2 + HO_2$	1.4E+12	0.0	3.60e+03
$O + H_2O_2 \rightarrow OH + HO_2$	1.4E+13	0.0	6.40e+03
$OH + H_2O_2 \rightarrow H_2O + HO_2$	6.1E+12	0.0	1.43e+03
$H + OH + M \rightarrow H_2O + M$	2.2E+22	-2.0	0.00e+00
H_2O 6.0d0			
$H + H + M \rightarrow H_2 + M$	6.4E+17	-1.0	0.00e+00
H_2O 6.0d0			
$H + O + M \rightarrow OH + M$	6.0E+16	-0.6	0.00e+00
H_2O 5.0d0			
$H + O_2 + M \rightarrow HO_2 + M$	2.1E+15	0.0	-1.00e+03
H_2O 16.0d0			
H_2 2.0d0			
$O + O + M \rightarrow O_2 + M$	6.0E+13	0.0	-1.80e+03
H_2 1.0d0			
$H_2O_2 + M \rightarrow OH + OH + M$	1.2E+17	0.0	4.55e+04
H_2O 15.0d0			

Table A.1: *19 step Reaction mechanism of Jachimowski [4]. Third body factors are given below the respective reactions.*

Reactions	A	B	E_a (kj/kmol)
$H + O_2 \Rightarrow O + OH$	1.86E+14	0.00	16790.
$O + OH \Rightarrow H + O_2$	1.48E+13	0.00	680.
$H_2 + O \Rightarrow H + OH$	1.82E+10	1.00	8900.
$H + OH \Rightarrow H_2 + O$	8.32E+09	1.00	6950.
$H_2O + O \Rightarrow OH + OH$	3.39E+13	0.00	18350.
$OH + OH \Rightarrow H_2O + O$	3.16E+12	0.00	1100.
$H_2O + H \Rightarrow H_2 + OH$	9.55E+13	0.00	20300.
$H_2 + OH \Rightarrow H_2O + H$	2.19E+13	0.00	5150.
$H_2O_2 + OH \Rightarrow H_2O + HO_2$	1.00E+13	0.00	1800.
$H_2O + HO_2 \Rightarrow H_2O_2 + OH$	2.82E+13	0.00	32790.
$HO_2 + O \Rightarrow OH + O_2$	5.01E+13	0.00	1000.
$OH + O_2 \Rightarrow HO_2 + O$	6.46E+13	0.00	56160.
$HO_2 + H \Rightarrow OH + OH$	2.51E+14	0.00	1900.
$OH + OH \Rightarrow HO_2 + H$	1.20E+13	0.00	40100.
$HO_2 + H \Rightarrow H_2 + O_2$	2.51E+13	0.00	700.
$H_2 + O_2 \Rightarrow HO_2 + H$	5.50E+13	0.00	57800.
$HO_2 + OH \Rightarrow H_2O + O_2$	5.01E+13	0.00	1000.
$H_2O + O_2 \Rightarrow HO_2 + OH$	6.31E+14	0.00	73860.
$H_2O_2 + O_2 \Rightarrow HO_2 + HO_2$	3.98E+13	0.00	42640.
$HO_2 + HO_2 \Rightarrow H_2O_2 + O_2$	1.00E+13	0.00	1000.
$H_2O_2 + H \Rightarrow HO_2 + H_2$	1.70E+12	0.00	3750.
$H_2O + M \Rightarrow H + OH + M$	2.19E+16	0.00	105000.
$HO_2 + H_2 \Rightarrow H_2O_2 + H$	7.24E+11	0.00	18700.
$H + OH + M \Rightarrow H_2O + M$	1.41E+23	-2.00	0.
$H + O_2 + M \Rightarrow HO_2 + M$	1.66E+15	0.00	-1000.
$HO_2 + M \Rightarrow H + O_2 + M$	2.29E+15	0.00	45900.
$H_2O_2 + M \Rightarrow OH + OH + M$	1.20E+17	0.00	45500.
$OH + OH + M \Rightarrow H_2O_2 + M$	9.12E+14	0.00	-5070.
$O + H + M \Rightarrow OH + M$	1.00E+16	0.00	0.
$OH + M \Rightarrow O + H + M$	7.94E+19	-1.00	103720.
$O_2 + M \Rightarrow O + O + M$	5.13E+15	0.00	115000.
$O + O + M \Rightarrow O_2 + M$	4.68E+15	-0.28	0.
$H_2 + M \Rightarrow H + H + M$	2.19E+14	0.00	96000.
$H + H + M \Rightarrow H_2 + M$	3.02E+15	0.00	0.

Table A.2: *34 step Reaction mechanism derived from larger methane mechanism by Westbrook [5].*